Abstract

BODNARUK, ETHAN WESLEY. Design and Implementation of a Digital Positron Annihilation Lifetime System for Measurements in Graphite. (Under the direction of Ayman I. Hawari.)

A digital Positron Annihilation Lifetime Spectrometer was designed and used to perform measurements on three graphite materials, reactor grade graphite, pyrolytic graphite, and a foam graphite developed by Oak Ridge National Laboratory. Positrons are a useful probe of the microstructural features of matter since they are attracted to open-volume pores and defects where the electron density is lower than in other parts of the material. Various types of graphite were studied because of their importance in nuclear technology, including as a moderator in nuclear reactor cores.

A lifetime spectrometer consists of a scintillation detector, photomultiplier tube, and equipment to perform timing analysis on the detected radiation. This equipment can either consist of analog pulse shaping and timing electronics or a system that digitizes and processes the radiation pulses. A new type of scintillation material, Lanthanum Bromide [$LaBr_3$(Ce)], was tested and compared to the scintillator usually used for lifetime experiments, Barium Fluoride. The Lanthanum Bromide was expected to perform somewhat better than BaF_2 based on its scintillation properties, and this was confirmed.

The digital system was tested and its performance optimized. The digital lifetime spectrometer shared some similar equipment with a standard analog spectrometer and as such, both could be used simultaneously to take measurements. The digital spectrometer showed improvement in its timing resolution over the analog system. The measurements on graphite were more conclusive for the digital system than for the analog system, as results from the former matched published data well and were more consistent in general. This was due to the greater flexibility in timing methods and opportunity for optimization afforded by the digital system.

Measurements on the graphites supported other work in the literature showing a lifetime of approximately 200 ps in the reactor grade and pyrolytic graphites with a second lifetime on the order of 410 to 425 ps. In the reactor grade graphite the second lifetime was about 410 ps while for the pyrolytic graphite it was about 425 ps. The second lifetime is higher in the pyrolytic graphite and it is attributed to its greater disorder. The 200 ps lifetime is explained as the lifetime of positrons in a perfect graphite crystalline structure while the 400 ps lifetime is explained as the lifetime of positrons at grain boundaries or defects between different regions in the graphite. Data fits involving a third lifetime for the materials were not satisfactory in terms of fitting statistics or results related to physical phenomena.

Measurements on the foam graphite yielded two lifetimes of approximately 125 ps and 340 ps. The first value matches the lifetime of para-positronium, a bound state of an electron and positron known to form in porous materials. The theoretical lifetime of this type of positronium is 129.3 ps. The 340 ps lifetime is most likely the result of positron annihilation in the graphite structure of the foam reflecting positron annihilation in both the perfect crystal structure of the graphite and in grain boundaries. This lifetime is close to the 334 ps mean lifetime found in the reactor grade graphite. Further work and improvements in the experimental technique and equipment could provide more insight into the measurements on graphite.

Design and Implementation of a Digital Positron Annihilation Lifetime Spectrometer for Measurements in Graphite

by
Ethan W. Bodnaruk

A thesis submitted to the Graduate Faculty of
North Carolina State University
in partial fulfillment of the
requirements for the Degree of
Master of Science

Nuclear Engineering

Raleigh, North Carolina

2008

APPROVED BY:

_____	_____
Dr. Man-Sung Yim	Dr. John Blondin

_____
Dr. Ayman I. Hawari
Chair of Advisory Committee

BIOGRAPHY

Ethan Bodnaruk was born November 17, 1981 in Tucson, Arizona to Peter and Judith Bodnaruk. In August 2000, he moved to Claremont, California to study engineering at Harvey Mudd College, a small school of 700 students with a focus on science and engineering. He served as the Vice President of the Tau Beta Pi Engineering Honor Society, active in tutoring core engineering courses and planning service activities for the group. Interest in nuclear nonproliferation and an internship at Sandia National Laboratories with the Yucca Mountain project after his junior year of college cemented his desire to pursue nuclear engineering. After graduating with high distinction from Harvey Mudd College in May 2004, the author decided to pursue an advanced degree in nuclear engineering at North Carolina State University.

Before beginning graduate studies, however, the author decided to pursue other interests for a year and lived at two different monasteries in the United States. He began studies at North Carolina State in Fall 2005, and by the spring semester decided to work with Dr. Ayman Hawari supporting the high intensity slow positron beam project and later transitioned to positron annihilation lifetime spectroscopy. In Summer 2007, he accepted a nonproliferation graduate fellowship with the National Nuclear Security Administration, part of the Department of Energy, and worked to complete his thesis while employed at the NNSA full time. The author plans to continue working at the NNSA.

ACKNOWLEDGEMENTS

The author would like to thank Dr. Ayman Hawari for the opportunity to work on the project and for his guidance and support. The author would also like to thank Dr. Man-Sung Yim and Dr. John Blondin for serving on his graduate committee, with a special thanks to Dr. Yim for his support, friendship, and conversations throughout the author's time at NC State.

The author would also like to extend his thanks to Dr. Jeremy Moxom for his help and expertise shared in the laboratory with the pulse processing equipment used in this work, as well as with experimental methods and helping with ideas of how to test the digital system. Finally, the author would like to thank his family for their continual encouragement and presence in his life.

TABLE OF CONTENTS

LIST OF TABLES

LIST OF FIGURES

Chapter 1

Introduction to Positron Annihilation Lifetime Spectroscopy (PALS)

1.1 Introduction

Positron Annihilation Lifetime Spectroscopy (PALS) is a radiation detection technique by which the lifetime of positrons implanted in condensed matter is measured. The lifetime of the positron from creation to annihilation is directly related to the microstructure of the material and so is extremely useful in the study of many materials. The positron is the antiparticle of the electron, having the same properties as the electron except for opposite charge. Its existence was predicted in 1928 by Dirac [1] and was first observed by Anderson in 1932 as a product of cosmic radiation in a cloud chamber [2]. It was the first antiparticle discovered and its annihilation with an electron provided a concrete example of Einstein's famous mass to energy conversion equation, $E = mc^2$. Whenever a particle and its antiparticle come into contact, the result in a short period of time (picoseconds to nanoseconds) is annihilation, in which both particles cease to exist, and their mass and energy is carried away in electromagnetic radiation [2]. The detection of this radiation from the positron-electron annihilation forms the basis of the PALS technique.

The first experiments utilizing positrons focused on probing the electronic structure of metals and alloys [1]. Three main techniques were used: angular correlation of the annihilation quanta (ACAR), Doppler broadening, and positron annihilation lifetime

spectroscopy (PALS). These techniques are all independent experimental methods and progressed rapidly in the 1950s and ‘60s. By the end of the 1960s, it was discovered that the characteristics of the annihilation phenomenon (i.e. lifetime and intensity) were sensitive to lattice imperfections in the microstructure of matter. Specifically, the positron is attracted to and may become trapped in open-volume crystal defects. In such locations the lifetime of the positron is increased due to a lower electron density. This behavior was conclusively shown by MacKenzie et al. (1967) for thermal vacancies in metals, Brandt et al. (1968) in ionic crystals, and by Dekhtyar et al. (1969) in semiconductors subjected to plastic deformation [1]. The above works marked the beginning of the study of defects via positron annihilation in these materials. Positron annihilation techniques were at first carried out mostly in metals and alloys, but the advance of computer semiconductor technology beginning in the 1980s fueled an increase in semiconductor studies that has continued to this day [1].

Positron techniques for the characterization of crystal defects are powerful and useful tools due to the sensitivity of positrons to open-volume defects and features such as vacancies and pores. Such a defect constitutes an attractive potential toward positrons since such vacancies by definition lack a nucleus that otherwise would be present in the crystal structure. This in effect removes the positive charge that would repel the positively charged positron, creating a localized region with an attractive potential. Pores also present an attractive potential toward positrons since they have a lower concentration of positive charges. The sensitivity of positron techniques is due to the high number of atoms that the positron probes before annihilating. A positron will diffuse a distance on the order of 100

nm through the lattice structure resulting in a microstructural sensitivity of about one vacancy per 10^7 atoms [1].

1.2 Positron Physics

The PALS technique rests upon the physics of the positron's interaction with matter, beginning with its creation and ending in its annihilation.

1.2.1 Creation

Positrons used in PALS and other laboratory applications are produced predominantly by one of three methods: β^+ (positron) decay of radioactive isotopes or by the pair production phenomenon in either a nuclear reactor or from a linear accelerator. Positron decay can occur for neutron-deficient isotopes – two commonly used isotopes being ^{58}Co and ^{22}Na. The ^{58}Co isotope is the most efficient choice for experiments requiring a high intensity of positrons over a short period of time, such as positron diffraction and microscopy. High-activity samples can be purchased for a fraction of the price of a ^{22}Na source with similar activity due to the former isotope's short half-life of 71 days [3].

Sodium-22 is the optimal choice for PALS experiments, however, because of its longer half-life (2.7 yrs) and most importantly due to its nearly-simultaneous emission of a 1.27 MeV gamma ray upon β^+ decay [3]. This gamma ray serves as the detectable signal of the birth of the positron, allowing the lifetime of each positron from its creation to annihilation to be measured. The decay reaction of the isotope is $^{22}\text{Na} \rightarrow {}^{22}\text{Ne} + \beta^+ + \nu_e + \gamma$. The neon nucleus is created in an excited state and then de-excites by emission of a 1.274

MeV gamma ray. This de-excitation gamma ray is included in the decay reaction above. The decay scheme is shown in Figure 1.1.

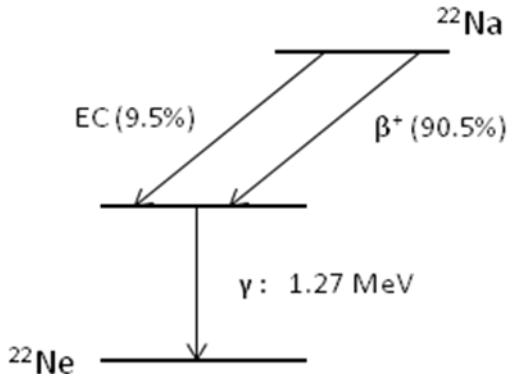

Figure 1.1. Decay scheme of ^{22}Na showing the 90.5% positron decay rate and the 1.27 MeV gamma created from the de-excitation of the excited ^{22}Ne state [1].

The isotope decays by positron emission 90.5% of the time and the 1.27 MeV gamma is emitted 3.7 ps after the positron decay. This time is sufficiently short compared to the lifetime of the positron such that the two events can be considered to be simultaneous [3]. Electron capture (EC) is a competing process and does not result in the emission of a positron.

The second means of positron production at a level required for positron applications is the pair production phenomenon, essentially the reverse of positron-electron annihilation. One of the ways a high-energy photon can interact with matter is by the creation of a positron-electron pair involving the slight recoil of a heavy nucleus to conserve momentum. For this process to occur, conservation of energy must be satisfied such that the minimum photon energy for pair production is 1.022 MeV, the rest mass of the positron-electron pair.

The probability of pair production increases approximately as the square of the atomic number Z of the material involved in the process and increases approximately linearly with the photon energy [4]. Examples of a beam-based positron system are the positron facility at Delft University [5] and the High Intensity Positron Beam at the PULSTAR reactor at North Carolina State University [6]. Beam-based systems are often used for depth-profiling in extremely thin materials as thin as tens of atomic distances. Such slow positron beam systems offer control of the positron energy to create nearly monoenergetic beams up to just tens of keVs. The study of materials with PALS using ^{22}Na positrons directly incident on the materials is characterized as bulk studies since the positron energy is much higher than in a slow positron beam and thus penetrates deeper into the material. The ^{22}Na positron has a continuous energy spread with a maximum energy of 545 keV [3].

1.2.2 Implantation and Moderation

Energetic positrons incident upon a target material lose their kinetic energy through inelastic collisions with electrons, and at lower energies by plasmon excitation and at the eV level by energy exchange with phonons that excite the vibrational modes of the material. This loss of energy occurs within about 1 ps [3] and the rate of loss is highest at large energies due to core ionization processes [1]. The positron implantation profile for the ^{22}Na positron, related to the thickness of the sample probed, is given empirically by Equation 1.1 below,

$$\overline{P}(z) = e^{-\alpha z}, \text{ with } \alpha = \frac{17\rho}{E_{\max}^{1.43}}, \tag{1.1}$$

where α [cm^{-1}] is the positron absorption coefficient, E_{max} [MeV] is the maximum positron energy, and ρ [g/cm^3] is the mass density of the solid [1]. Figure 1.2 shows the mean depth of implantation ($\bar{z}$) and depth probed ($\hat{z}$) for various materials. The mean penetration or implantation depth is defined by P($\bar{z}$) = 1/e, and the probed or information depth is defined by P($\bar{z}$) = 0.999 [1].

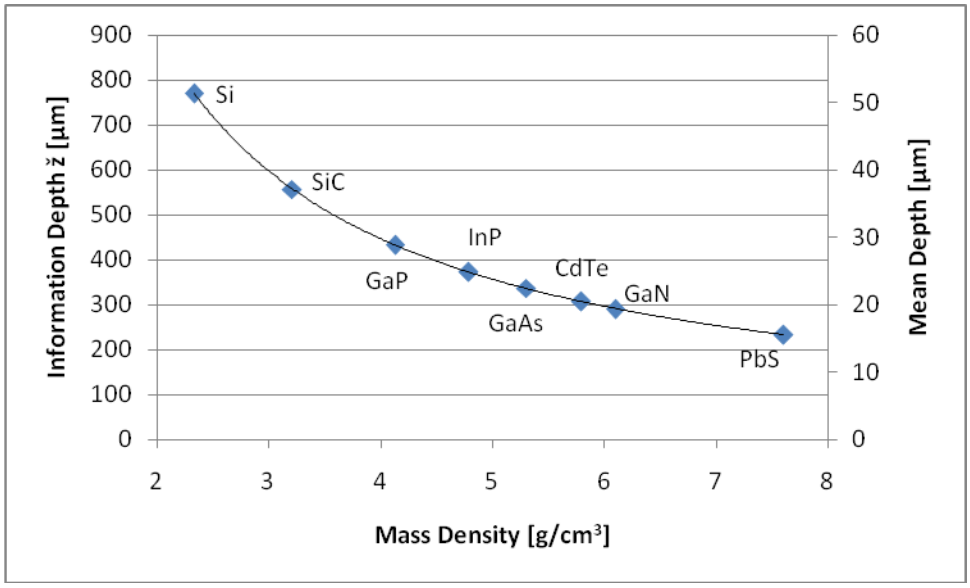

Figure 1.2. Positron depth profile versus sample density [1]

Once the positron has reached thermal energies it begins to diffuse through the crystal lattice of the target material. The positrons are repelled by nuclei and thus have the highest probability of being found in interstitials and vacancies. The diffusion process is akin to that of electrons at similar energies and can be described using semiclassical three-dimensional random-walk theory [1]. Because of the random walk nature of motion it is possible for positrons to diffuse back to the surface of the material and exit the material if it has a positron

work function that is negative. The work function for a given particle is the amount of energy required to remove it from the surface of a solid material. Some materials have a negative positron work function, meaning that positrons diffusing near the surface may be emitted from the material gaining energy equal to the magnitude of the work function [3]. This phenomenon is not common for the positron energies from ^{22}Na in bulk samples, however. The source-sample sandwiched geometry used in PALS also prevents the positrons from escaping, as discussed later. Some positrons do annihilate in the support foil and these require a source correction that is of utmost importance in PALS.

A parameter describing the diffusion of the positron is the positron diffusion length, L_+, which is limited by the finite lifetime of positrons in the defect-free bulk of the material, τ_b, as follows [3]

$$L_+ = \sqrt{\tau_b D_+} \quad \text{with} \quad D_+ = \tau_r \frac{k_b T}{m^*}, \tag{1.2}$$

where τ_r is the relaxation time for the dominant scattering process at a given energy. The term m^* is the effective positron mass and is between 30% to 70% greater than the free positron rest mass because of phonon scattering, the periodic lattice, and the effect of screening by electrons [1]. The diffusion length is a measure of the distance a positron will diffuse before annihilating. That is why the positron lifetime also enters into the equation. Positron diffusion is described in general by the time-dependent diffusion equation

$$\frac{\partial}{\partial t} n_+(\mathbf{r},t) = D_+ \nabla^2 n_+(\mathbf{r},t) - \nabla[\nu_d n_+(\mathbf{r},t)] - \lambda_{eff} n_+(\mathbf{r},t), \tag{1.3}$$

where n_+ $(\mathbf{r},t)$ is the positron density at position $\mathbf{r}$ and time t, and ν_d is the positron drift

velocity. This equation takes into account the effect of positron trapping resulting from an effective annihilation rate

$$\lambda_{eff} = 1/\tau_b + \kappa(\mathbf{r}) \tag{1.4}$$

and the effective positron diffusion constant

$$D_+^{eff} = L_+^2 \lambda_{eff}, \tag{1.5}$$

where $\kappa(\mathbf{r})$ is the positron trapping rate which must be a function of position since the vacancies, interstitials, and dislocations are located in different positions within the overall crystal structure. This trapping rate can be determined from the results of PALS using the trapping model [7].

1.2.3 Positronium

After thermalizing, a positron may form a bound state with an electron, known as positronium (Ps). This occurs at air- or vacuum-surface boundaries and in low density condensed matter such as liquids or some solids with sufficient free space in the lattice, for example ice [2,8]. The Ps atom is similar to the hydrogen atom in its mathematical description except that the reduced mass of the Ps must be used, which is half the electron mass. The Schrödinger equation accurately describes the Ps atom with this reduced mass correction. Other equations such as the eigenvalue equation for the Ps center of mass yield very similar results as compared to that of hydrogen [1]. The reduced mass is responsible for a decrease in the Ps energy level separations relative to the hydrogen atom such that the Ps binding energy is only 6.8 eV. Additionally, the positron's magnetic moment is 658 times larger than that of the proton with the result that the Ps fine and hyperfine energy levels

deviate from those in the hydrogen atom. Other QED effects also contribute to this difference [3].

The quantum state of the Ps is a major factor in determining how the Ps annihilation process takes place, as shown by Yang (1949), and Wolfenstein and Ravenhall (1952) [3]. It can exist in one of two spin states, $s = 0$ or $s = 1$. The former state is known as para-positronium (p-Ps) and consists of anti-parallel positron and electron spins, which is a singlet state. The $s = 1$ state is a triplet state in which both spins are aligned. Yang, and Wolfenstein and Ravenhall, derived a selection rule for the annihilation of positrons correlating the number of photons created and the spin, s, and orbital angular momentum, l, values of the positronium as follows:

$$(-1)^p = (-1)^{l+s}, \tag{1.6}$$

where p is the number of photons created [3]. For the case of p-Ps, $s = 0$ and $l = 0$ and so the number of photons created at the time of annihilation must be even. For ortho-Ps, $s = 1$ and $l = 1$ so the number of photons must be odd. Although "allowed", higher order annihilations, such as four-gamma p-Ps annihilation or five-gamma o-Ps annihilation are exceedingly rare. For o-Ps, the most common form of annihilation is the three-photon process; the one-photon process is also extremely rare [3].

1.2.4 Annihilation

All positrons in contact with condensed matter will eventually annihilate with an electron. In this process both particles are quantum mechanically converted to energy in the form of photons. Only positrons isolated in vacuum can be preserved or stored for a long

period of time. By far the most common mode of annihilation is the two-photon annihilation in which two photons sharing the rest mass and kinetic energy of the positron and electron are created [3]. These are observed to possess approximately 511 keV of energy and have opposite momentum, thus obeying the conservation laws.

The two photons exhibit an energy that only slightly deviates from the value of 0.511 MeV, because of the small contribution of the electron's momentum before annihilation. This small but detectable difference forms the basis for Doppler Broadening spectroscopy with positrons [3]. The detection of the annihilation quanta provides the signal for determination of the end of the positron lifetime for PALS studies.

1.3 Positron Annihilation Techniques

The three major positron annihilation experimental techniques are Doppler broadening, Angular Correlation of Annihilation Radiation (ACAR), and PALS. Although PALS is the focus of this work it is worthwhile to briefly explore the other two before concentrating on PALS exclusively.

1.3.1 Doppler Broadening

As mentioned above, Doppler broadening is based on the detection of slight differences in energy of the 0.511 MeV annihilation quanta due to the energy and momentum of the electron in the positron-electron annihilation. A distribution spectrum of the number of counts versus annihilation quanta energy in a given material is collected, resulting in a nearly Gaussian-looking peak at 0.511 MeV. Positrons favor trapping and subsequent annihilation in open-volume vacancies lacking a nucleus and thus lacking energetic bound

core electrons. As a result the positron annihilates with a low-energy valence electron which adds negligible momentum to the positron-electron system resulting in annihilation quanta with energy right at 0.511 MeV. When a positron annihilates with a core electron, however, the electron contributes a significant momentum to the system and the annihilation quanta may have energies as high or as low as 520 keV or 500 keV, respectively [3]. Thus the more defects present the sharper the profile will be since more positrons annihilate with low energy electrons resulting in more 511 keV quanta. Two variables *S* and *W* are used to quantify this, *S* being the area under the central part of the peak and *W* the ratio between the area under the wings of the peak and the total area. A material with a higher *S* value will have more defects than a material with a lower *S* value [3].

1.3.2 Angular Correlation of Annihilation Radiation

Angular Correlation of Annihilation Radiation (ACAR) is a method that reveals information about the electronic structure of the bulk of, and the defects present in, a material. It is observed that annihilation quanta can exhibit a slight deviation from collinearity or 180º back-to-back emission. While the Doppler broadening effect is due to the conservation of momentum in the direction of the annihilation quanta's propagation, ACAR is due to momentum conservation in the other two perpendicular spatial dimensions making up three-dimensional space. The annihilation quanta are measured in coincidence by position-sensitive detectors to determine the angles $\Theta_{x,y}$ of deviation from 180 degrees [1].

The system utilizes electronics that filter the coincident events and store the deviation in memory. This effectively saves the two-dimensional electron momentum distribution and can be plotted with contour or perspective plots. In order to acquire defect-specific

information and plots, however, a normalization based on the trapping of positrons in all types of defects must be performed. This is provided by positron lifetime (PALS) measurements which yield the fraction of positrons annihilating in each type of defect. Contour plots can also be compared to theoretical calculations to add to the knowledge of the electronic structure of a given defect. The ACAR technique provides greater resolution than Doppler Broadening but requires a stronger positron source and longer collection time [1].

1.3.3 Positron Annihilation Lifetime Spectroscopy

The PALS measurement is based on the measurement of the time interval between the detection of a 1.27 MeV gamma ray emitted by a ^{22}Na source and the detection of the corresponding 0.511 MeV annihilation photon created by the annihilation of the positron from the ^{22}Na decay [1]. The ^{22}Na source is usually deposited on a thin foil and sealed with another layer of the same foil. This foil or support structure is placed between two samples of a material to study. As mentioned in the above sections, the positron goes through a process of implantation, thermalization, diffusion, and finally annihilates either somewhere in the perfect crystal lattice of the material or trapped in an open-volume defect or feature.

A PALS measurement is made by collecting and storing the individual lifetimes of positrons in a histogram or the channels of a multichannel analyzer (MCA), resulting in the positron lifetime spectrum. A sufficient number of annihilation events must be captured to ensure adequate statistics in the overall results and in each channel. A lifetime spectrometer is characterized by its time resolution, which refers to its ability to resolve pulses that are exactly in coincidence. Due to various detector, radiation interaction, and pulse shaping effects a spectrometer processing only pulses in exact coincidence would still show a spread

in the effective time difference between the pulses. The shape of the spread is the resolution function of the system and is characterized by its full width at half maximum (FWHM), known as the time resolution.

The time resolution of the PALS spectrometer is characterized by a single value related to its resolution function. The timing resolution is defined as the full width at half maximum (FWHM) of the resolution function, which is $2\sqrt{2\ln 2}\,\sigma_s$, or approximately $2.35\sigma_s$. This is a key parameter and its minimization is the focus of much research in the field. Values in the range of 200 to 280 ps are common for the PALS timing resolution. The crux of this value is that positron lifetimes less than 50 ps cannot be resolved and that materials with multiple lifetimes of similar value are difficult to resolve. This is an issue for metals, many of which have bulk lifetimes of 50 ps or under. The uncertainty of lifetimes that can be resolved can be as low as 1-2 ps [1].

Another important parameter in the PALS measurement is the coincidence count rate, or the rate at which data is collected. This depends mainly on the geometry of the setup and the source used. A PALS measurement usually takes between several hours and a day to collect a spectrum with good statistics. Some efforts to decrease the time resolution increase the counting time so there is an important tradeoff there to be managed. The research performed in this work strove to both attain a better timing resolution and to obtain new positron lifetime data for different graphite materials in consideration for use in future Generation IV nuclear reactor designs.

1.4 Digital and Analog Implementation of PALS

The conventional method of PALS measurements involves an analog spectrometer which consists of the radiation detectors and analog electronics that process and extract information from the detector pulses. A newer PALS implementation relies on digital processing and information extraction from the detector pulses [9]. Such a digital method uses either analog to digital converters or a digital oscilloscope [9,10]. Recent work has focused on achieving lower time resolution in both types of systems and this has been successful but with varying degrees of usefulness in performing actual PALS measurements [10]. A digital PALS system has been shown to have better time resolution than an otherwise equivalent analog system [9]. This work also shows that a digital system can provide a better time resolution.

1.5 Purpose of Studying Graphite

Nuclear energy is experiencing a renaissance in the United States and elsewhere in the world, especially in developing countries. The world population is growing exponentially and per capita electricity use is also increasing, resulting in a rapidly growing demand. It is estimated that the world demand for electricity will increase by over 55% by 2030 compared to 2004 [11]. Nuclear energy promises to help meet this demand while avoiding the emission of greenhouse gases associated with most types of base load energy production. As the climate for the expansion of nuclear energy is ripe, new reactor concepts are being designed that increase the overall safety of the system and that also produce less nuclear waste. Graphite is a key component in some of these systems.

Graphite is a carbon material that has been used as a neutron moderator in various nuclear reactor designs. Neutron moderation is important because Uranium-235, the

principal isotope that fissions in a nuclear reactor, has a much higher fission cross section for slower, thermalized neutrons than for fast neutrons. The neutrons born in fission are mostly fast neutrons, so the moderation of these leads to a greater number of fissions [12].

Graphite is well suited for neutron moderation since it has a low cross section for neutron absorption and an atomic mass not prohibitively greater than that of the neutron. This latter property is a major factor in the efficiency of neutron moderation. The smaller the mass of the nucleus the neutron collides with (down to the mass of the neutron itself), the larger the maximum and average energy the neutron loses in a single collision. In terms of size alone, the nucleus of the hydrogen atom – having nearly the same mass as the neutron – is the ideal moderator since the neutron can lose practically all of its energy in a single collision. Hence water is another common moderator in reactor designs such as those found in the PWR and BWR commercial nuclear power plants. The downside of such light water moderation is that the water has a large neutron capture cross section, resulting in a decrease in the efficiency of the fission process due to removal of neutrons. Heavy water, or water consisting of the ^{2}H isotope instead of the ^{1}H isotope, is also a good moderator in terms of its size compared to the neutron. It is better compared to light water, though, because ^{2}H has a much lower neutron capture cross section since it already contains an extra neutron compared to ^{1}H [12]. The choice between water, heavy water, and graphite as moderator for a given reactor design involves economic tradeoffs as well as political and nonproliferation considerations.

For these reasons and others, graphite is the moderating material future thermal spectrum Generation IV nuclear reactors are designed to use. For such designs the need

exists to understand the properties and behavior of graphite in more detail. After an extended period of time in a reactor, graphite experiences significant neutron irradiation leading to the creation of many dislocations and vacancies at the microstructural level. This has important safety implications for its mechanical properties. Evidence also exists that open-pore defects in graphite affect its nuclear properties related to neutron interactions [13]. Finally, for one design in particular, the Very High Temperature Reactor, graphite will be subject to much higher temperatures and radiation doses at which the understanding of the graphite microstructure is poor. All of these factors call for the increased study of graphite. One tool which is well-suited for this is the PALS technique.

Chapter 2
Description and Theory of Spectrometer

2.1 Analog PALS Spectrometer

The analog PALS spectrometer measures the lifetime of each positron absorbed in the test material and its supporting structures. The measurement is initiated by the detection of the ^{22}Na 1.27 MeV gamma that is liberated in coincidence with the positron from each nucleus's decay. The end of the positron's lifetime is marked by the detection of its 0.511 MeV annihilation quanta [1]. The analog system as a whole consists of the radiation detectors, signal amplification hardware and shaping signal processing/timing hardware, and a computer on which to store and view the data. The appropriate detector for this application is a scintillation detector, based on the conversion of the gamma rays to scintillation light given off as the detector material absorbs the energy of the gamma ray. The scintillation photons are then collected and converted to an electrical signal with characteristics related to the quantity and timing of the photons produced. This is accomplished by photomultiplier tubes (PMTs) which convert the light to electrons and send them through a series of amplification stages, creating an electrical pulse that is processed by subsequent electronics. The PMTs require a high voltage power supply to power this process of electron signal amplification based on secondary electron emission [14].

A total of two detectors are used: one to record the birth of the positron, and one to record the annihilation. For an analog implementation, the detector events are processed by a

conventional analog pulse processing chain consisting of time pick-off using constant fraction discriminators (CFD), a time to amplitude converter (TAC) and multi-channel analyzer (MCA). The CFD uses the constant fraction principle to mark the time of occurrence of the radiation event based on the rising edge of the pulse. It outputs a fast, square logic pulse that is led to the TAC to trigger it [15]. Thus the first input to the TAC marks the time at which the positron was born and the second the time at which it annihilated.

Upon receiving the START signal, or the signal from the first discriminator that performed the time-pickoff on the 1.28 MeV gamma, the TAC begins charging a capacitor. The capacitor stops charging when the STOP signal is received from the detector set to the 511 keV annihilation quanta, producing a stored charge on the capacitor proportional to the time difference. This potential discharges, sending a voltage pulse to the MCA which digitizes and records the maximum voltage. The MCA digitizes each pulse it receives from the TAC. It stores this information across its 8192 channel range, creating a lifetime spectrum similar in concept to a pulse height spectrum in energy spectroscopy [1]. Instead of a distribution of pulse heights, however, a distribution of time differences representing the positron lifetime is obtained. The conversion from pulse height stored in the MCA to time interval is based on the approximately 50 ns range of the TAC split across the 8192 channels. Tests using delayed pulses from a pulse/delay generator are also used to determine the time interval per channel, which was approximately 6.8 ps/ch.

A schematic of the analog PALS system is shown below in Figure 2.1, showing a not-to-scale rendition of a source/sample sandwich. Two different setups were used for the

analog system, varying only the detector and its associated photomultiplier tube. The first was the relatively new $LaBr_3$(Ce) scintillation material, obtained from Saint-Gobain Crystals under the trademark name BriLanCe 380© and the second was BaF_2, a fast scintillation material that has been in use for decades and was also obtained from Saint-Gobain Crystals. Both detectors were purchased as a package with their PMT and voltage divider base, the detector crystal having been coupled to the PMT by the manufacturer. The divider bases chosen were one of the standard commercially available options, optimized for timing performance [16,17]. The BaF_2 crystal was coupled to the XP2020/Q PMT while the $LaBr_3$ detector was coupled to the XP20D0 PMT with voltage divider model AS-20. The high voltage supplies used were Ortec model 556.

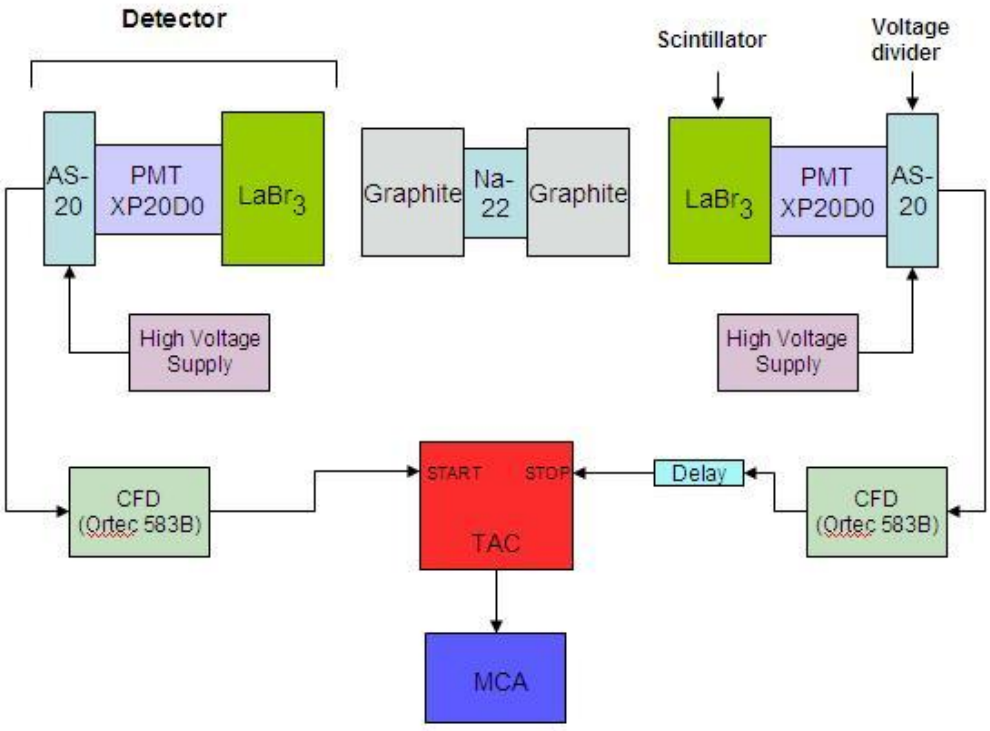

Figure 2.1. Schematic of the analog PALS system

$LaBr_3$ and BaF_2 were chosen as detector materials because of their balance of high collection efficiency, light output, and short pulse rise time. The rise time is especially important for the time resolution of the system [14]. Barium Fluoride (BaF_2) detectors are also commonly used in PALS because they have the best rise time of inorganic scintillators [14]. The $LaBr_3$ was also chosen because it was a new material that had not been used for this application before but was expected to have similar or better performance than BaF_2. It has a decay time of 16 ns and a rise time on the order of 3 ns depending on the PMT and operating voltage. Its decay time is among the best of scintillators but is poorer than BaF_2. Its 63 photon/keV light emission, however, is superior to the BaF_2 1.8 photon/keV light emission meaning that the $LaBr_3$ yields more scintillation photons per unit of energy deposited in the crystal. A figure of merit parameter defined as the ratio of the decay time to the light emission is one indicator of a material's performance in coincidence timing. The figure of merit for BriLanCe 380 $LaBr_3$ is 0.25 while that of BaF_2 is 0.44, where a smaller figure of merit is desirable [18]. As far as is known from conversation with personnel at Saint-Gobain Crystals, this study was the first PALS application using any of the BrilLanCe® series scintillator materials. A 25 mm diameter, 25 mm thick crystal was chosen for both types of detectors. This was a compromise between cost, transit time of the gamma rays due to the size of the crystal, light reflection, and the efficiency of collection.

2.1.1 Source and Test Material Sample Configuration

The ^{22}Na source is sandwiched tightly between the two test samples – for this work, either graphite or high purity silicon used for calibration – to ensure that all positrons are

absorbed so none escape to form Ps at an air-surface boundary. Since ^{22}Na is expensive, it is not feasible to deposit the isotope directly on each sample. The general procedure is to deposit the ^{22}Na on a thin foil and to seal it in order to create a reusable source for use in PALS studies. A sheet of 25μm thick kapton foil was obtained from McMaster-Carr for this purpose. Kapton is a polyamide polymer that is known to exhibit only one positron lifetime of 382 to 386 ps [19-20], allowing for a simpler source correction in the PALS spectrum accounting for the positrons that annihilate in the kapton. The 25 μm thickness foil was the thinnest available from McMaster Carr, and later it was noticed that most researchers use even thinner foils to minimize the number of positrons annihilating in the foil.

An aqueous 10 μCi ^{22}Na solution was deposited on a small square piece of the 25 μm foil with a small eye-dropper and placed under a heat lamp until it evaporated, leaving only the dried ^{22}Na crystals. Another identical piece of kapton was placed on top and was sealed with kapton tape, and together this is referred to as a source/kapton sandwich. This sandwich is shown below in Figure 2.2. One of the high purity silicon samples used in the testing is shown underneath the kapton for color contrast.

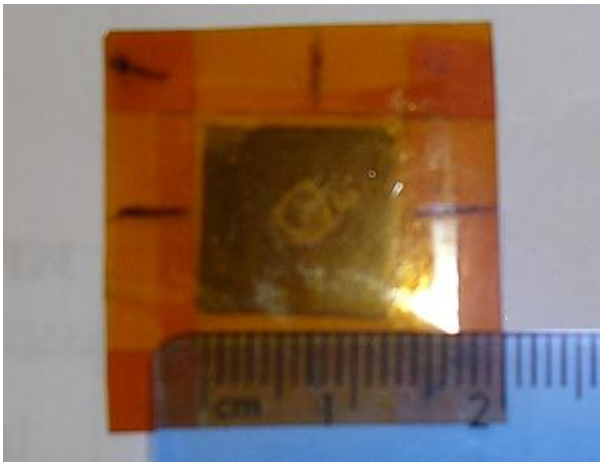

Figure 2.2. White ^{22}Na crystals seen at the center of the orange kapton foil

The whitish spot in the center is the dried ^{22}Na, and the darker orange regions on the foil are where layers of kapton overlap to seal the source. Immediately above and below the source spot, however, is only one layer of kapton. It is seen from the figure that the diameter of the source is approximately 4 mm. In a PALS measurement the source is surrounded by two samples of the desired test material, such as silicon, and this is referred to as the source/sample sandwich or source/kapton/sample sandwich. The sandwich is held tightly together to eliminate any air gaps between the kapton and sample. This helps prevent positronium formation at surface boundaries [1].

The ^{22}Na source activity was small enough to ensure that there is only one positron on average in the material at any given time. A 10 μCi source is equivalent to 3.7×10^5 disintegrations per second, and with a 90% positron branching ratio this corresponds to an average of 3.3×10^5 positrons created per second, or one positron every three microseconds. Since an individual positron lives on the time scale of hundreds of picoseconds to nanoseconds, this activity ensures that only one positron will be processed by the system at a time, preventing the overlap of signals or triggering from separate annihilation events [1]. In addition, the smaller the activity the better the ratio of true coincidences to chance coincidences, giving a higher true coincidence peak to background ratio [14]. Because the foil is so thin (not to scale in Figure 2.1) most of the positrons emitted from the sodium source enter the specimens.

Kapton foil is used because it is "well-behaved" when it comes to positron lifetimes, i.e. it has a single lifetime parameter with thickness-dependent intensity so its contribution can be subtracted out of the experimentally determined spectrum [19-21]. This is known as a

source correction and is determined by performing a PALS test on a specimen of extremely high purity silicon or other material known to have just one positron lifetime, as discussed later. The literature shows a single lifetime component of 219 ps for such silicon [10]. The high purity silicon is used to determine the spectrometer time resolution function since its lifetime and the kapton lifetime are known, providing the needed degrees of freedom to calculate the function.

2.1.2 Photomultiplier Tube (PMT) and Voltage Divider Base

The photomultiplier tube (PMT) converts the light produced in the scintillator into an electrical pulse. It accomplishes this using a photocathode that produces a yield of electrons from the incoming scintillation light. The photocathode is followed by a series of stages that amplify the electrical signal [14]. The Photonis XP20D0 PMT is designed for optimal timing performance with the BrilLanCe® series of scintillator material. It is used in fast scintillation detection and has good linearity and high energy resolution. The AS20 voltage divider base provides optimum timing performance amongst commercially available bases, achieving a 1.5 ns rise time [16]. The base supplies specific voltages to the photocathode and dynode stages in the PMT to optimize the signal amplification.

The Photonis XP2020/Q was used for the BaF_2 detectors. This is the standard PMT for this scintillation crystal as it has an excellent quoted rise time of 1.5 ns and good linearity as well [17]. Another PMT that has been used with BaF_2 is the Hamamatsu H3378 (R2083Q), which has a quoted rise time of 0.7 ns and has been used successfully in PALS studies [22].

2.1.3 Constant Fraction Discriminator, TAC and MCA

The Ortec 583B CFD is a fast differential discriminator with built-in single channel analyzer (SCA) [15]. It uses the constant fraction discrimination principle to pick off the time at which birth and death events occur. Constant fraction discrimination is a time pick-off method that greatly reduces amplitude walk, which is variation in time pick-off due to varying pulse amplitude. The built-in SCA allows energy selection criteria to be added. The CFD in the "start" chain is set to accept scintillator pulses corresponding to gamma ray energies in the vicinity of 1.27 MeV, the energy of the gamma ray marking the birth of the positron. The CFD in the "stop" chain is set to accept scintillator pulses corresponding to the collection of light from gamma rays in the vicinity of 0.511 MeV, the energy of the annihilation quanta. These selection criteria ensure that only pulses arising from the birth and death of the positron are processed. Furthermore, it ensures that the "start" chain of the system only processes 1.27 MeV quanta and the "stop" chain only processes the 0.511 MeV annihilation quanta. This is important since both types of gamma rays deposit energy in each detector. The energy selection reduces noise in the system and improves the time resolution [14].

At the moment of the time pick-off, the CFD unit produces a standard output logic signal accepted by the TAC, which for the PALS system marks either the birth (start signal) or death (stop signal) of the positron. During the time interval between the start and stop signals a capacitor in the TAC is charged so that the amplitude of the output pulse of the TAC is proportional to the time difference between start and stop signals and thus proportional to the lifetime of the positron. The output pulse travels to the MCA where it is

digitized and stored in a bin based on its amplitude, yielding a distribution of time differences, i.e. the lifetime spectrum. As seen in Figure 2.1, the output from the "stop" chain between the CFD and TAC is delayed in time. This is accomplished by using a longer coaxial cable, adding a fixed delay time which serves to increase the time difference to a region of linear response in the TAC. The MCA used in this work was an MCA PCI card placed on board a computer via a PCI slot, and included the Maestro 32 data acquisition and MCA emulation software used to acquire and view the data.

The system is characterized as a fast-fast coincidence system since both the energy and timing selection are fast. The energy selection is fast because the 583B constant fraction discriminator is a fast differential discriminator, and the timing is fast because the detectors produce fast pulses with nanosecond rise time. In the past, the 583B and other fast timing units with energy selection were not available [14].

2.2 Digital PALS Setup using Fast Digital Oscilloscope

As an alternative to the analog pulse processing chain used in PALS, a digital PALS system can be implemented. This eliminates the need to optimize the electronics in Figure 2.1, namely the constant fraction discriminator. This is useful since the optimization of the CFD is a tedious process and because digital methods provide more flexibility in timing than the CFD hardware and give the user access to the pulses themselves. Digital systems can be designed without the use of the analog CFD-TAC-MCA chain using a coincidence unit or custom circuit for triggering [9,10,22]. The analog chain, however, can serve as a means of triggering the oscilloscope solely on coincident events, and if the output of the TAC is split

to both the oscilloscope and to an MCA then the resulting system is capable of collecting both analog and digital lifetime spectra with separate and independent timing calculations. This allows for direct comparison of the results from the same set of detection events for both systems. The combined analog and digital PALS approach was chosen for this work because of the utility of the direct comparison. A schematic of the system is shown below in Figure 2.3.

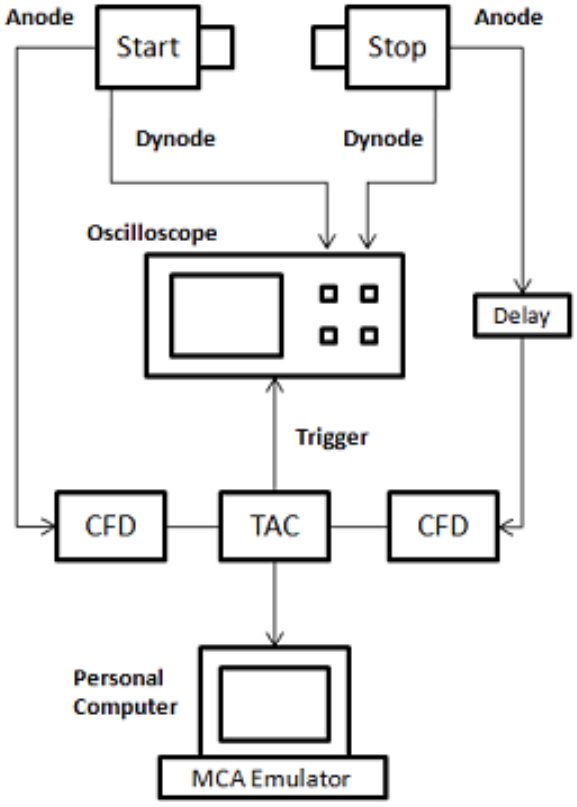

Figure 2.3. Combined digital and analog PALS system. The setup allows data to be collected simultaneously from both digital and analog processing methods.

For the digital system used in this work, the output of the scintillation detectors is taken directly from the PMT dynode and transmitted by RG-58C/U coaxial cable to the channel 1 and channel 2 inputs of a WaveRunner 6100A oscilloscope from LeCroy. The

TAC signal contains the timing information about the pulses based on the time pickoff performed by the CFDs. A key difference is that the digital system does not use the output of the TAC for its timing calculation. The digital system utilizes this signal only as a trigger to indicate that a given event is a coincident event. The actual timing measurement is performed by the oscilloscope on the leading edge of the digitized pulses from the dynode – not via the CFDs. The CFDs still perform their pick-off operation in order to determine if a given pulse pair is in coincidence, but this is not used in the digital calculation of the time difference. Thus the operations are independent and do not affect one another, yet the results of the two systems can be directly compared knowing that experimental conditions are identical for each system.

The digital system gives flexibility to optimize its timing calculations based on the constant fraction value and opens the possibility of defining other timing algorithms, rejection criteria for spurious pulses, and pre-processing of the pulses. It gives the user access to the detector pulses themselves in a way not possible in the analog system. The CFD, on the other hand, is hard-wired to perform the constant fraction time pick-off at a fixed constant fraction of the pulse amplitude.

The LeCroy WaveRunner 6100A has a sampling rate of 10 GHz and a 3 GHz bandwidth. The sampling rate translates into a data acquisition rate of 1 sample every 100 ps, which yields 20 to 30 sample points on a 2 ns to 3 ns leading edge, depending on the rise time of the detector and its electronics. This is more than enough points to ensure that all high frequency information is captured [10]. The oscilloscope has an 80GB hard drive and runs the Microsoft Windows XP platform like a desktop computer. Furthermore, it supports

Excel, MATLAB, and programming languages within the oscilloscope interface. With the XMATH Advance Math Package software upgrade, it can build histograms of up to one billion data points, easily accommodating a positron lifetime spectrum [23]. The histogram may be saved to the hard drive for transfer to other computers and to be analyzed by programs that analyze lifetime spectra. Individual detector pulses may also be saved to the hard drive at each trigger signal, but this was not feasible for PALS spectra due to the millions of pulses that would be saved and their prohibitive size on the hard disk. Other researchers have used digitizers in place of a digital oscilloscope and saved all data to hard drive and subsequently performed offline time pick-off and pulse processing [9,10]. Online pulse processing was convenient and avoided the writing of more complicated computer codes but could be a bottleneck for the maximum coincidence count rate, as discussed later.

The dynode pulses are slightly faster than the anode pulses as they come from an earlier stage in the electron signal amplification process within the PMT. The dynode pulses are also smaller in amplitude than the anode pulses for the same reason and do not fall into the amplitude range recognized by the CFDs. The dynode pulse amplitude is acceptable for the oscilloscope, however, and this is why the anode pulses are led to the CFD while the dynode pulses are led to the oscilloscope, as shown in Figure 2.3 above.

2.3 Theory of Scintillation and the Pulse Shaping Process

2.3.1 Scintillation Detectors

Both detector types are categorized as fast inorganic scintillators, meaning they are composed of non-organic elements and have a fast scintillation response. The $LaBr_3$ detector

is an activated inorganic scintillator while BaF_2 is an unactivated inorganic scintillator. The difference arises from the fact that the $LaBr_3$ detector requires a dopant, specifically the element cerium, in order to be an effective scintillation material. The BaF_2 material, on the other hand, does not require such a dopant or activator. The origin of the scintillation effect in both materials lies in the energy structure of the electrons in the given material's crystal lattice. The electrons in these materials as well as other insulators and semiconductors have discrete energy values that are allowed, determined by quantum mechanics. A lower group of energies known as the valence band corresponds to electrons that are bound to nuclei at specific locations in the crystal lattice. A higher group of electron energies known as the conduction band corresponds to electrons that diffuse freely through the lattice. Electron energies do not exist between the valence and conduction bands. Because of this discrete structure only certain energy transitions are available [14]. Since scintillation photons are produced at electron energy transitions it follows that the frequency and energy of photons produced by a specific scintillator are limited. The frequency of a scintillation photon is related to the energy difference in the electronic transition by the formula $E = h\nu$ where h is Planck's constant.

Gamma rays lose energy in a scintillator primarily through two interactions, photoelectric absorption and Compton scattering. Pair production, essentially the opposite of annihilation, is rare compared to the other interactions for energies just above 1 MeV and for lower Z materials such as those used in this work. In photoelectric absorption, a gamma ray is absorbed by an atom and an atomic electron is ejected with energy equal to the difference of the gamma ray energy and the binding energy of the electron. For the Compton effect, a

gamma ray has an interaction or collision with an individual electron imparting some of its energy to the electron based on the conservation of energy and momentum. If a struck electron was already in the conduction band of the material it would simply gain more energy and begin to transfer that energy to other electrons. If the original struck electron was in the valence band, however, then it would be stripped from its lattice position creating an electron hole and would have energy equal to the difference of the energy imparted from the interaction and the binding energy of the electron. The high-energy electrons slow down in the material through Coulombic interactions with other electrons, creating more electron-hole pairs. As electrons from the conduction band fall into these holes scintillation light is given off [14]. A simplified diagram of the scintillation process is shown below in Figure 2.4.

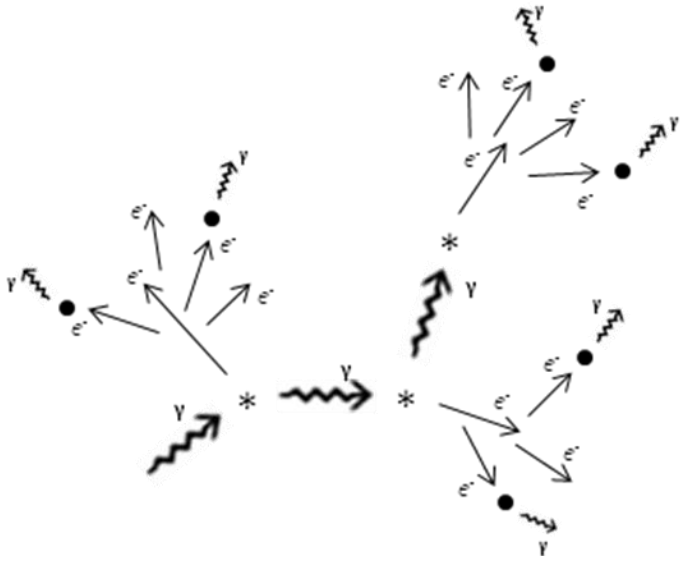

Figure 2.4. Illustration of the scintillation process showing a high-energy gamma ray represented by a large wavy arrow causing many subsequent interactions. An asterisk either represents a Compton scattering where the gamma ray loses some energy and imparts it to an electron, or a photoelectric absorption. After such absorption the gamma ray no longer exists and a single electron is liberated. Both effects create a high-energy electron that then creates secondary electrons and electron holes. Eventually an electron will fall into a hole represented by a small filled circle, giving off a low-energy scintillation photon represented by a small wavy arrow.

The diagram shows Compton interactions, photoelectric absorption, secondary electrons, and scintillation photons created when an electron falls into a hole represented in the figure by a filled black circle. An undesirable effect in scintillators occurs when scintillation photons are reabsorbed in the material. This can occur because it takes roughly the same amount of energy to create an electron-hole pair in a pure crystal as is liberated when an electron recombines with the hole. This results in significant self-absorption of scintillation light which reduces the amount of signal collected by the photomultiplier tube. A dopant, or activator, can reduce this problem by adding its own different allowed energy levels to the structure as seen in Figure 2.5.

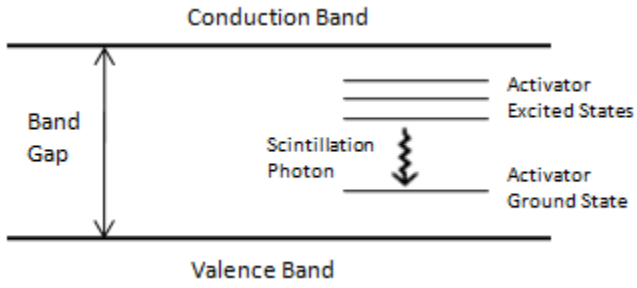

Figure 2.5. Illustration of the atomic energy structure in an activated scintillator material. The material itself has a valence band energy corresponding to electrons bound to a positive ion, and a conduction band representing electrons that are free to diffuse about the lattice. When an activator or dopant is present, its energy levels are added to the system and can improve the performance of the scintillator.

If the activator's energy levels fall between the conduction and valence bands of the pure crystal then transitions between activator excited states and the ground state will be of lower energy and scintillation photons will have a lower frequency that will fall in the visible or near-visible light portion of the electromagnetic spectrum. This increases the proportion of visible light scintillation photons but most importantly these scintillations due to the

activator material will not lie in an energy range that can be absorbed by the pure crystal structure. As a result the doped scintillator produces a useful visible light scintillation with low self-absorption [14]. Cerium plays the role of activator in the $LaBr_3$(Ce) scintillation material used in this work.

The BaF_2 material has a fast scintillation component with shorter wavelengths of scintillation photons in the ultraviolet region of the electromagnetic spectrum. Quartz is sensitive to this wavelength so widows of this material are used to couple the BaF_2 detector to its photomultiplier tube [24]. The fast scintillation mechanism is due to the creation of a hole in the outer core band of the ionic crystal and the subsequent combination of this hole with an electron from the valence band. Although this process has a fast transition time, it does not has a low light output due to self-absorption and other effects [14]. The $LaBr_3$(Ce) detector, in contrast, has a high light output due to the activator phenomenon described above.

2.3.2 Theory of the Pulse Shaping Process

Scintillation light is produced as photons lose energy from collisions with electrons in the scintillator or are absorbed by scintillator atoms, and from the subsequent energy deposition of secondary electrons. These electrons are then slowed down continuously as charged particles in a "sea" of charges. This energy loss leads to the excitation of other electrons boosting them up in energy level. When these de-excite, a photon is given off. The energy difference between levels is such that this energy is in the visible or near-visible light portion of the electromagnetic spectrum. Because the BrilLanCe® 380 and BaF_2 materials have a fast decay time, the photons are given off extremely quickly after the entrance and

interaction of the birth (1.27 MeV) or annihilation quanta in the sample. This results in a narrow pulse of light with respect to time known as a fast timing pulse. The pulse enters the photomultiplier tube which converts the visible light photons into low-energy electrons that can be contained and directed through the PMT [14]. A diagram of a PMT is shown below in Figure 2.6.

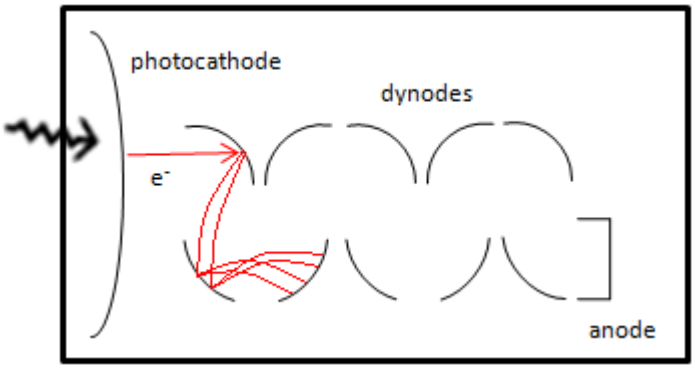

Figure 2.6. Illustration of the Photomultiplier Tube. A scintillation photon enters the tube and liberates an electron from the photocathode. The electron is then guided by subsequent stages of dynodes at high voltage. At each dynode multiple electrons are liberated since the electron is accelerated in the electric fields created by the dynodes, gaining more energy. Final collection of the electron signal occurs at the anode.

After multiple steps of electron signal amplification and acceleration by voltage biased stages, a pulse of electrons with high correspondence to the original light pulse is directed to the anode, or output, of the PMT. Here, the anode collects this pulse of electrons and converts it to a voltage pulse [14]. This process is characterized by the time constant of the anode circuit. For this application, the time constant is chosen to be small (set by the manufacturer) compared to the decay time of the detector material. This results in a voltage pulse with leading edge characterized by the anode time constant. The time constant is shorter than the scintillator material's time constant or decay time, so it is very fast. The tail

of the pulse has an exponential decay behavior with time constant equal to that of the scintillator decay. This means that the pulse tail has the same behavior as the photon pulse tail from the scintillator [14].

The signal coming out of the PMT going to the CFD is thus a fast voltage pulse, defined as a pulse with rise time on the same or lower order of magnitude as its transit time. The PMT pulse is called a linear pulse because its height and width carry information about the detected radiation. In this situation, the pulse specifically carries the timing information about the birth or death of the positron. This linear pulse enters the 583B CFD unit, is accepted if it is in the correct energy range corresponding to the 1.27 MeV gamma energy for one detector and the 511 keV annihilation energy for the other detector. The pulse is then shaped according to the principle of constant fraction discrimination. It is shaped into a bipolar signal where the zero crossing occurs at a specified (constant) fraction of the original pulse height. The fraction used usually varies between 0.1 and 0.2 [14]. For the 583B unit, it is internally set at 0.2 [15]. The time at which this shaped pulse has the zero crossing is then used as the point of reference for the positron event. The time picked off from this pulse shows very little amplitude walk and little timing jitter, so is an accurate time pick-off method. When the signal crosses the zero-crossing, a logic pulse is created and is output by the CFD unit [15]. This signal corresponds to the time of the positron event. The logic pulse is a square wave of standard size and shape and is accepted by the TAC, either at its start input or stop input [1]. The square wave has a very sharp leading edge so that the TAC recognizes the beginning of the signal with extremely good precision [25]. A block diagram of the process is shown below in Figure 2.7.

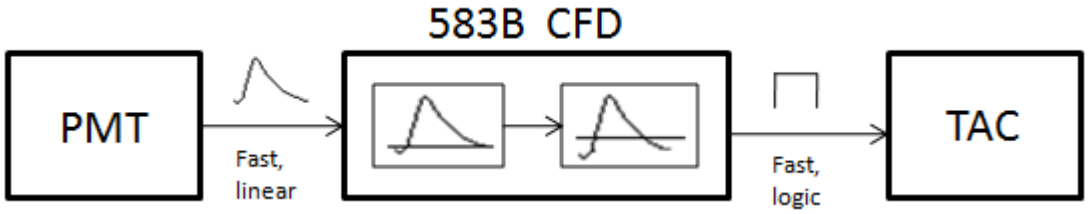

Figure 2.7. Signal chain diagram from the PMT to the TAC. The CFD unit shapes the pulse so that its zero-crossing occurs at the internally set fraction of the pulse amplitude

The 583B unit provides user-adjustable external Constant-Fraction Shaping Delay via inputs for a 50-ohm cable that sets the delay. The shaping delay is optimized through experimentation with the length of the cable used. The delay value must be greater than the time the detector signal takes to reach its maximum amplitude from the triggering fraction of 0.2 [14,26].

For every positron lifetime captured, the TAC creates a pulse with amplitude proportional to the elapsed time between start and stop signals. The maximum allowed time interval between start and stop signals for the TAC 566 unit is set by a control on the unit's front panel [25]. It is important that the maximum time range be small compared to the average spacing between signal pulses. This way the TAC unit is not likely to receive multiple pulses during the maximum time range [14]. The 10 μCi ^{22}Na source meets this criterion using the minimum TAC range allowable, 50 ns. This was the setting for the TAC range used in all PALS experiments and optimization. Based on the ^{22}Na activity there is an average of 0.0165 positrons per 50 ns TAC range. Thus it was unlikely that multiple signals would be received by the TAC during one time range. In general, the TAC can resolve time differences ranging in magnitude from 10 ns to 2 ms [25]. Since the lifetimes involved in PALS are on the order of hundreds of picoseconds, a delay cable was needed in the stop

branch of the PALS system. The delay extended the time difference between start and stop signals to a magnitude the TAC could process.

2.3.3 Pulse and Cable Considerations

The fast nature of the signal to be processed by the PALS chain brings up the important issues of signal reflection, high frequency attenuation, and device impedances which affect signal/voltage attenuation. For a chain of connected components it is desirable for the output impedance of each component to be as low as possible. A low output voltage impedance results in a small voltage drop so the signal is minimally attenuated as it traverses the electronics chain. This is easily visualized with the voltage divider equation below, where Z_O is the output impedance of a component and Z_L is the input impedance (or load) of the next component [14].

$$V_L = V_S \frac{Z_L}{Z_O + Z_L} \tag{2.1}$$

The voltage pulse containing the timing information that reaches the next component in the processing chain is attenuated by the factor on the right hand side of Equation 2.1. It is easily seen that the smaller the output impedance, Z_O, the larger the voltage the next component (V_L) sees, up to a maximum of the original voltage, the source voltage V_S. Thus, if every component in a signal processing chain has a small output impedance compared to the input impedance of the next component then minimal signal attenuation will be achieved [16]. Since this issue is common to all nuclear measurement techniques, industry has designed all standard equipment with this in mind. The Ortec 566 TAC, for instance, has an output

impedance < 1Ω, input impedance >1k Ω [25] and the MCA has an input impedance of about 1 kΩ [27].

Changes in the impedance of various components lead to signal reflection which is more undesirable than signal attenuation. Such reflection can alter the shape of the pulse and not just the amplitude, throwing off the pulse's timing information. This is important to consider in the network of coaxial cables connecting the PALS system components. As a result the problem of reflection involves both the impedances of devices/components used as well as the characteristic impedance of the coaxial cables used to connect the components [14].

The solution is to ensure that all cables are terminated in their own characteristic impedance. The characteristic impedance of a cable is determined by the amount of resistance it provides when being initially charged. If a cable is terminated in its own characteristic impedance, i.e. if the total impedance at the next stage is equal to the characteristic impedance then there are no reflection issues. The current drawn by the cable is constant during the transient charging of the cable and after current is being delivered to the load at the end of the cable. This termination is the effective impedance of the next component in the chain and can be altered if necessary by series or shunt terminators. Most coax cables used in nuclear pulse processing have a 50-ohm characteristic impedance and as a result, the nuclear instrument industry has designed most of the circuits designed for pulse processing to have an effective input impedance of 50 ohms. When all of the circuits and cables have matched impedances then reflections are eliminated. The oscilloscope, for instance, was set to have an input impedance of 50 Ω through an internal setting. Reflection

arises from abrupt changes in impedance and is similar in concept to optical reflection between media of different index of refraction [14]. Thus the coax cables used in this design all have 50-ohm characteristic impedance. Coax cables also have more severe signal attenuation for high frequency components (fast signals) than for lower frequencies, so it is beneficial to use coax cable with better attenuation properties. RG-58C/U coaxial cable is commonly used in nuclear applications. It has a 50-ohm characteristic impedance and has adequate high frequency characteristics [14]. This type of cable was used in the PALS system.

2.4 Timing Theory of the PALS Systems

In the digital PALS system, pulses from the dynode of the PMTs are led directly to the inputs of the oscilloscope and the output of the TAC is also led to the oscilloscope for triggering. Triggering was set up on the oscilloscope such that events were processed and displayed only when the TAC output signal was present. This was accomplished by triggering on the rising edge of the TAC signal at an arbitrary voltage of approximately one volt. The detector part of the system was essentially identical to the analog, and as a result the main theory involved with the digital system relates to the processes and calculations taking place in the oscilloscope: those related to the time pick-off method, the major difference between the analog system that accounts for the improved time resolution of the digital system. The following section prepares this discussion by laying out the sources of the time resolution spreading.

2.4.1 Sources of Spreading in the Time Resolution

The time resolution of the system is the quadrature sum of the various sources of timing uncertainty or spreading. The components that affect the resolution are related to the interaction of radiation in the detector crystal, transit time spread in the PMT, uncertainty inherent in the time pick-off method, and jitter inherent to the oscilloscope or electronics. The following equations show the sources of timing resolution for the digital and analog system [22]:

$$\sigma_{DIGITAL}^{\ 2} = \sigma_L^2 + \sigma_{edge}^2 + \sigma_{TTS}^2 + \sigma_{CF_{dig}}^{\ 2} + \sigma_{scope}^2, \text{ and} \tag{2.2}$$

$$\sigma_{ANALOG}^{\ 2} = \sigma_L^2 + \sigma_{edge}^2 + \sigma_{TTS}^2 + \sigma_{CF}^{\ 2} + \sigma_{elec}^2, \text{ where} \tag{2.3}$$

σ_L = spread of the resolution function caused by variation in optical path length of gamma rays and scintillation lights in detector crystal;

σ_{edge} = spread caused by variation of the shape of the rising edge of the pulse;

σ_{TTS} = spread due to transit time spread of the electrons in PMT;

σ_{CF} = resolution spread due to the Constant Fraction or other time pick-off method used;

σ_{scope} = time jitter of the oscilloscope, < 3ps;

σ_{elec} = spread due to the TAC and MCA electronics chain (insignificant) [22].

The σ in the above equations characterizes the spread of the Gaussian resolution function in terms of its width, where the timing resolution, or FWHM, is 2.35 σ [22].

The first three terms of the right hand side of Equations 2.2 and 2.3 are identical for the analog and digital systems as they depend solely on the detector which is comprised of the crystal and PMT. Of these, the first term represents the timing uncertainty due to optical

path length variation in the crystal. Scintillation light is emitted isotropically in the crystal and in order to increase collection at the PMT the crystal surfaces are made to be diffusely reflective, reflecting the light toward the PMT. As a result, scintillation photons travel different path lengths adding to the spread of the signal [14]. This effect depends on the crystal geometry and is therefore not subject to much control or manipulation. Small crystals were purchased (1" diameter x 1" length) to minimize this effect. Thinner crystals have been used in the literature [9,10,22] but the direct effect of this has not been quantified.

The second term on the right hand side of Equations 2.2 and 2.3 is related both to the uncertainty in the number of photoelectrons emitted from the photocathode of the PMT and the duration of the leading edge of the detector pulse. The more photoelectrons that are produced at the photocathode of the PMT the less the uncertainty in the resolution and the less the fluctuation in pulse shape. Photoelectron production is a statistical process so the more scintillation photons created the more photoelectrons produced, and at large numbers statistical fluctuations exhibit a smaller proportion of the overall number of carriers and thus have less of a deleterious effect on the time resolution [14]. In this regard, the Brillance 380 detectors have an advantage over the BaF_2 detectors since the former have a much larger scintillation light output per keV of energy absorbed. BaF_2 detectors, however, have a faster rise time than Brillance 380 detectors because of the faster decay of excited states in the crystal. The detectors are expected to have similar timing resolution characteristics based on the tradeoff between these two factors, although the $LaBr_3$ is expected to be somewhat better. The duration of the rising edge is also dependent on the type of photomultiplier used. The

XP2020/Q PMT has a typical quoted rise time of 1.5 ns and a Hamamatsu H3378 (R2083Q) has a rise time of 0.7 ns, while the XP20D0 is 1.5 ns [16,17,24].

The third term on the RHS of Equations 2.2 and 2.3 represents the transit time spread of the electrons as they traverse the PMT. Photons entering the PMT liberate electrons at the photocathode. These electrons and subsequent electrons from the stages travel slightly different paths than one another and so the signal is spread because of this. Stray magnetic fields and even the earth's field also can contribute to the spreading due to the magnetic alteration of the electron paths. Much of the recent setups seeking to reduce the time resolution of PALS systems utilize Helmholtz coils to cancel any magnetic fields in the vicinity of the PMTs. This reduces the transit time spread in the tubes but its effect has not been known to be isolated and characterized in the literature. Magnetic shielding of the tubes has also been used in the literature but Helmholtz coils are reported to be superior [28].

The fourth term in Equations 2.2 and 2.3 is the timing uncertainty due to the CF method used. This represents the major advantage of the digital implementation and the cause of the reduction of the digital timing resolution compared to the analog timing resolution reported by Becvar et al. Becvar and his coworkers reported that their digital method was superior to the otherwise identical analog method based on Monte Carlo simulations but provided little detail or reasoning [9]. In this work, the digital method proved superior mostly because the constant fraction percentage used was optimized from the built-in 20% value inherent to the CFD hardware. Other factors such as rejection of spurious pulses and energy/voltage criteria similar to setting energy windows with an SCA were not as fruitful for the time resolution, as discussed later.

2.4.2 Time Pickoff Methods

Time measurement techniques necessary for experimental procedures such as PALS rely on a method to identify the time of occurrence of an input linear pulse. In an analog system this is done by time pick-off units, such as a CFD, and the method relies upon the generation of a logic pulse whose leading edge indicates the time of occurrence of the linear pulse. For a digital system time pick-off can occur on the digitized linear pulses themselves. Uncertainty in timing derives from noise in the pulses, shape fluctuation, and amplitude fluctuation between pulses. Uncertainty in timing from pulses with stable amplitude is called jitter and involves noise or shape variations. Amplitude variation that contributes to timing uncertainty is known as walk. The underlying cause of jitter in the system is noise inherent in the detector and PMT system as well as shape variations caused by the discrete number of scintillation photons (information carriers) created by the system. Although the $LaBr_3$ detector creates 35 times more scintillation photons per unit of energy deposited than BaF_2 these shape variations are still an important factor since scintillation counters create few carriers compared to other types of detectors [14].

Different methods of time pick-off have contrasting strengths and weaknesses with respect to the types of uncertainty. Because of this, a separate term for the contribution of the time pick-off method to the time resolution was included in Equations 2.2 and 2.3 in Section 2.4.1. Common forms of timing include leading edge, crossover, amplitude and rise time compensated, and finally constant fraction timing. Leading edge timing is the simplest method, in which the time of occurrence of the pulse is defined as the moment it reaches a particular set voltage. This method is especially prone to both amplitude walk and time jitter.

As such it serves as an excellent visual illustration of the two processes, as seen in Figure 2.8. Signals identical in all respects except for the presence of random noise will show a considerable difference between time pick-off instances as a result of the signal fluctuation. Amplitude and/or rise time variation between pulses also causes significant skew in timing of otherwise identical signals as the following figures indicate [14].

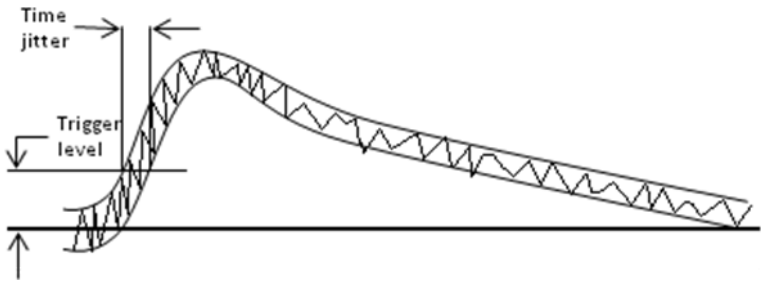

Figure 2.8. Time jitter due to signal noise. For a fixed trigger level the instance of time pickoff can occur almost anywhere within the envelope that bounds the noisiness of the curve.

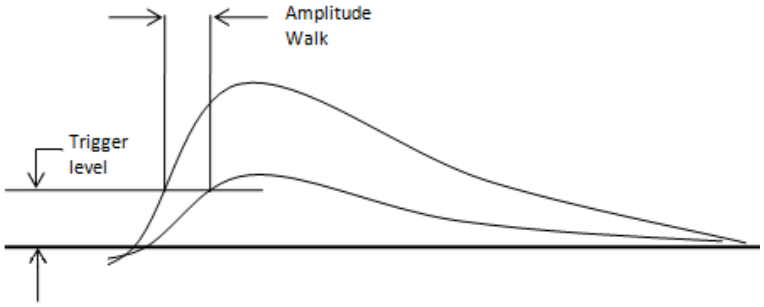

Figure 2.9. Amplitude walk due to varying pulse amplitude**.** The potentially significant difference in the pickoff time at a constant voltage level for two pulses with similar shape but different amplitude is easily seen.

Figure 2.8 shows a noisy pulse enclosed by an envelope roughly bounding the noise. For a set trigger level (equivalent to leading edge timing), the time pickoff can occur anywhere in the range of the envelope at that level causing a time jitter shown in the figure. Figure 2.9 illustrates two pulses with similar shape but different amplitude. For a set trigger

level there is a different pick-off time for each pulse as seen in the figure, and the amplitude walk is the difference in these times.

Crossover timing can be useful for pulses that are bipolar in shape. This technique registers the time pick-off at the instance the signal crosses the baseline voltage of the pulse. It has been shown in some situations to reduce walk in bipolar signals with significant amplitude variation. The constant fraction method, like the leading edge method, determines the time coordinate of the pulse when it crosses a certain voltage threshold. Instead of a constant threshold, however, it is set to be a constant *fraction* of the pulse amplitude. Thus the trigger point is independent of pulse amplitude for signals with little shape variation. The constant fraction method is the standard in scintillation counting applications involving timing. The electronic implementation of the constant fraction method requires manipulation and transformation of the signal into a bipolar pulse. The input pulse is multiplied by the constant fraction value (i.e. 20%) hardwired into the unit creating an attenuated signal. The original signal is inverted and delayed by an amount of time set by the experimenter. This signal is added to the attenuated signal creating a signal where the zero crossing corresponds to a constant fraction of the pulse height [14].

With the digital oscilloscope the time pickoff method was carried out via an algorithm written in Matlab. In order to implement the constant fraction method the algorithm measures the amplitude of the pulse and finds the time at a given fraction of the pulse amplitude. No pulse processing with electronics was required on the pulse to the oscilloscope. The pulses created in the PALS system showed variation in the rise time from pulse to pulse. Because of this a new rise-time modified constant fraction method was

attempted which tried to take into account the effect of the rise time variation in the pulses. It was realized that pulses exhibiting the same amplitude and originating at the same time would yield different pick-off times if their rise times differed as shown in Figure 2.10 below.

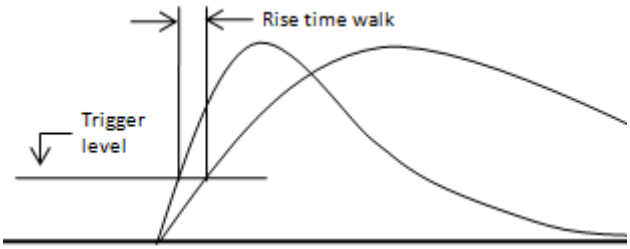

Figure 2.10. Illustration of rise time walk due to rise time variation. The pulses have the same amplitude but different rise time and as a result the pickoff time for each pulse is different. This difference is the rise time walk.

The pulses in the figure above have essentially the same amplitude but each take a different amount of time to reach its full value. A rise time modified constant fraction (RTMCF) method was created to try to compensate for such behavior by calculating the rise time of each pulse and adjusting the constant fraction percentage to decrease the walk. This was explored in this work but proved less effective than optimized CF timing.

Chapter 3
Performance and Optimization

Four variations on a PALS system were tested to find which had the best timing resolution – the two different detectors, $LaBr_3$ and BaF_2, and two different system types, analog and digital. Each detector with its PMT was first tested to ensure proper functionality and adherence to quoted energy resolution specifications provided by the manufacturers. For the analog versions, each detector setup was tested separately and ran at the optimal high voltage for the PMT with optimized CFD settings found by experimentation. The functioning of the digital timing algorithm was verified by performing timing measurements on split identical outputs from a pulser, and then from a single detector. With identical pulses the actual time difference is known to be zero, so the algorithm's results provide a check on its functionality and a measure of the inherent spread in timing. Optimization of the timing resolution with Co-60 was performed on the digital system for different timing methods and constant fraction percentages, and also based on rejecting pulses with spurious behavior or characteristics that fell outside of the norm. Co-60 was used because it emits a 1.17 MeV gamma in coincidence with a 1.33 MeV gamma, thus serving as a convenient measure of the spectrometer's response to coincident events.

3.1 Initial Testing of Detectors and Equipment

Prior to shipment, each detector was tested by the manufacturer for its proper operation and its energy resolution for the Cs-137 662 keV full energy peak. Each detector

came with a sheet detailing the energy resolution for a given operating voltage. Upon receipt, the two $LaBr_3$ detectors obtained from Saint Gobain Crystals were tested with a small Cs-137 source and high voltage supply of -750 volts, the same voltage the manufacturer had tested them at. The detectors had an energy resolution of 2.8% and 2.9%, defined by the ratio of the FWHM of the full energy peak (in channels) to the channel number at the center of the full energy peak. These values matched the manufacturer specifications, and similarly, the BaF_2 detectors also matched the manufacturer specifications of 9.2% energy resolution on the Cs-137 full energy peak. To perform this energy spectroscopy, the output of the detector (anode) was connected to an Ortec 671 Spectroscopy Amplifier and its output was connected to the computer-based MCA as seen in Figure 3.1.

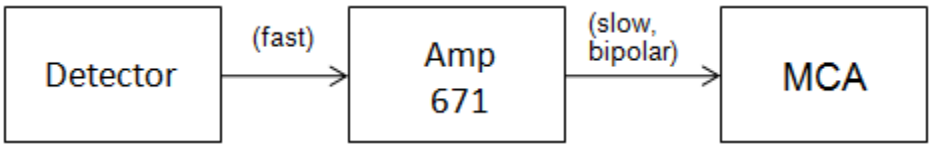

Figure 3.1. Hardware configuration used to test the detector energy resolution. The detector pulse amplitude was too small to be directly led to the MCA so it had to be amplified first.

The amplifier was needed to increase the voltage to a level detectable by the MCA. The amplifier shapes the fast detector pulse into a longer slower pulse on the order of a 2 μs rise time with the stable and accurate pulse height needed for pulse height discrimination [29]. The energy resolution results for the new Brillance 380 detectors are shown below, in Figures 3.2 and 3.3.

The voltages used above were not optimal for timing resolution – they were set at typical voltages for energy resolution applications. Generally speaking, the higher the

voltage a PMT is operated at the better the timing performance since the electrons are accelerated more, thus minimizing the effect of initial path length differences after the photocathode. The BaF_2 detectors were operated at -2500 V, the maximum safe operating voltage specified by the manufacturer/designer [17]. The maximum voltage for the $LaBr_3$ detectors was -2000 V but it was found that the detector functioned poorly at this level, as all energy spectra collected at this voltage were unrecognizable due to pulse saturation [16].

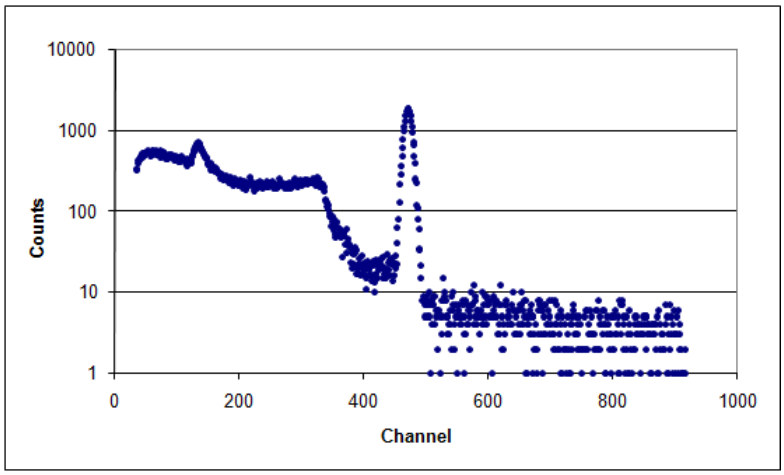

Figure 3.2. Cs-137 energy spectrum from Brillance 380 detector

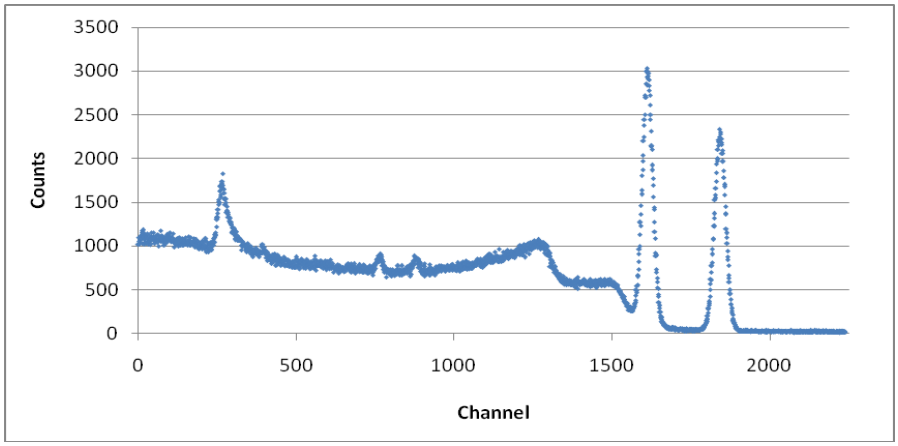

Figure 3.3. Co-60 energy spectrum from Brillance 380 detector

As a test of the optimal operating voltage, the energy resolution and pulse rise time was investigated for a range of voltages up to the maximum allowable. The pulse rise time was determined from viewing on the digital oscilloscope and from the built-in rise time function that measures the rise time on the oscilloscope. Rise time values were histogrammed, noting the most common value and the range of values. For the BaF_2 detectors rise time improved as voltage increased and the energy resolution remained stable. The maximum operating voltage of -2500 V resulted in the best rise time, and was used for PALS testing as reported in all the literature utilizing BaF_2 detectors [22,28]. The $LaBr_3$ detectors showed a similar trend but at voltages above -1500 V the quality of the energy response function drastically diminished. Rise time results for the $LaBr_3$ detectors are shown below.

Table 3.1: Detector Pulse Rise Time for Different PMT Operating Voltages

Voltage (V)	**Rise Time (ns) [Most common]**	**Rise Time (ns) [Range]**
-750	4.8	3.2-6.0
-1000	4.6	3.5-4.6
-1250	3.5	3.4-3.7
-1500	3.4	3.3-3.6
-2000	2.9	2.7-3.1

The optimal voltage for the $LaBr_3$ detectors was found to be -1500 V based on the combination of the rise time and quality of the energy spectrum.

3.2 Analog PALS Optimization

The analog system was set up as in Figure 2.1, with the detectors connected to the CFD-TAC-MCA analog electronics chain. The only difference from the setup shown in the

figure was that a Co-60 source was used in place of the source/sample sandwich which is used for actual PALS measurements. Since Co-60 emits two high energy gammas in coincidence it serves as an approximation of the inherent timing resolution of the system. Thus initial tests and attempts to optimize the timing resolution focused on using the Co-60 source.

There are two main electronic features that can be used to improve the time resolution: the energy window/SCA settings on the CFDs, and the optimization of the CFD settings related to the constant fraction timing pick-off. In the first case, the narrower the CFD energy windows are set around the 1.17 and 1.33 MeV energy peaks, the better the resolution. The improvement in time resolution from this is limited, however, and also comes at the cost of decreased count rate since as the energy windows are set more narrowly more of the broadened full energy peak is rejected. Setting the energy windows involves experimentally determining the SCA settings on the CFDs as set by the discrimination threshold potentiometers. The potentiometers, one setting the upper limit discrimination threshold and one setting the lower limit, define for each discriminator the range of pulse heights and thus energies that the CFDs accept [15].

A way to monitor the energy spectrum in real time as the SCA settings were varied was necessary since the conversion between energy and the potentiometer voltage setting is not generally known. To do this, the configuration shown in Figure 3.4 below was used. Both the anode and dynode outputs of a given detector were used to provide a pulse to the CFD for discrimination and a pulse to the MCA through the amplifier. The amplified pulse contains the pulse amplitude information in a range the MCA could accept and process,

while the timing pulse from the discriminator was sent to a gate/delay generator, the output of which was led to the gating input of the MCA. The discriminator produces an output pulse only when the pulse from the detector fell between the voltage range set by the discrimination levels. The resulting output is a fast logic pulse which activates the gate/delay generator. This then outputs a square wave serving as the gating signal for the MCA, and is delayed by the proper time so that it overlaps with the pulse going to the MCA from the amplifier. The overlap is assured by viewing both pulses on an oscilloscope and adjusting the delay on the gate/delay generator. Once accomplished, this ensures that the MCA only accepts pulses from the detector that meet the energy range set in the CFD. The delay is needed because the chain with the amplifier is a slow chain (i.e. a slow pulse is produced after the amplifier) and the chain leading to the gate/delay generator is fast.

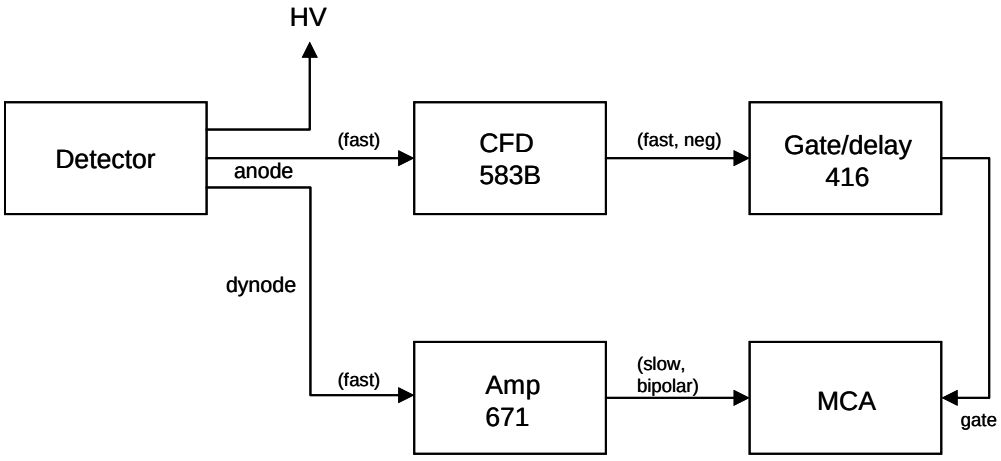

Figure 3.4. System setup for setting the discriminator energy windows. This setup is used for each discriminator, and allows the changes in the energy spectrum to be viewed on the MCA as the discriminator settings are varied.

With this configuration, all pulses making up the energy spectrum of the Co-60 source were sent to the CFD but only the ones corresponding to the range selected at the

CFD were displayed on the MCA. This made it an easy matter to adjust the discrimination settings until only the desired portion of the energy spectrum was observed on the MCA, for example just the 1.17 MeV peak. In this way, one detector could be set to accept pulses belonging to the 1.17 MeV full energy peak and the other set to the 1.33 MeV peak.

Once this was set up, the next step was to optimize the timing portion of the CFD. As discussed previously, the CFD takes an attenuated version of the signal and adds to it a delayed and inverted version of the signal in order to produce a bipolar pulse with zero crossing at a fixed constant fraction of the original pulse's amplitude. In order to do this the delay must be greater than the rise time of the pulse but must not be too large. The delay is determined by the length of cable connecting the two BNC connections on the CFD labeled *cable delay*. The optimal length must be found by experimentation by using different lengths of cable [15]. For each cable length the delayed coincidence spectrum of the Co-60 source was recorded and saved in the MCA. Its FWHM was then determined within the Maestro program and confirmed by fitting the spectrum to a Gaussian using the statistics program *SigmaPlot*.

Different lengths of cable were made by cutting cable and adding crimp-on BNC connectors with a crimping tool. This is one aspect of the optimization that is very time consuming and is not needed for the digital system. The Ortec operating manual for the CFDs suggested an initial guess of delay time equal to 0.7 ns plus a factor of 1.1 times the 10% to 90% rise time of the pulse [15]. For the BaF_2 detectors a rise time of 2.7 ns was common, and so by this formula a delay time of 3.67 ns was necessary. The signal propagation speed in the RG-58C/U coaxial cable was 0.659c, where c is the speed of light in

vacuum [14]. Performing the conversion for the length of cable needed to create this delay time resulted in 28.5 inches. The first coaxial cable made was 28.6 inches in length. Lengths surrounding this value were tested for both detector types, plotted against timing resolution as measured by FWHM, then data points were filled in as necessary by additional testing. The results for the BaF_2 detectors are shown below in Figure 3.5.

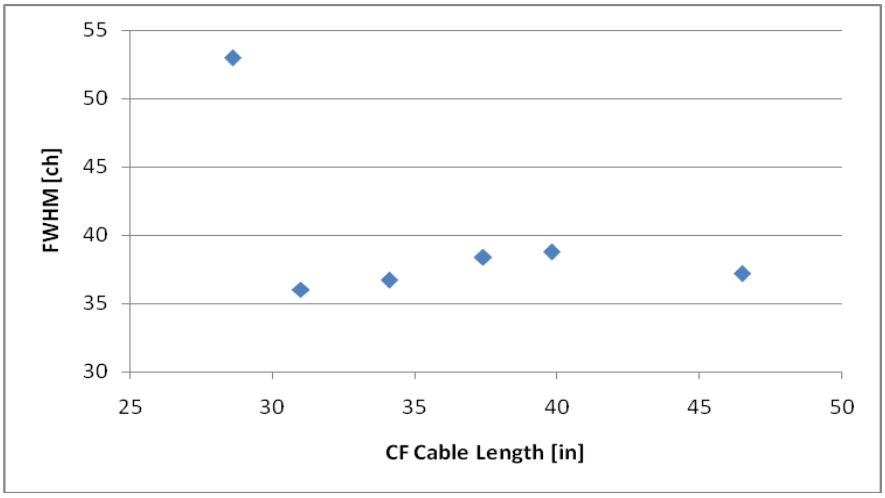

Figure 3.5. Time resolution versus constant fraction cable length for the BaF_2 detectors.

Values of the FWHM varied by tens of picoseconds for lengths within a few inches of the optimal value but were off by 50% or more at shorter lengths that did not produce the minimum delay needed to carry out the constant fraction method. The best timing resolution was found at 32 inches and this length of cable was used for the cable delays on the CFDs for the BaF_2 detectors.

The coincidence count rate for the analog system with energy windows set around the individual peaks was only 0.5 to 1 counts per second. Five thousands counts were collected for each cable length tested. The time resolutions achieved for the optimized system were 210 ps and 192 ps for the BaF_2 and $LaBr_3$ detectors, respectively.

3.3 Digital PALS System

3.3.1 Oscilloscope setup

The digital system was also tested and optimized using the Co-60 source and the $LaBr_3$ detectors. The signal from the TAC in channel 3 of the oscilloscope was used as the trigger for coincident events. The TAC signal and the detector pulses were separated in time by about two nanoseconds on the oscilloscope display. The time scale was adjusted to 50 ns, which is 5 ns per division with a total of 10 divisions shown on the scope, and the signals shifted so that both would remain on the screen. This was important for the use of the timing algorithm because the scope would only process what was on the screen. In doing this, the entire detector pulse was easily seen on the scope as well as significant portions of the pulse baseline before and after the pulse. The above setup was needed to perform pulse rejection based on spurious pulses and on the pulse baseline, such as the baseline mean or rms value over a user-defined range.

Upon setting up the proper time scale, the TAC channel display was turned off to improve the sampling rate, since the scope samples at 10 GHz for 2 channels displayed or 5 GHz for three or four channels displayed. At 10 GHz sampling rate, the waveforms on the scope consisted of points at 100 ps intervals with the option of interpolation between points. Linear and sinx/x interpolation were standard options and cubic interpolation was available with the XMATH package [23]. A cubic interpolation script was also written in Matlab for comparison purposes and for use before the XMATH package was purchased. Their performance in terms of timing was identical, although the Matlab interpolation resulted in a greater dead time or decreased throughput rate for processing events since it involved

communication between different computer programs. Cubic interpolation was found to yield better performance than sinx/x interpolation and linear interpolation, which agrees well with the prevalence of cubic interpolation found in the literature [9-10].

Interpolation was used to obtain more points on the leading edge of the pulse in order to perform more accurate timing calculations. With a non-interpolated 100 ps/pt sampling rate, for instance, it would be difficult to pinpoint the time at which a constant fraction of the pulse voltage occurs. Cubic interpolation by a factor of 20 was used to produce a voltage data point every five picoseconds. At this frequency of data points, the time pickoff of the constant fraction could be off by a maximum of 2.5 picoseconds. For example, if the pulse amplitude was 2.0 volts and the baseline was at zero volts, then the 20% constant fraction level would be 0.4 volts. With a 100 ps/pt data frequency, there might only be 20 data points on the curve, and the seventh point could have a voltage of 0.35 volts and the eighth point could have a voltage of 0.44 volts. Thus if the seventh or eighth point was used as the time pickoff, this time would be off by about 50 ps, or half of the sampling interval. For one data point per 5 picoseconds, the points surrounding the constant fraction value are guaranteed to be less than 2.5 picoseconds off the time at the constant fraction value.

In addition to data interpolation, the scope could also perform data smoothing. The pulse waveforms without smoothing were noisy, leading to timing jitter. The scope's built in math function called *eres*, Enhanced Resolution, uses a process similar to a digital moving average filter to smooth out noise in the signal. The choices for smoothing were 1, 1.5, 2, 2.5, and 3 bit enhanced resolution filtering. At 2.5 and especially 3 bit filtering some pulse amplitude attenuation was visible due to high frequency attenuation from the frequency

response of the digital filter. Experimentation showed that 2.5 bit filtering was optimal, followed by 3 bit filtering. Data smoothing was also an important part of all other work involving a digital PALS system [9,10,22].

3.3.2 Testing of Constant Fraction Algorithm

In order to test the basic functioning and legitimacy of the constant fraction algorithm it was used to calculate the delayed coincidence spectrum for a series of pulses derived from the split output first of a pulser and second of a single detector. A total of three tests were performed. The output of an Ortec Model 480 pulser was split with a standard tee and led to the inputs of the oscilloscope. Since both channels were receiving identical inputs there would be no time resolution spreading due to pulse shape variations or amplitude variations as there was with the Co-60 source, even though with the Co-60 source it is known that both gammas are given off in coincidence. A second test used the output of a single $LaBr_3$ detector, similarly split with a tee and led to the inputs of the oscilloscope. In this test the CFD energy windows were set narrowly so that there was very little amplitude variation between pulse sets. In the third test, the CFD energy windows were wide open such that pulse sets showed significant variation in pulse amplitude. For each of these tests various types of timing were tested using the digital algorithm program: different constant fraction percentages and leading edge timing based on time pick-off at a set voltage instead of at a constant fraction of the pulse amplitude. Each of these was also performed for different levels of smoothing with the Enhanced Resolution feature of the oscilloscope. These tests were performed in real-time on the scope since the output from the pulser and single detector was of sufficient frequency that each test could be performed in a short period of time. In

these tests, the time difference between the pulses was measured by the time pick-off method and histogrammed. Each test was performed until 10,000 counts were collected. The results were plotted and the FWHM determined.

Constant fraction timing performed similarly to leading edge timing which was expected because leading edge timing is excellent when there is no pulse shape variation and little amplitude variation, such as with identical split signals [14]. Results were similar for the tests from the single detector and for the detector with amplitude variation. The latter showed a worsening in the time resolution that was expected because of the greater amplitudes and variations in shape across these. A summary of the testing results is shown below in Figure 3.6.

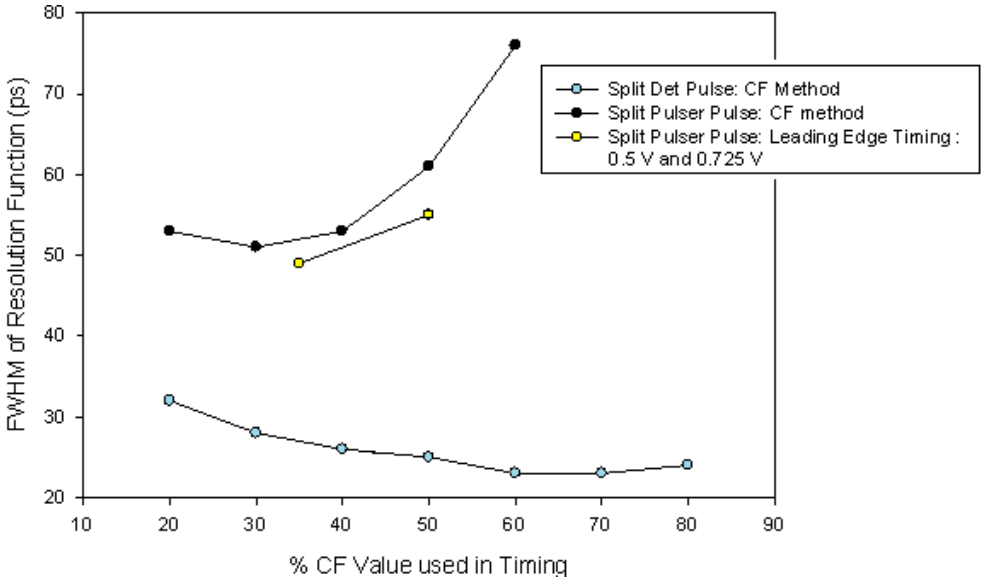

Figure 3.6. Results of tests to determine the timing resolution of the digital system and algorithm for split pulser and detector pulses

The split detector pulses had the best resolution because they were the fastest pulses, while the pulser produced a much slower pulse on the order of microseconds instead of

nanoseconds. The low timing resolution achieved shows that the digital timing algorithm functions properly.

3.3.3 Optimization of the PALS System for Co-60 Coincidences

Although the tests in the previous section showed that the digital algorithm functioned properly it did not necessarily follow that the same values and settings that produced the optimal timing resolution on the split pulses would be appropriate for the system measuring the Co-60 delayed coincidence spectrum or for the PALS experiment with ^{22}Na. In order to address this, the digital PALS system was optimized using sets of pulses from the Co-60 source that were saved to the oscilloscope for analysis and testing. Two sets of 10,000 pulse pairs were saved for each detector type. One set using the $LaBr_3$ detectors was run with PMTs supplying a high voltage of -1500 V and another of -1600 V. Both BaF_2 sets were obtained running the PMTs at -2500 V. In all cases, one CFD was set to accept pulses from the 1.17 MeV full energy peak and the other CFD was set to accept pulses from the 1.33 MeV full energy peak.

Cubic interpolation and digital smoothing were applied in real-time to the digitized pulses on the oscilloscope before the pulses were saved to the hard drive. The data was interpolated by a factor of 20 to produce a data point every 5 ps, and the smoothing was implemented using the 2.5 bit enhanced resolution feature.

The four sets of 10,000 pair pulses were saved to the oscilloscope and the timing algorithm applied offline, as post-processing. It took about three hours to collect this number of pulses. By saving the four sets of pulses to the hard drive, any number of timing methods and constant fraction percentages could be implemented on the same set of data. Performing

the timing online would require the collection of 10,000 pulse pair for each change in the timing algorithm, while offline processing only took about 10 minutes. Offline processing on unchanging sets of data also increased confidence that differences in timing performance were due to the changes in timing parameters and not any experimental differences that might have arisen over the course of the testing, such as an inadvertent movement of the detectors or source.

The effect of the constant fraction percentage on the timing resolution was tested first, followed by the effect of selective pulse rejection, as described later. Pulses from the detectors were all bipolar in shape, with a small falling edge to the minimum voltage then the rising edge to the maximum voltage. Constant fraction timing was optimal on the rising edge of the pulses for both detector types, and results of the constant fraction testing are shown below in Figures 3.7 and 3.8 for the $LaBr_3$ detectors and BaF_2 detectors, respectively.

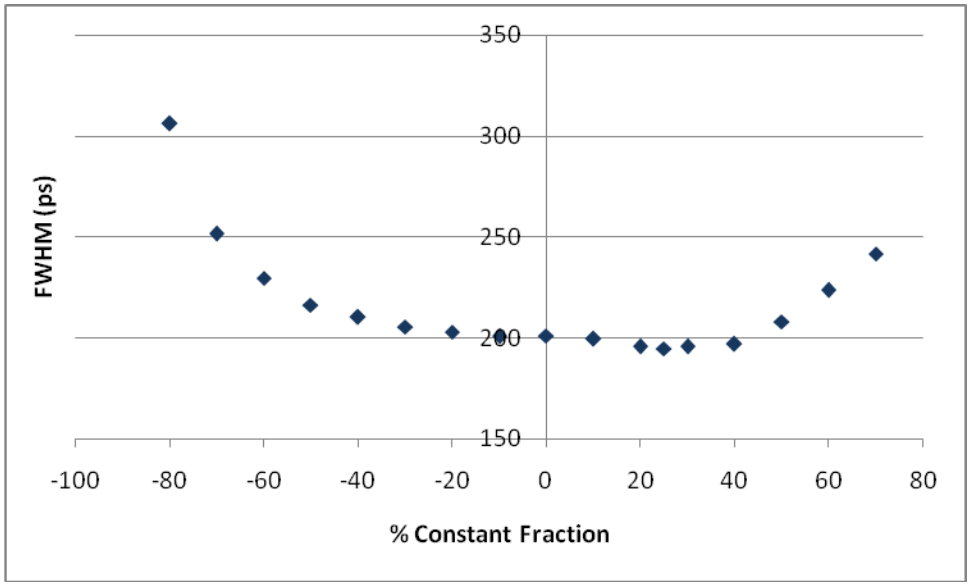

Figure 3.7. Optimization of the $LaBr_3$ timing resolution based on the constant fraction value used for timing. Negative values of the constant fraction correspond to the falling edge of the pulse while positive values correspond to the rising edge.

As seen in Figure 3.7, the optimal constant fraction for the $LaBr_3$ detectors was at 25% of the height of the rising edge. The independent axis in the figure shows positive and negative constant fraction percentages. The negative values pertain to timing on the falling edge of the pulse while the positive values pertain to timing on the rising edge. The best timing resolution was obtained at a constant fraction of 25%, with a resolution of 194 ps. The timing resolution for the BaF_2 detectors was optimal at the minimum of the pulse, or 0% constant fraction measured from the rising edge. Figure 3.8 shows the constant fraction in the same way as Figure 3.7, with negative values corresponding to the falling edge and positive to the rising edge. The optimal timing resolution was 182 ps compared to the analog resolution of 210 ps.

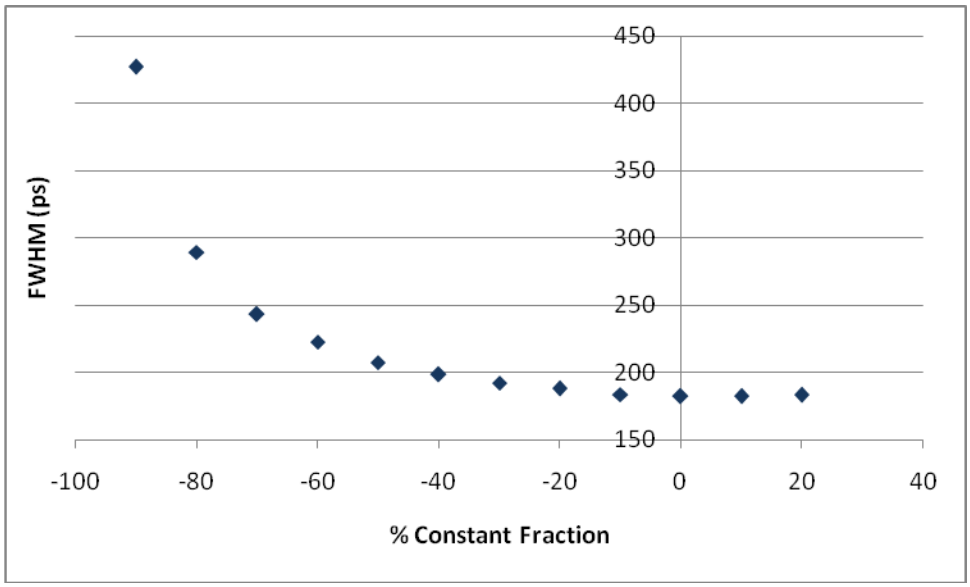

Figure 3.8. Optimization of the BaF_2 timing resolution based on the constant fraction value used for pulse timing

Furthermore, it was observed that some pulses exhibited spurious behavior; such pulses were not even visually recognizable as pulses deriving from the absorption of Co-60 gamma rays, as the voltage baseline and pulse shape were completely off. Another spurious

case occurred when both pulses had reasonable shape but one pulse was shifted in time on the order of a few nanoseconds. This cannot be due to a scattering event between detectors or other nearby materials because the transit time corresponding to a distance traveled in 1 to 3 ns is approximately 30 cm to 100 cm, which is much larger than the detector spacing. Since this is not feasible it is concluded that this time shift is due to a chance coincidence from an unrelated pulse. Examples of both types of spurious pulses are shown below in Figure 3.9 for 5000 pulses saved from a $LaBr_3$ detector with energy windows set to 1.33 MeV corresponding to one of the Co-60 gamma rays. Most of the pulses seen fall within a common range of time and voltage, but some are shifted with respect to time, voltage, both time and voltage, or are completely spurious.

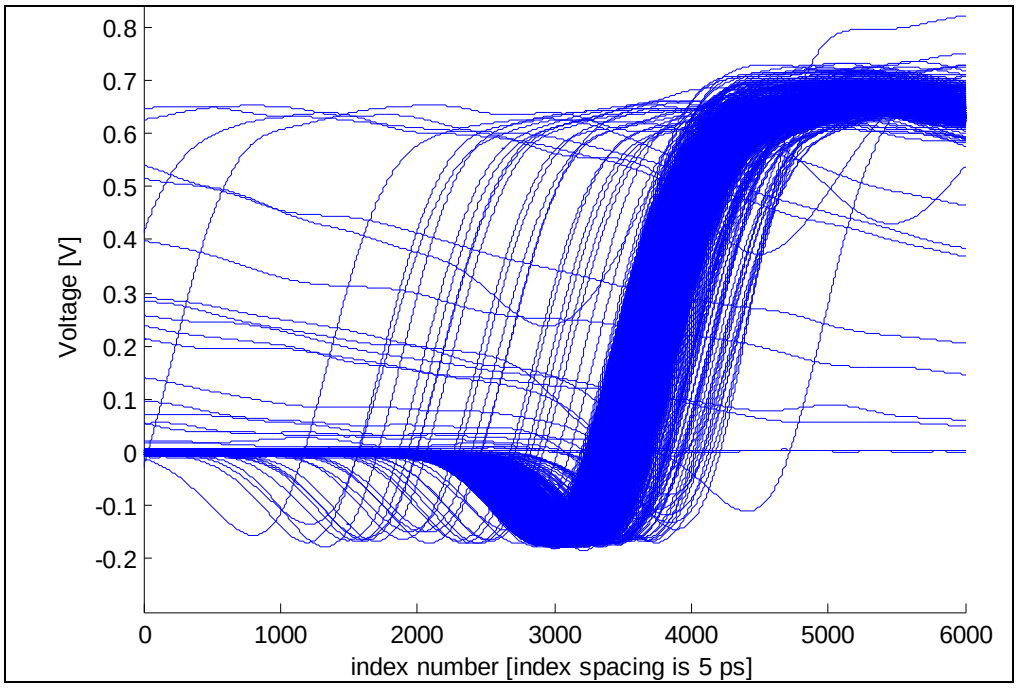

Figure 3.9. Pulses from the $LaBr_3$ detector with a Co-60 source

Another deviation from normal pulse behavior that was observed on the oscilloscope was the occurrence of a drift in the baseline voltage value in a span of nanoseconds before

the leading edge of the pulse. Such a drift could change the slope, shape, or rise time of the pulse somewhat, possibly leading to an addition timing spread. As a result of these observations it seemed logical to filter out pulses based on criteria related to the pulse amplitude, baseline voltage, maximum and minimum voltage, and time occurrence of the pulse minimum or maximum. Becvar et al. had implemented a similar filtering scheme in their digital timing algorithm [9]. Two measures of the drift in voltage over a given region are the mean of the baseline and the root mean square (rms) defined as

$$V_{rms} = \sqrt{\frac{1}{b-a}\sum_{i=a}^{b} V_i^2} \quad , \tag{3.1}$$

where a is the first data point in the region of interest and b is the last, and V_i is the voltage at each data point i.

The timing algorithm was modified to calculate the baseline mean and rms and to display them on the scope in order to observe typical and atypical values. This however, was not very robust, so another method was needed. The oscilloscope had the ability to save pulses to the hard drive whenever it was triggered, so this provided the means to perform a large series of tests all on one set of data at a time. Sets of 10,000 pair pulses were saved for each detector type.

A Matlab code (.m file), shown in Appendix A, was written to calculate and histogram the various baseline parameters, voltage maxima and minima, and time of occurrence of the voltage maxima and minima for each of the saved pair pulses. The baseline parameters calculated were the baseline RMS value, the baseline mean value (voltage offset) and the difference between the baseline RMS value and the absolute value of

the mean, i.e. RMS - |mean|. The latter was chosen because it was observed that this quantity was small and usually showed little variation such that the difference between the two terms was usually less than 0.2 mV but occasionally as high as 1 mV. Examples of histograms are shown below in Figures 3.10 and 3.11 showing the distributions of minimum pulse voltage and time of occurrence of the minimum, respectively.

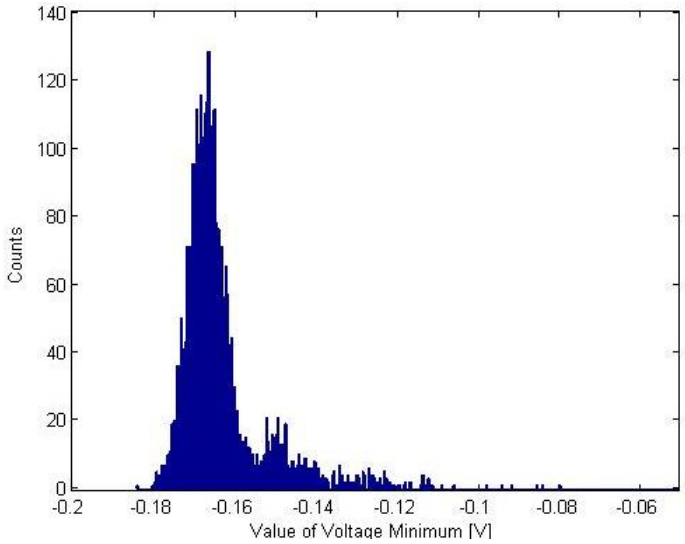

Figure 3.10. Distribution of the $LaBr_3$ detector pulse minimum voltage

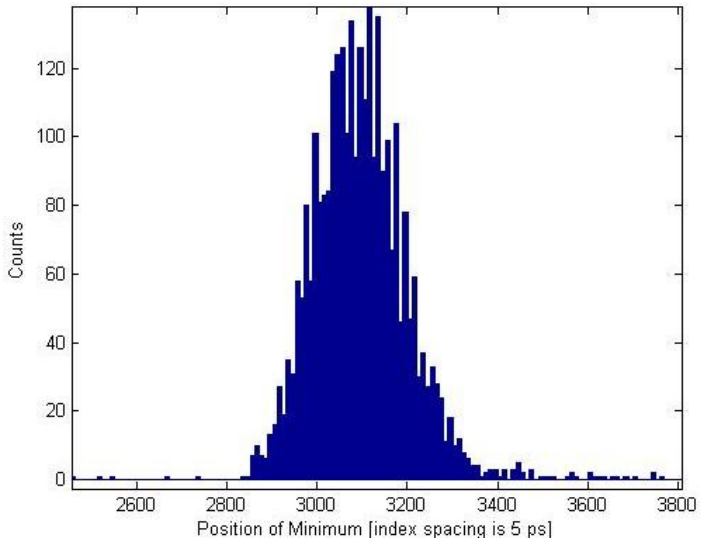

3.11. Distribution of the $LaBr_3$ detector pulse minima time of occurrence

The histograms provided a solid basis for the choice of a specific range of values to accept and conversely a range of values to reject the pulses. The time difference for rejected pulse pairs was not calculated and thus they were removed from the calculation. In the Matlab code this was accomplished by creating an upper and lower limit for each criteria based on the histogram, and checking if each pulse in the pulse pair met the criteria. If they did meet the criteria, the logical expression would be true and the program would calculate the time difference between the pulses via the digital constant fraction method. If the criteria were not met, a logical expression would be set to the value false and the program would not calculate the time difference. A flowchart of this process is shown below in Figure 3.12.

The time resolution achieved and the percentage of pulses rejected were the main factors by which the efficacy of the limits was tested. A rejection scheme that improved the resolution by 10% but cut the effective count rate by 90% (such that only 10% of incoming pulses were accepted) would not be desirable, for instance.

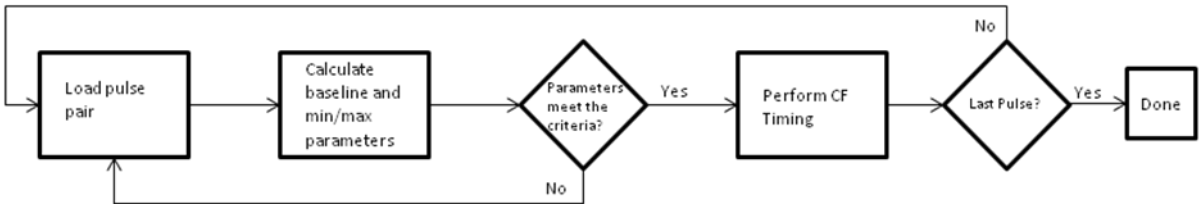

Figure 3.12. Flowchart of the pulse rejection process. If the calculated pulse parameters did not meet the criteria then the pulse would be ignored and the next pulse would be loaded. If the parameters did meet the criteria, then the constant fraction timing would be performed. After this the next pulse pair would be loaded unless it was the last pair in the set.

The histograms for the baseline, voltage maxima and minima, and time coordinate position of the voltage maxima and minima values were studied and specific values chosen that corresponded to 1) eliminating only spurious values in the histogram (those outside the

tail of the Gaussian distribution), 2) values cutting into the Gaussian distribution by approximately 5% on each side, and 3) values cutting approximately 10% of the pulses on each side (i.e. 1000 pulses on each side, leaving 8000 in the main part of the distribution). This scheme resulted in three variations for each type of test (e.g. voltage maxima, voltage minima, position of each, and so on). Each parameter was tested individually to ascertain its effect on timing resolution then criteria values that improved the timing resolution were combined with others that also improved the resolution in order to determine the aggregate response of many of these factors, all in a methodical and repeatable fashion. Figure 3.13 below shows the same set of pulses as in Figure 3.9 but after rejection of spurious pulses corresponding to option (1) above.

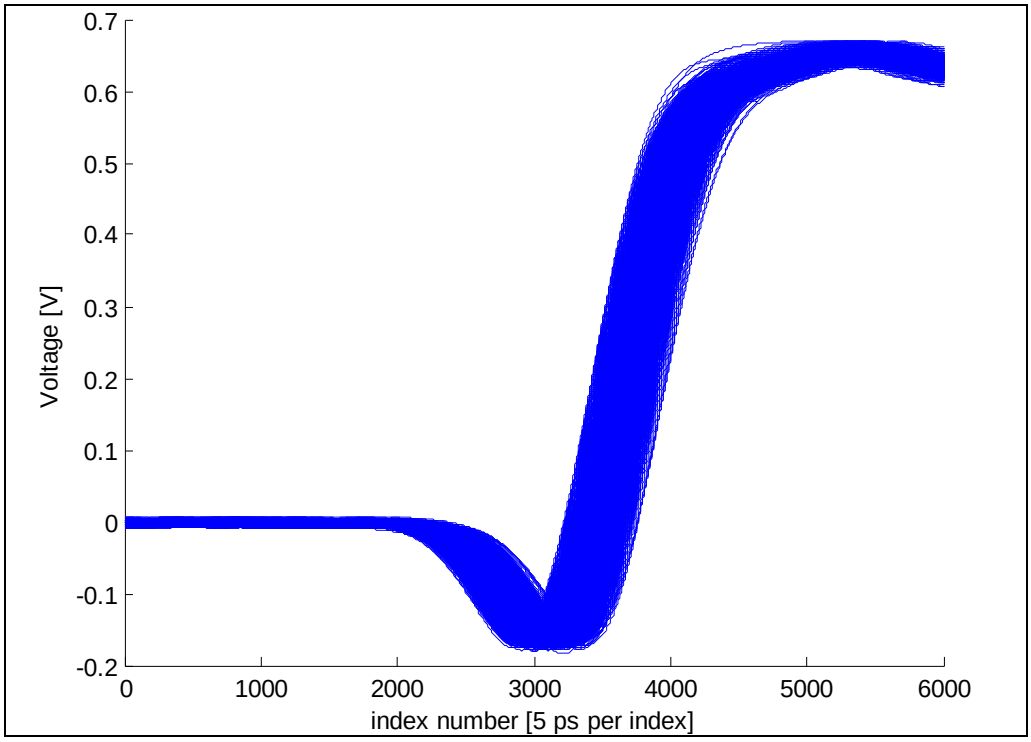

Figure 3.13. Pulses from the $LaBr_3$ detector with Co-60 after rejection of spurious pulses

For the BaF_2 detectors it was found that the pulse rejection did not improve the time resolution, but optimizing the constant fraction percentage did. For the $LaBr_3$ detectors, two factors were found that improved the time resolution. First was optimizing the constant fraction percentage and second was rejecting pulses based on their maximum and minimum voltage, as shown in the table in Appendix B.

3.3.4 Digital/Analog Comparison and Discussion

The time resolution performance for Co-60 of the optimized analog and digital systems for both types of detectors is shown below in Table 3.2. The uncertainties cited in the table are derived from the computer program *SigmaPlot*, which was used to determine the width of the timing response function by fitting it to a Gaussian. The time resolution values for the $LaBr_3$ detectors are better than those shown in Figure 3.8 in Section 3.3.3 because the latter only shows optimization based on constant fraction percentage. The values below take into account optimization based on pulse rejection as well.

Table 3.2. Summary of spectrometer time resolutions

Detector Type	**Voltage**	**Analog Time Resolution (ps)**	**Digital Time Resolution (ps)**
$LaBr_3$	-1500 V	192 ± 3	176 ± 3
$LaBr_3$	-1600 V	196 ± 3	178 ± 2
BaF_2	-2500 V	214 ± 3	187 ± 3
BaF_2	-2500 V	210 ± 2	182 ± 2

The $LaBr_3$ detectors were chosen for the graphite PALS testing because they had better time resolution than the BaF_2 detectors and because their application to PALS was new.

Chapter 4
PALS Measurements

PALS measurements were performed on reactor grade, pyrolytic, and foam graphite provided by Poco® Graphites, as well as high purity silicon for the determination of the resolution function of the spectrometer. Lanthanum Bromide [$LaBr_3$(Ce)] Brillance 380 detectors were used since they had a better timing resolution compared to BaF_2 as determined from testing with Co-60. The detectors and associated equipment were set up such that data was simultaneously collected from the analog chain and the digital oscilloscope providing a point of comparison between the two systems based on identical input.

4.1 Positron Annihilation Lifetime Spectroscopy

The PALS measurement in this work is based on the measurement of the time interval between the detection of a 1.27 MeV gamma ray emitted by a ^{22}Na source and the detection of the corresponding 0.511 MeV annihilation photon created by the annihilation of the positron from the ^{22}Na decay [1]. As mentioned in Chapter 1, the positron goes through a process of implantation, thermalization, diffusion, and finally annihilates either somewhere in the perfect crystal lattice of the material or trapped in an open-volume defect or feature.

The usage of the term *lifetime* can be somewhat confusing. Each positron exists for a finite amount of time before its annihilation – this duration can be thought of as that individual positron's lifetime. The lifetime that is the quantity of interest in PALS is the *parameter*, τ, that describes the behavior of a large number of positrons and is a material-

dependent property depending on the structure of the material as well as each of its types of open-volume defects or features. This is a concept analogous to that of radioactive decay – each individual nuclear decay occurs randomly and the time until the next decay is like the lifetime of the individual positron. On a macroscopic scale, however, the decay for a given radioisotope is described by its half-life, which is a time constant analogous to the lifetime τ. A radioisotope can be characterized by its half-life, and in PALS, a given sample will be characterized by a lifetime for the bulk material and a lifetime for each type of defect or other open volume feature. Each lifetime is associated with a parameter called its *intensity*, which is a measure of the relative strength or dominance of a lifetime compared to the other lifetimes. A perfect sample free from all defects would therefore be characterized by just one lifetime and that lifetime would have an intensity of 100%.

A PALS measurement is made by collecting and storing the individual lifetimes of positrons in a histogram or the channels of a multichannel analyzer (MCA), resulting in the positron lifetime spectrum. A sufficient number of annihilation events must be captured to ensure adequate statistics in the overall results and in each channel [1]. The number collected must be balanced with collection time, the number of channels used, and the time scale, for example. The sample-specific decay spectrum, related to the experimental spectrum, is given by

$$D(t) = \sum_{i=1}^{k+1} I_i \exp(-t/\tau_i) \tag{4.1}$$

where each I_i is the intensity, τ_i is the lifetime of each type of defect, and k indicates the number of defects or other open-volume features the material contains [1]. The similarity

and analogue of this equation to the radioactive decay equation is clear, especially when considering the case of $k = 0$. The ideal positron lifetime spectrum is described by [1]

$$N(t) = \sum_{i=1}^{k+1} \frac{I_i}{\tau_i} \exp(-t/\tau_i). \tag{4.2}$$

This is the absolute magnitude of the time derivative of the positron decay spectrum [1]. Two major differences in the experimental data exist compared to the ideal equation above. First, the spectrometer itself does not have a perfect or ideal response function. For a detector system that was measuring the energy E_0 of a monoenergetic gamma emitter, for example, the ideal measurement would show a spike or delta function at the energy value E_0. This would mean that the detector counted a certain number of gammas that deposited energy equal to E_0 in the detector. In real conditions, however, the gamma is backscattered, undergoes Compton scattering, some of the energy escapes, and other processes occur that result in a range of energies that are detected. This energy response is akin to the timing response function of the PALS spectrometer. Were the spectrometer to measure the time difference between gammas from a source that emits two gamma rays in coincidence, the ideal result would be a spike or delta function at $t = 0$ (or $t = t_0$ if a constant time shift was introduced). This is never the case because of the broadening of the time peak due to effects in the detector and electronics that make up the PALS spectrometer. This non-ideal response is the resolution function of the spectrometer and the data obtained from the spectrometer is the convolution of the resolution function with the ideal positron lifetime spectrum N(t) from Equation 4.2 [1]. The resolution function is also affected by the geometry of the setup due to scattering of gamma rays between detectors, as discussed later.

Another minor departure from the ideal lifetime spectrum above is due to the practice of intentionally delaying or shifting the spectrum by time t_0 such that the portion of the spectrum located at $t < t_0$ arising from the resolution function is not cut off. This also serves to ensure that the signals reaching the Time to Amplitude Converter (TAC), which measures the time difference between the 1.27 MeV and 0.511 MeV quanta, fall in a well-behaved, linear region of the TAC. The effect of this delay is to replace t by (t-t_0) in Equations 4.1 and 4.2 [1].

The timing resolution function of the spectrometer can be approximated by a sum of three Gaussians, each characterized by a different full width at half maximum (FWHM) and centroid location in time. The origin of this resolution function has to do with the Gaussian spreading mentioned above and also issues related to interactions in which the full energy of the gamma is not deposited in the detector, as discussed in Section 4.2. Early PALS studies represented the resolution function by a single Gaussian [30] centered at the delay time t_0. A single Gaussian function is expressed by [1]

$$G(t) = \frac{1}{\sigma\sqrt{\pi}} \exp[-(\frac{t-t_0}{\sigma})^2], \tag{4.3}$$

where σ defines the width of the Gaussian such that the width at half its maximum value is $2\sqrt{2\ln 2}\ \sigma$, or approximately 2.35 σ. The convolved spectrum is the convolution of Equation 4.1 with the resolution function, $F_t(t)$, which consists of a sum of Gaussians. The convolution is expressed by [1]

$$D_f(t) = \int_{-\infty}^{\infty} D(t-t')F_t(t')dt'. \tag{4.4}$$

The experimental data is thus the lifetime data convoluted with the system's resolution function. In order to obtain the desired positron lifetimes and intensities, the data must be unfolded and decomposed using computational techniques. A number of fitting programs based on non-linear least squares fitting are accessible to do this, one of the most common being PositronFit Extended by Kierkegaard et al. 1989 [31]. A more recent version of this software called PALSfit [32] features a Windows platform and GUI interface. It allows the user to determine the resolution function of the spectrometer and use this to decompose the spectra for material samples of interest. Inherent in this process is the source correction, in which the positrons annihilating in the foils supporting the isotope are accounted for. Further details are listed in sections dealing with data analysis and the PALSfit routine.

A key parameter in the PALS measurement is the coincidence count rate, or the rate at which data is collected. This depends mainly on the geometry of the setup and the source used. A PALS measurement usually takes between several hours and a full day to collect a spectrum with good statistics. Some efforts to improve the time resolution decrease the coincident count rate creating an important tradeoff to be managed.

4.2 The Spectrometer Timing Resolution Function

4.2.1 Resolution Function

The analytical mathematic expression of the positron decay spectrum in Equation 4.2 describes the annihilation of positrons in the bulk crystal structure of a test material and in different types of open-volume vacancies, defects, or pores [1]. The shape of this function is that of a decaying exponential. The experimentally obtained spectrum, however, is different

from this ideal positron decay spectrum, most notably in the portion to the left of the peak as seen in Figure 4.1. The portion to the right of the peak is nearly a straight line which on a log scale represents exponential decay. The portion on the left, however, is due to the spectrometer resolution function – its response to events exactly in coincidence, similar to the concept of the impulse response of a system in systems engineering and analysis. The resolution function is also related to the geometry of the setup through the scattering of start and stop signals (detector cross talk and other scattering) and the ratio of the scattering and backscattering solid angles relative to the source-detector solid angle [33-35]. The experimental data collected in an actual PALS experiment is the convolution of this response function with the positron decay spectrum [1].

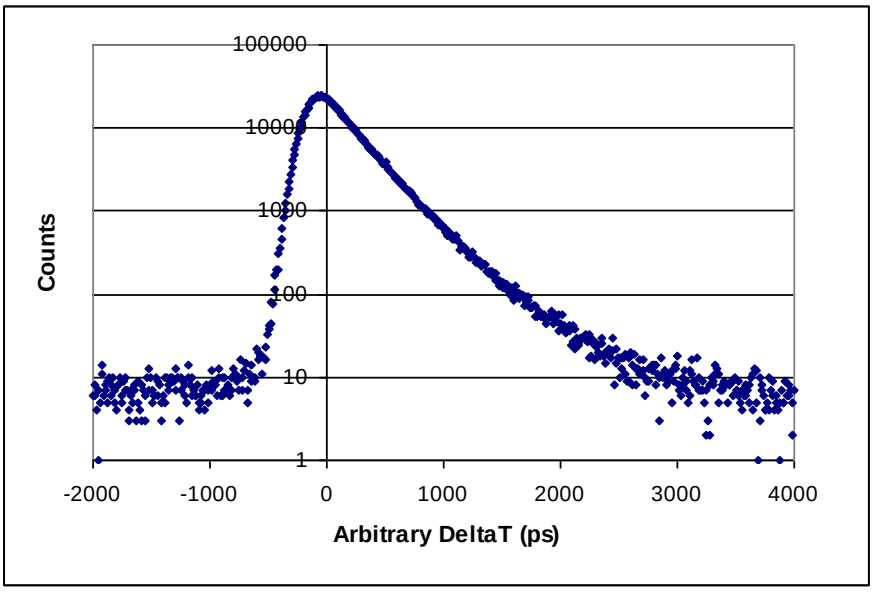

Figure 4.1. PALS Spectra for high purity silicon. The portion to the left of the peak is an effect due to the resolution function of the spectrometer.

Since the resolution function of the spectrometer is an integral part of the data collected, its proper mathematical description is essential. Once determined, a non-linear least squares

fitting procedure that takes into account the resolution function is used to create a model of the spectrum and the experimental data is fit to the model [1,32, 36]. Generally speaking, there are two ways to determine the resolution function. Based on the definition of the resolution function above, the resolution function could be experimentally obtained by recording the response of the spectrometer to a source that emits two coincident gamma rays of the same energies utilized in a PALS experiment [34]. Such a source does not exist, however, but Cobalt-60 is a readily available isotope used to obtain an approximation of the resolution function as it emits a 1.17 MeV gamma ray in coincidence with a 1.33 MeV gamma ray. Experience with this method, however, showed that the use of Co-60 in defining the resolution function producedinconsistent and incorrect results [31,37]. The true resolution function differs from the Co-60 response as it depends on the energy of the gamma rays and their specific interactions with the detectors and surrounding materials. An example spectrometer response to Co-60 from the analog system with $LaBr_3$ is shown below in Figure 4.2.

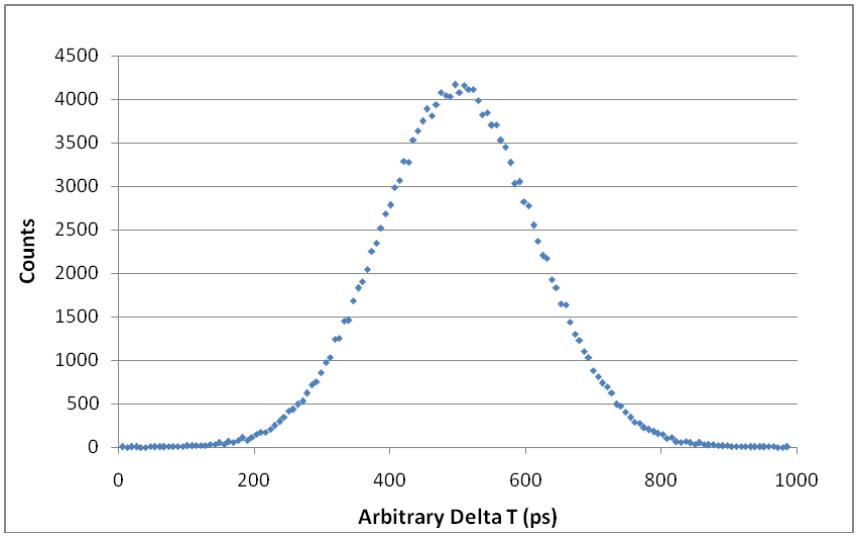

Figure 4.2. $LaBr_3$ spectrometer response to Co-60.

The Co-60 response is still useful because it shows that scattering does have an effect on the resolution function and because it provides a close approximation to the time resolution, or resolving power, of the spectrometer based on the width of the Co-60 response function. If the time resolution of the system in an actual PALS experiment deviates much from this value it is an indication that there is some error in the system [32]. As seen above, the shape is similar to a Gaussian curve but is slightly asymmetrical and otherwise deviates from Gaussian behavior at the tails. The Gaussian-like shape is due to the sources of resolution spreading outlined in Section 2.4 but the deviation from this shape is due to scattering.

The second and only method successfully used in the PALS community is to derive the resolution function from a PALS spectrum of a material with a single, well-known lifetime such as high purity silicon, highly annealed iron, or highly annealed molybdenum [1,36]. Using a PALS spectrum fitting program such as PALSFit, the single positron lifetime and source/foil lifetime of this calibration material can be input as fixed constants providing the necessary degrees of freedom needed to fit the resolution function to a given model. The evolution of fitting programs over the few decades of PALS experiments shows the progression of the models used to describe the resolution function. Positronfit written by M. Eldrup, et al. allows the resolution function to be modeled as a single Gaussian, defined by its position and width [30]. The programs PFPOSFIT (1983) [38] and DBLCON (1978) [37] modified Positronfit to allow for the description of the resolution function by an exponential sided Gaussian (ESG), which is a Gaussian convoluted with two exponential decaying functions at its tails. These exponential functions are each defined by a decay constant and

intensity (τ and I). Eldrup produced another version of his program in 1974 called Positronfit Extended that allowed for the fitting of the resolution function by a sum of up to seven Gaussians, each with two fitting parameters, the position (or shift) x, and width σ [31]. A more recent version of PositronFit called PALSFit featuring a graphical user interface was created in 2006 for the Windows operating system. It allows for the fitting of up to three Gaussian curves to the resolution function [32]. A summary of selected lifetime fitting programs is shown below in Table 4.1.

Table 4.1. Summary of selected positron lifetime fitting programs and the method used to model the spectrometer resolution function.

Principal Developer	**Program**	**Date of Release**	**Modeling of Resolution Function**	**Comments**
Kierkegaard	Positronfit	1972	Single Gaussian	Single Gaussian did not produce consistent results
Kierkegaard	Positronfit Extended	1974	Up to seven Gaussians	Two Gaussians tested and also found to produce inconsistent results
Wharburton	DBLCON	1978	Exponential Sided Gaussian	Produced satisfactory results
Puff	PFPosfit	1983	Exponential Sided Gaussian	Produced satisfactory results
Olson	PALSFit	2006	Up to three Gaussians	Program based on Kierkegaard and reflects accepted usage of three Gaussians

Wharburton showed using simulated spectra (those generated from user input for lifetimes, intensities, and resolution function) that the representation of the resolution function by a single Gaussian was insufficient, especially for materials with multiple lifetimes of similar values [37]. Kirkegaard et al. also found that a single Gaussian often failed and that the error was worse as more lifetimes were fit and the analysis became more complicated [31]. The exponential sided Gaussian form was found to produce more consistent results than a sum of two Gaussians; however, a sum of three Gaussians has

become standard practice [1,9,10,22,28,32]. Using a superposition of three Gaussians gives the flexibility and degrees of freedom needed to accurately reproduce a resolution function.

4.2.2 Deviation of the Resolution Function from a Purely Gaussian Shape

A few researchers have performed experiments linking the geometry of the spectrometer setup to the resolution function as approximated by the use of Co-60. Dorikens-Vanpraet et al. investigated the effect detector and source geometry plays in the resolution function. Plastic scintillators were used in a collinear fashion with the source centered between the detectors and in line with their axis. The spectrometer response to Co-60 is shown in Figure 4.3 below for three different source-detector separation lengths [33].

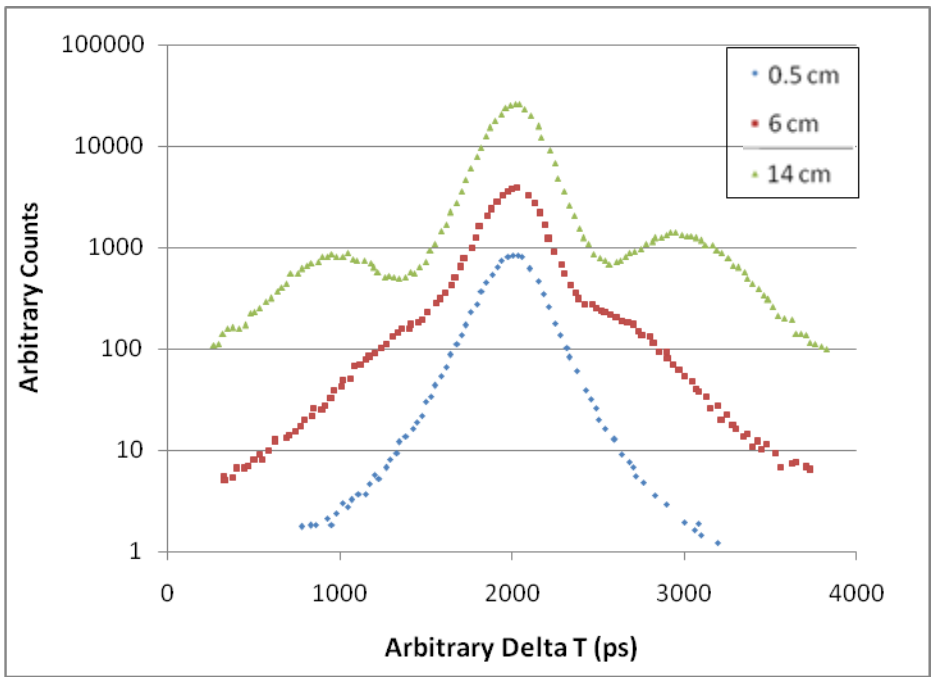

Figure 4.3. Response of a spectrometer to Co-60 for different detector separation distances [33]. The differences are due to scattering between the detectors. The effect gets pushed out farther for increasing separation distance.

The green curve at the top of Figure 4.3 is the result from the detectors with a 14 cm source-detector spacing, or 28 cm detector to detector spacing. The blue curve is the result

from the detectors with the least spacing – 0.5 cm. Backscattering of the Co-60 gamma rays was responsible for these effects, as the locations of the peaks in the green and red curves correspond to the time of flight for a backscattered gamma. As the detector spacing is decreased, the backscatter distance and time of flight is decreased so the two peaks at the edges get pushed in toward time zero, where their effect is still present but is more washed out by the higher number of counts toward time zero. This phenomenon does still lead to a greater number of counts towards the tails of the response even though it is not sufficient to create additional peaks. Experimentation with other geometries in addition to detector spacing in the collinear fashion by Dannaefer, et al also showed an increase in distortion of the resolution function and increase in the FWHM as the ratio between the backscatter solid angle and the detector-source solid angle increased [35]. From tests on simulated spectra, Dannaefer also concluded that collecting more counts in a spectrum leads to more reliable and resolvable results than improving the time resolution at the cost of the count rate by setting a very narrow energy selection range in the CFDs. This is due to the fact that narrowing the energy windows too much drastically reduces the coincidence count rate while only marginally improving the timing resolution. With fewer counts in the spectrum Dannaefer found that resolving multiple lifetimes was difficult, especially for lifetimes with similar values close to each other [35]. This has also been observed by Somieski et al [39].

H. Rajainmäki et al. investigated backscattering for BaF_2 detectors, which have a high probability of detecting both the 1.274 MeV gamma the twin of the 511 keV gamma detected in the stop detector. Any energy deposited and time delay by this twin (the second annihilation photon that is incident upon the start detector not the stop detector) would

contribute to the resolution function and could also scatter into the other detector. PALS experiments on annealed Molybdenum were found to be off established values in the collinear setup but normal in a "triangular" geometry where the source is located outside of the axis of the detectors, forming a triangle between the source and detector crystals as shown below in Figure 4.4. This altered geometry disallows the entry of both 511 keV annihilation quanta into the detectors and was used in this work [34].

Figure 4.4. Triangular detector-source geometry that prevents the entry of annihilation quanta from the same annihilation event into both detectors. The small circle represents the ^{22}Na source and the other two figures are detector crystals attached to a photomultiplier tube.

The spectrometer resolution function is affected by the scattering of gamma rays between detectors and because of this the resolution function must be represented by a function more complex than a single Gaussian or even a pair of Gaussians. Using three Gaussians gives sufficient degrees of freedom and flexibility to accurately describe a complex resolution function. When three Gaussians are used, two generally exhibit a FWHM near that of the overall resolution function and have a combined intensity of over 95%. The third Gaussian is wider and more shifted [22,28,32]. The three Gaussians together are needed to accurately represent the resolution function.

4 .3 Graphites and Silicon

An extremely high purity silicon sample approximately 12 mm on a side and about one millimeter thick obtained from Oak Ridge National Laboratory was used for the determination of the spectrometer resolution function. As mentioned earlier, such silicon is

an ideal material for this purpose because of its nearly defect-free crystalline microstructure. The PALS spectrum from this material contains only two lifetimes – one for the positron lifetime in the silicon crystal lattice and one for the kapton foils. Knowledge of these lifetimes allow for the determination of the resolution function via nonlinear least squares fitting. Such silicon is well-characterized in the literature and is shown to have a lifetime in the range of 218 to 220 ps [1,40].

Reactor grade graphite refers to any graphite designed for use as a moderator in a nuclear reactor. It has a very high chemical purity and is composed of grains of graphite with no bulk or long-range orientation. The lack of orientation leading to varied grain boundaries could give rise to additional lifetimes [7,42-43]. Any defects caused by a manufacturing process could also contribute one or more lifetimes. The reactor grade graphite samples were approximately 51 mm square and 6.4 mm thick. The density of the graphite samples was about 1.7 g/cm^3.

Pyrolytic graphite has a close packed hexagonal structure with a varying degree of crystallographic orientation of the c-axes perpendicular to the graphite surface, depending on the grade of the pyrolytic graphite [41]. Various grades of pyrolytic graphite are commercially available and distinguished by their mosaic spread, or the degree of alignment between stackings of graphite layers. Highly oriented pyrolytic graphite (HOPG), for instance, is a pyrolytic graphite with an angular spread of the c-axes of the crystallites of less than one degree, and is formed by chemical vapor deposition of carbon atoms or stress annealing at high temperature [41]. The highest grades of HOPG are used in monochromators and have a mosaic angle as low as 0.4 deg [44]. Lower grade pyrolytic

graphite will still have regions of high orientation within a grain, for example, but with an increased spread in mosaic angle. Imperfections in the crystal structure are expected at regions where different grains are not aligned. The pyrolytic samples used in this work were not HOPG and were noticeably thinner and denser than the reactor grade graphites studied. They were approximately 50 mm square and 3.2 mm in thickness, with a density of about 2.2 g/cm^3.

The foam graphite was developed by Oak Ridge National Laboratories and is manufactured by Poco Graphite, Inc. It has a thermal conductivity comparable to aluminum but is significantly less dense and thus lighter. The foam is under investigation for use in many different heat transfer and thermal management systems and for use in nuclear applications [45]. The manufacturer quotes a porosity of 0.75 and open fractional porosity of 0.98. The porosity is defined as the ratio of pore volume to total volume and the open porosity is defined as the ratio of the pore volume that is connected to the surface of the sample to the total volume [46]. Because the foam is porous it is expected to exhibit significantly different positron lifetimes than the other standard graphitic materials [42,47]. It was received in rectangular blocks about 50 mm on a side and 11.25 mm thick. The measured density was 0.41 g/cm^3.

4.4 Setup of the Spectrometer for PALS Measurements

A triangular geometry for the source/sample and detector setup, as in Figure 4.4 in Section 3.2.2, was chosen to eliminate the simultaneous detection of 511 keV annihilation quanta in both detectors. The size and dimensions of the graphites were not conducive to placing the source/sample sandwich close to the detectors to optimize the coincidence count

rate. As a result, the graphites were cut to dimensions similar to the silicon and sanded down on a rotating grinding plate with sandpaper to reduce their thickness. The samples were cut to be approximately 17 mm on a side. The reactor grade graphites were sanded down to a thickness of about 3.2 mm, the thickness of the pyrolytic samples. The foam samples were not sanded down because they were easily ground away and because thinner samples were more prone to indentation when held in place to create a tight source/sample sandwich. All graphite samples were more than thick enough to stop all incident positrons as they were much thicker than the silicon. The 17 mm dimension was chosen for the graphites for ease of handling and because this size did not impact the sample-detector placement. Figures 4.5 and 4.6 below show some of the cut and uncut graphite samples.

Figure 4.5. Cut graphite samples, labelled in the figure.

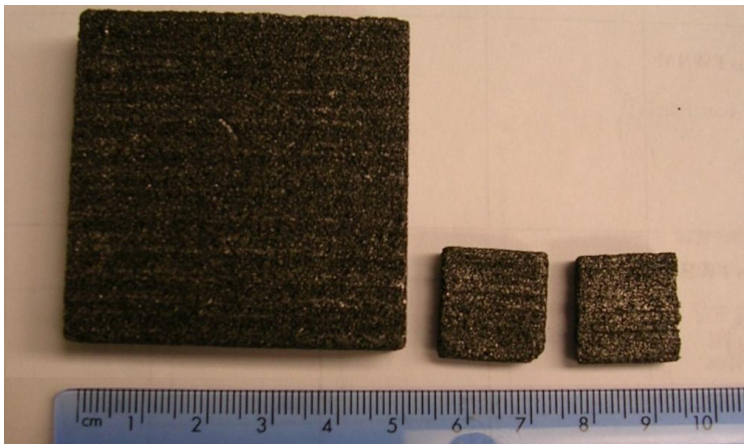

Figure 4.6. Uncut and cut graphite foam samples

Figure 4.7 shows the source/sample and detector setup and Figure 4.8 shows the experimental setup from more of a distance, including a full view of the polyethylene blocks used to hold the detectors. These were placed on top of a hollow cardboard box to raise the system further above the table to decrease potential scattering from nearby materials. Not all scattering can be avoided since the detectors and whatever they are held in will also contribute somewhat to scattering.

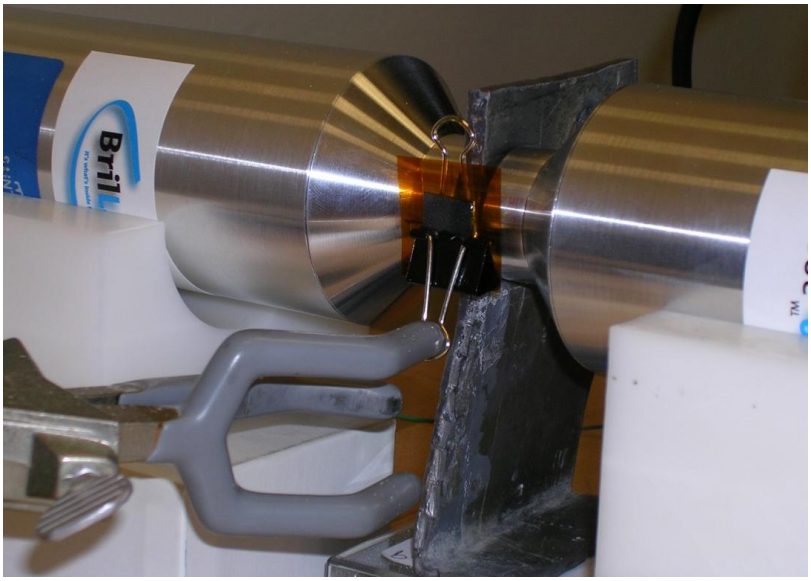

Figure 4.7. Source/sample sandwich and experimental setup

Figure 4.8. Experimental setup showing the detectors, source, and lead between the detectors

Since the resolution function of the spectrometer is dependent on the geometry of the experimental setup it was important to maintain the same geometry and configuration between all measurements in a given set. In this work the geometry between all three sets of data was kept constant. The limiting factor in the source distance was the foam thickness since it was the thickest of the samples. In order to determine the geometry of the setup, the source sandwich was assembled with the foam graphite samples and placed snugly against the detectors such that the source was aligned with the center of the height of the detector crystals but just outside the axis of the detectors. In this way, the distance from the edge of the crystals' housing to the source was equal the thickness of the foam graphite sample with an additional small distance due to the clip.

The distance between the detector faces was 8 mm, while the lead was 4.5 mm thick. The closest achievable distance with the foam (thickest) sample was 21 mm outside of the detector radius, measured from the edge of the detector to the kapton foil between the samples. This distance was therefore used for each type of graphite. To ensure the proper alignment of the source, small marks were made on the kapton foil indicating the location of the ^{22}Na salt spot that was visible when the samples covered the spot, as shown in Figure 4.9.

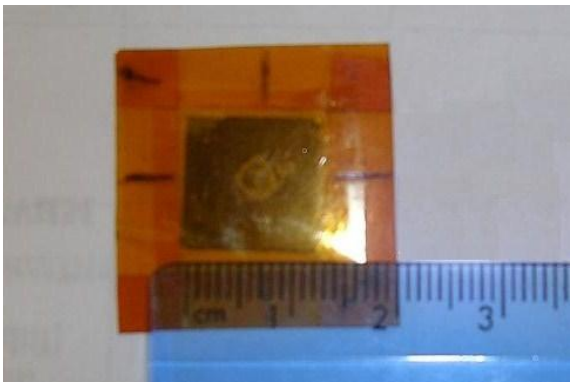

Figure 4.9. Kapton/source sandwich with position markings

The energy windows of the detectors were set via the procedure described in Section 3.2. The Start and Stop detectors were set to 511 ± 100 keV and 1270 ± 100 keV, respectively, with each detector capturing its respective broadened full-energy peak but excluding essentially all other energy ranges. This range was a compromise between keeping a practical coincidence count rate and including only the full energy peaks, and the count rate obtained allowed collection of over one million counts in less than 24 hours. Collection times much longer than this become impractical for routine PALS use. Collection times varied somewhat across all data sets due to the impracticality of changing the samples every 24 hours.

Three sets of measurements were made, with a set consisting of an approximately 24-hour measurement of the silicon, followed by the foam, reactor grade, and pyrolytic graphites. Data was viewed between sets to ensure that no obvious errors occurred in the measurement or setup, including comparison of the data sets to one another. The first set of measurements was made without digital pulse rejection criteria as a control for later sets that would include digital rejection of pulses. Digital pulse rejection criteria were determined from a saved set of 10,000 pulses similar to that done for the Co-60 tests, but in the experimental setup used for the test samples and with the Na-22 source. Various parameters from the 10,000 pulse pairs were calculated and histogrammed. The histograms were Gaussian-like but had some counts outside of the Gaussian distribution. Limits for position, voltage, and baseline characteristics (mean, rms, etc.) were selected from the boundaries of the major distribution eliminating all outliers. Limits from within the Gaussian portion of the histogram were not taken because this would increase the number rejected and because

earlier tests with Co-60 showed this was not fruitful. The algorithm used on the digital oscilloscope for timing was the same as for the Co-60 time resolution experiments with the exception of different limits and ranges for the rejection criteria unique to the ^{22}Na source.

The spectra for the first two sets of measurements showed spurious effects at the left edge of the spectra in the form elevated counts in the background count rate portion of the spectra as seen in the first two thirds of Figure 4.10 below.

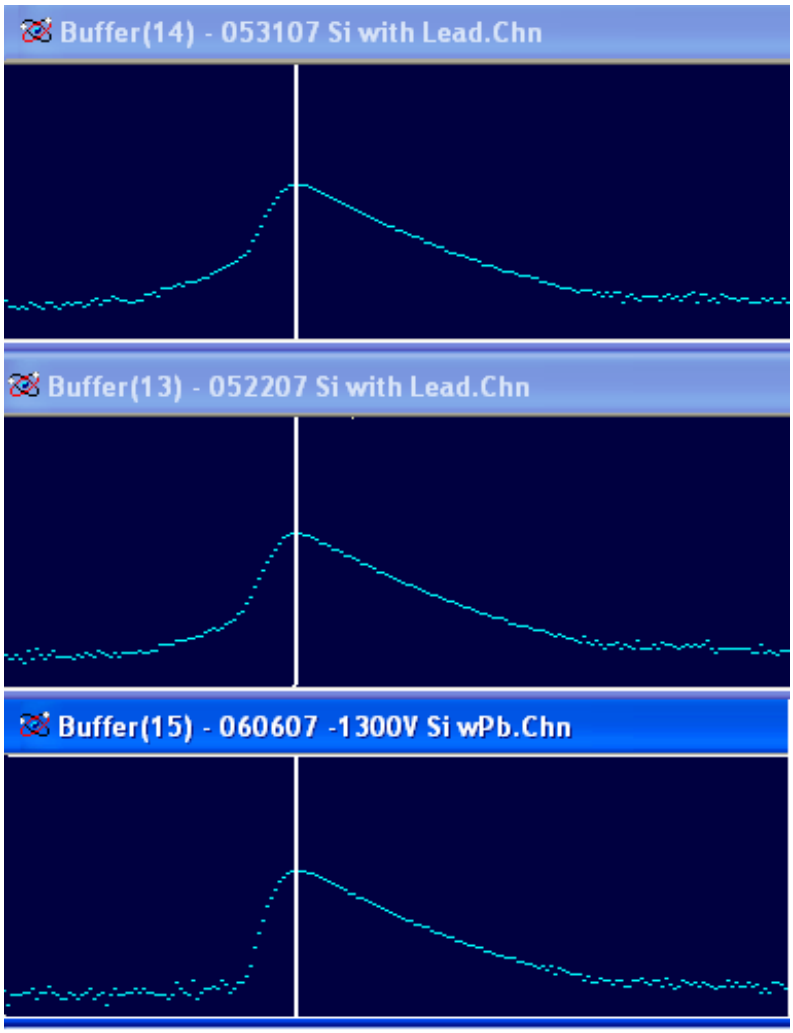

Figure 4.10. Silicon PALS spectra. Two were taken with the PMT at -1500 V high voltage and the last with the PMT at -1300 V. The portion to the left of the spectra peak marked by the white line is better behaved for the -1300 V case.

These spurious effects are coincident events that are produced from scattered quanta and distortions due to the high operating voltage. Viewing the detector pulses on the oscilloscope revealed that some pulses in the 1.27 MeV detector had two different pulse shapes – one was well-behaved and shaped, while the other showed variation in shape as well as rise and fall time. The existence of this second type of pulse was investigated over different operating voltages, and the highest magnitude voltage at which this did not occur was -1300 V. The operating voltage was adjusted and a sample run with silicon was taken for comparison. This spectrum showed a dramatic decrease in the effect, and so subsequent data was taken at this voltage. All of the data collected at -1300 V exhibited a more behaved spectrum to the left of the spectrum peak as seen in the last section of the figure.

4.5 PALS Measurement Data Sets

The PALS spectra of the four materials were plotted for each measurement set and are shown below in Figures 4.11-4.18. In order to access and plot the data, the analog spectra were exported to a text file from the Maestro MCA emulator program. The data from the digital spectrometer was saved directly as a text file from the digital oscilloscope. From these files the data was easily introduced into a graphing program and plotted. Further details on file structure are provided in Appendix C.

The data were manipulated to normalize the number of counts in the peak channel, i.e. the channel with the greatest number of counts. This way the differences between the spectra could be compared visually in a qualitative manner, showing which materials have shorter and longer positron lifetimes. This would be necessary even for data sets with the

same total number of counts since the distribution of the counts across the spectrum is different based on the material and its lifetime characteristics. In other words, two spectra with 1.5 million counts each will have a different distribution of counts and different peak value the farther apart the average lifetimes in the material are.

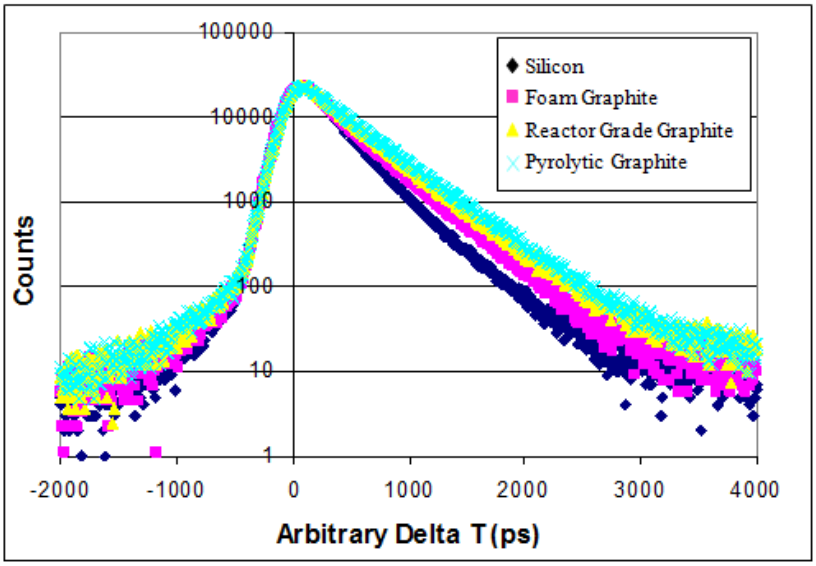

Figure 4.11. Analog PALS spectra, first dataset. The order of materials in terms of mean lifetime is silicon, foam graphite, reactor grade graphite, and pyrolytic graphite. The pyrolytic curve at the top has the longest mean lifetime since its exponential decay is the longest.

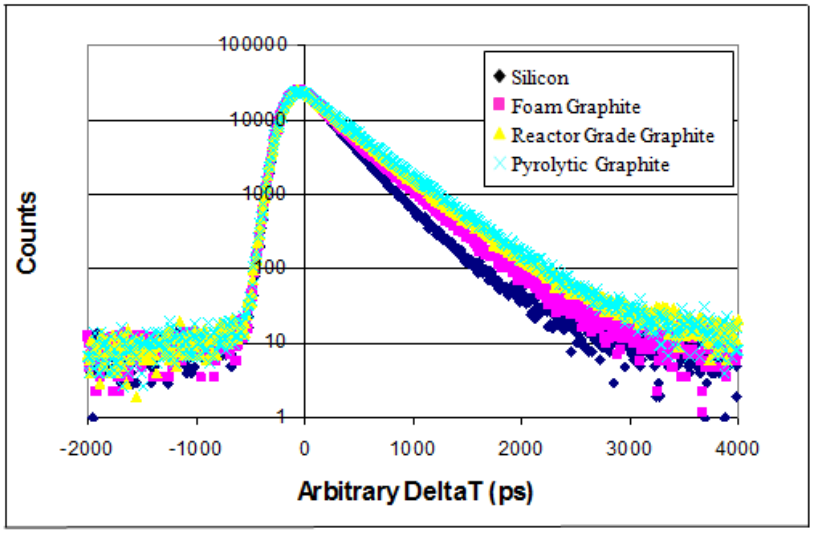

Figure 4.12. Digital PALS spectra, first dataset.

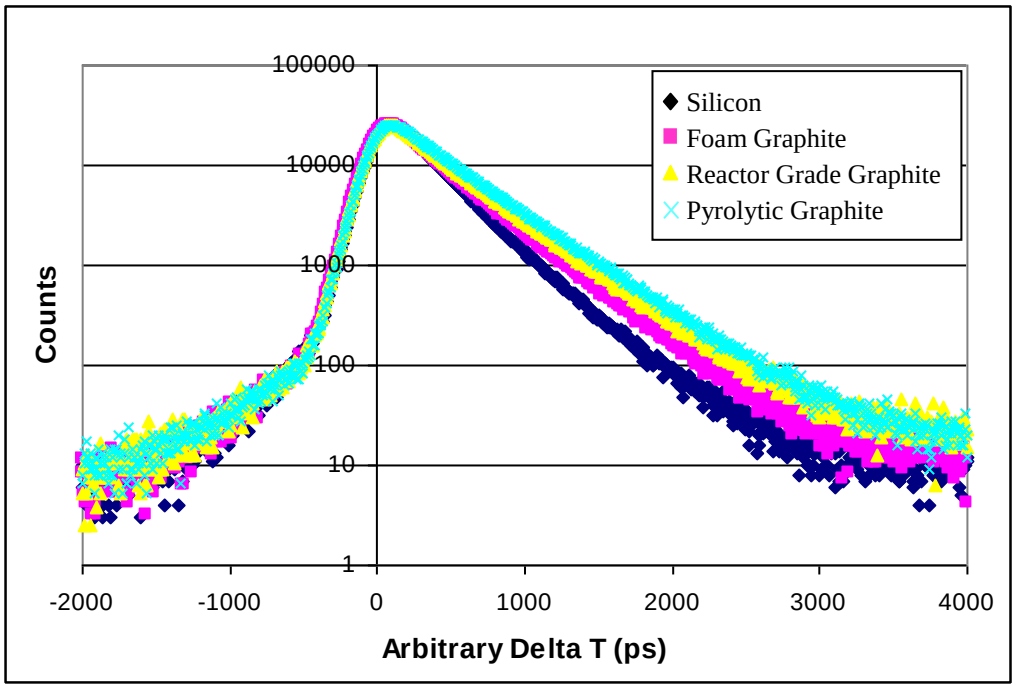

Figure 4.13. Analog PALS spectra, second dataset.

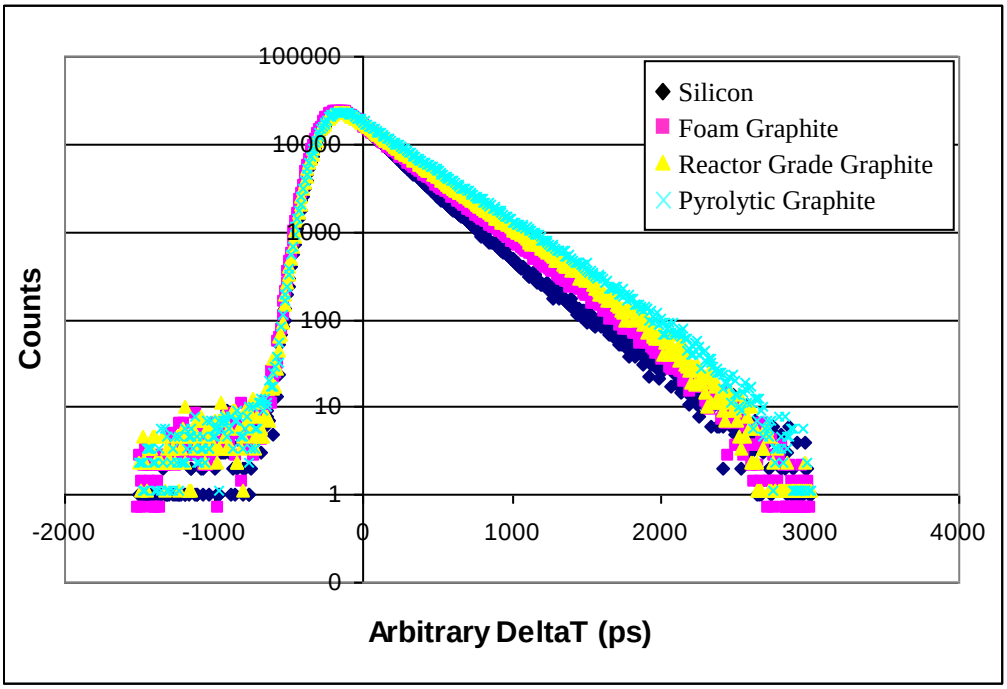

Figure 4.14. Digital PALS spectra, second dataset. Rejection criteria were used for this set, and this eliminated the backgrounds counts outside of the main part of the distribution.

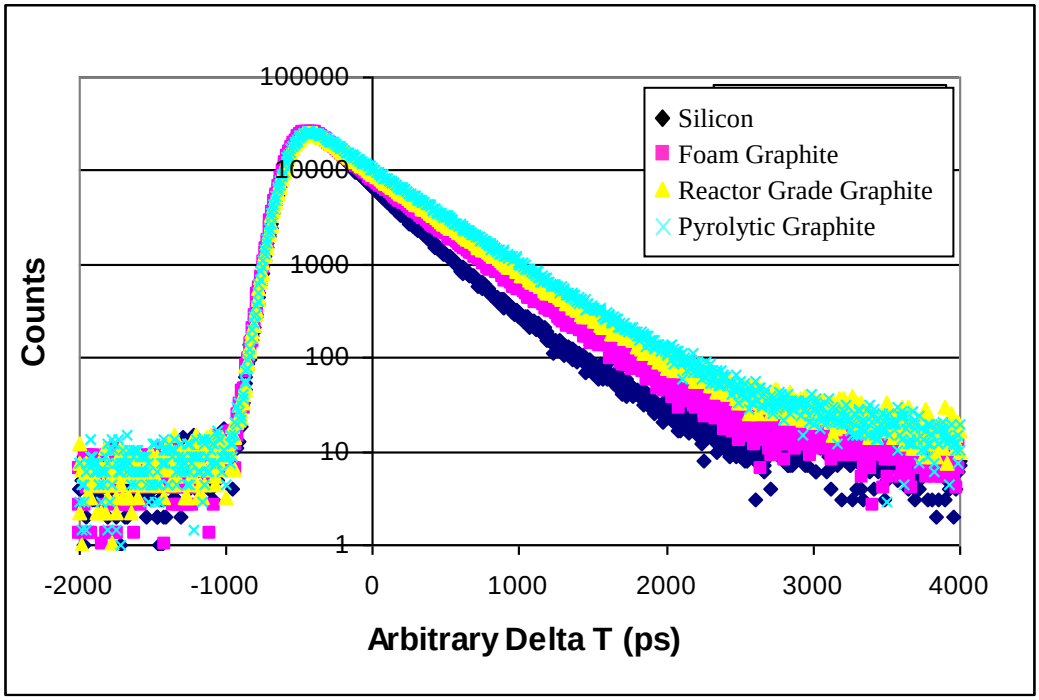

Figure 4.15. Analog PALS spectra, third dataset

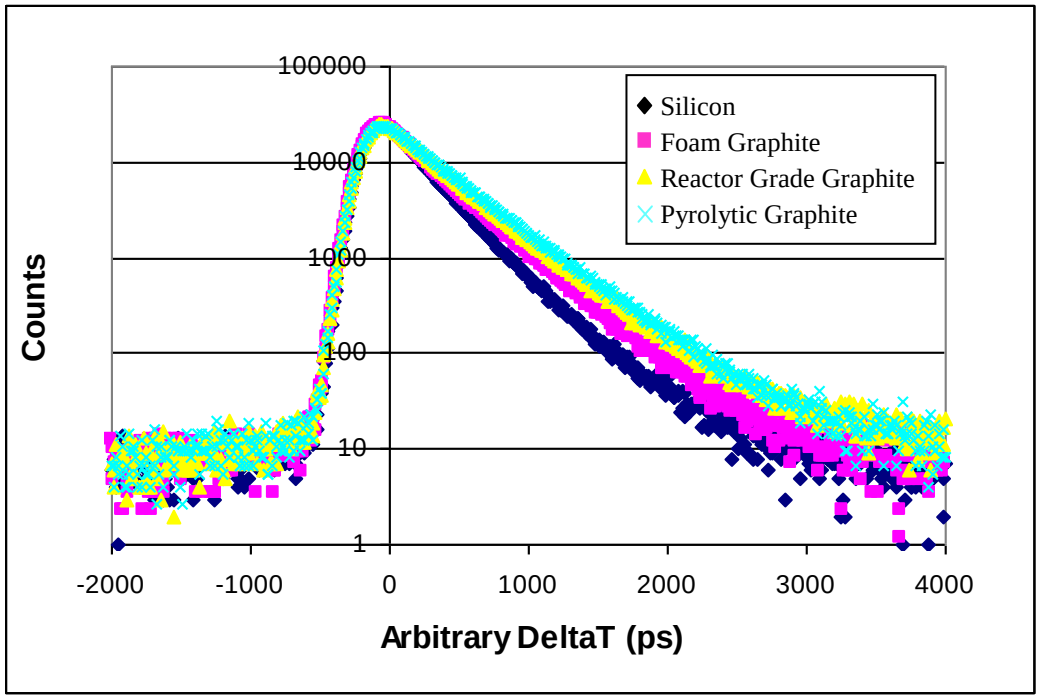

Figure 4.16. Digital PALS spectra, third dataset.

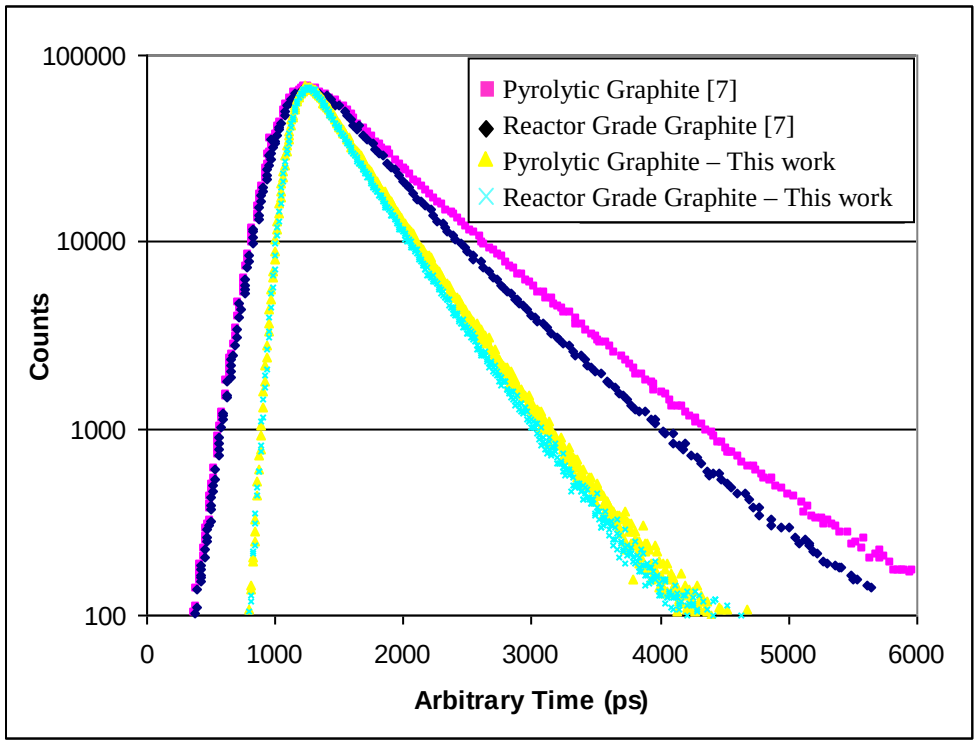

Figure 4.17. Comparison of the pyrolytic and reactor grade graphite PALS spectra from Iwata [7] and this work. Much of the difference between the two sets is due to the larger 240 ps time resolution of the Iwata spectrometer which broadens the Iwata spectra. The relative order between the two types of graphites in this work and between other graphites Iwata studied is correct.

The right hand side of the spectra representing the lifetimes and intensities (τ_i and I_i) fall into the following order of average lifetime from high to low: pyrolytic graphite, reactor grade graphite, foam graphite, and silicon. It is interesting to note that the foam has the smallest average lifetime of the graphites. Results from Iwata et al [7] also show a similar ordering amongst pyrolytic and reactor grade graphites as seen in Figure 4.13 above.

The data from Iwata was captured with a plot digitizer and the channel numbers were converted to arbitrary time using the reported 18.7 ps/channel MCA scaling factor so all sets of data could be compared on an equal time scale [7]. The data was also shifted to achieve alignment at the peak channel and was scaled so that the peak channels contained the same

number of counts in order to aid the visual comparison of the data. The difference in width and shape between the two sets of spectra are due to the time resolution, or width of the resolution function. The Iwata spectrometer had a time resolution of 240 ps with Co-60 compared to 190 ps with Co-60 for the spectrometer used in this study. Thus Iwata's data is more spread out since each experimental spectrum is the convolution of the ideal lifetime spectrum with the spectrometer resolution function.

The pyrolytic graphite used by Iwata had the largest mean lifetime of the graphite samples he tested, which additionally included annealed pyrolytic graphite, natural flake highly oriented pyrolytic graphite (HOPG), and monochromator grade HOPG. The pyrolytic graphite studied in this work was not HOPG and was found to have the highest mean lifetime of the graphites studied in this work, as seen in Figures 4.7-4.13, where the pyrolytic graphite spectrum is at the top of each figure with the longest decay. Thus the general ordering of the pyrolytic and reactor grade graphite spectra of this work are consistent with Iwata's data [7].

4.6 Data Analysis: PALSFit

4.6.1 Input to PALSFit

The program PALSFit was used to analyze the PALS spectra. PALSFit is a nonlinear least squares fitting program consisting of two modules, one to determine the spectrometer resolution function from a reference lifetime spectrum, and one to extract the positron lifetimes and intensities from a lifetime spectrum [32]. Both modules fit a model function to a set of experimental data points y_i forming the PALS spectrum. The data points are the number of counts recorded in each channel, or histogram bin, in an MCA or other system

such as the digital oscilloscope. The program iteratively minimizes the least squares difference between the data and the model with k parameters $b_1, \ldots b_k$ as follows:

$$\Phi = \sum_{i=1}^{n} w_i \left(y_i - f_i(b_1, \ldots, b_k) \right)^2 , \tag{4.6}$$

where n is the number of experimental data points, $f_i(b_1,\ldots b_k)$ is the model prediction for data point i and w_i is a fixed weight attached to the data point. The value of w_i used is $1/\sigma_i^2$, which is the estimated variance of y_i, and is equal to y_i itself under the assumption of Poisson statistics in the data. This weighting serves to give more statistical emphasis to channels with many counts where the uncertainty is smaller, avoiding an over-dependence on portions of the data yielding little information (i.e. the tail of the PALS spectra). The b_i parameters are the model-dependent variables such as the positron lifetimes, intensities and the various parameters describing the resolution function [32].

PALSFit requires the spectrum data to be entered in a particular FORTRAN-standard tabular format, as discussed in Appendix C. To get the data from the analog and digital systems into this format, two programs were written – one in Matlab and one in Fortran90. The Matlab program takes an arbitrary array of data and converts it into a single column of data. The Fortran90 program takes a single column of numbers and puts them into the 10f7.0 format. The actual coding language of the two programs is supplied in Appendix C.

PALSFit produces a result output file which can be viewed in the PALSFit graphical interface program or in a separate output file. The graphical interface also produces a plot of the spectrum before or after background subtraction and with options to show any range of the actual data points, the curve representing the model's predicted spectrum, or both overlaid together. The graphing section can also plot the residuals for each point, which is

the least squares difference between the plot and the model expressed in number of standard deviations. Both graphical options are useful in assessing the validity of a set of results.

4.6.2 Output of PALSFit

After performing the nonlinear least squares fitting of parameter values, PALSFit displays an output screen that summarizes the input parameters and displays the output results. It displays the number of iterations taken to reach optimized results and statistical information on the goodness of fit between the data and model. It displays the chi squared value, the number of degrees of freedom (the difference between the number of data points used in the fit and the number of free parameters), and chi squared divided by the number of degrees of freedom – also known as the reduced chi squared. It also displays the 'Significance of Imperfect Model' which is the probability of obtaining a chi squared value greater than or equal to the one that was calculated using the model parameters. This provides an indication of if the fit is too good, too poor, or is reasonable granted standard statistical scatter and sampling of a distribution [32,48]. A low or high percentage for this value suggests that the model used (number of lifetimes and any constraints on the lifetimes or intensities) is not correct or that the given lifetimes cannot be resolved properly.

4.7 PALSFit Results from the Silicon and Graphite PALS Spectra

4.7.1 Extraction of the Resolution Function from Silicon

The silicon spectra were analyzed in PALSFit to extract the spectrometer's time resolution function. Appendix D gives an overview of the PALSFit program, its use, and

structure. A two lifetime analysis was chosen for the determination of the resolution function, with the first lifetime fixed at 219 ps, the lifetime of positrons in a pure silicon crystal lattice structure. The second lifetime was an iterated value with an initial guess of 385 ps corresponding to the accepted range of kapton positron lifetimes from the literature. Initial guesses for the parameters of the Gaussian components of the resolution function were also provided from which PALSFit iterated to a stable solution. The body of PALS work shows that for a three-Gaussian resolution function, two of the Gaussians will have a FWHM near that of the Co-60 time resolution. The combined intensity of these Gaussians will be 96 or 97%. The third Gaussian has a greater FWHM, small intensity, and is crucial in accurately defining the spectrometer resolution function [9-10,28,31-32]. Variations in the initial guesses for FWHM and shifts did not change the PALSFit results for the resolution function.

Guesses of 200 to 220 ps were used for the FWHM of the first two components and a guess of 400-600 ps used for the third. The intensity used for the third component was 4%, which was arrived at after experimentation with this value, and is in agreement with other studies. Commonly used intensities for the first two components range from 63% and 33% to 52% and 44% [32]. Experience gained with PALSFit and the spectra show that the exact choice of these intensities does not affect overall results for subsequent materials. This is reasonable since the Gaussians are used to build the resolution function similar to how a set of basis functions summed together can be used to build a more complicated function. Each Gaussian has two degrees of freedom, its width (FWHM) and its centroid position, so any relatively small changes in the balance of intensities between the dominant Gaussians will be

reflected in small changes in their FWHM or shift so that the same function is still created. In other words, there is not one unique way to build the resolution function from three Gaussians. What is important for PALS is that the resolution function is represented accurately by whatever set of functions is used to build or represent it.

The results for the silicon data sets are shown below, first for the analog system and then the digital. Values are listed with their associated uncertainty calculated by PALSFit using linear perturbation analysis relating the deviation of the data points themselves to the parameters (lifetime, intensity, etc.). The values that do not have an uncertainty were used as fixed guesses (not iterated) and as such no uncertainty can be established by PALSFit [32]. The column labeled '*Probability* > χ^2' refers to the probability of obtaining a chi squared value equal to or greater than that calculated from the model and data.

Table 4.2. Lifetime and fitting results for silicon from the analog spectrometer

Silicon Dataset Number	τ_1 **(ps) [Silicon]**	τ_2 **(ps) [Kapton]**	I_1 **(%)**	I_2 **(%)**	τ_{avg} **(ps)**	χ^2/ν	**Probability** > χ^2 **(%)**	**No. Counts**
Set 1	219	387 ± 5.9	61.9 ± 2.7	38.1 ± 2.7	283	0.986	43%	1.73×10^6
Set 2	219	386 ± 3.2	62.4 ± 2.5	37.6 ± 2.5	285	1.023	63%	1.91×10^6
Set 3	219	385.9 ± 3.6	61.9 ± 1.5	38.1 ± 1.5	283	1.002	52%	1.89×10^6

Table 4.3: Resolution function results for the analog spectrometer

Resolution Function Parameters	**Gaussian 1**	**Gaussian 2**	**Gaussian 3**
Set 1: FWHM (ps)	210.2 ± 1.8	284.9 ± 7.9	691.3 ± 86
Intensity (%)	63%	33%	4%
Shift (ps)	0.0	-71.7 ± 5.3	8.3 ± 55
Set 2: FWHM (ps)	213.2 ± 1.3	281.1 ± 5.6	802.1 ± 60.3
Intensity (%)	63%	33%	4%
Shift (ps)	0.0	-93.0 ± 13.8	-20.6 ± 28.7
Set 3: FWHM (ps)	214.9 ± 2.7	249.4 ± 6.3	486.7 ± 29.9
Intensity (%)	58%	38%	4%
Shift (ps)	0.0	-17.2 ± 8.6	128.5 ± 24.5

Table 4.4. Lifetime and fitting results for the digital system with silicon

Silicon Dataset Number	τ_1 (ps) [Silicon]	τ_2 (ps) [Kapton]	I_1 (%)	I_2 (%)	τ_{avg} (ps)	χ^2/ν	Probability > χ^2 (%)	No. Counts
Set 1	219	384.0 ± 5.6	72.6 ± 1.5	27.4 ± 1.5	**264**	0.933	22%	1.05×10^6
Set 2	219	387	70.1 ± 0.4	29.9 ± 0.4	**269**	0.965	37%	1.12×10^6
Set 3	219	377.8 ± 4.3	70.8 ± 0.9	29.2 ± 0.9	**265**	1.092	83%	1.16×10^6

Table 4.5. Resolution function results for the digital spectrometer

Resolution Function Parameters	Gaussian 1	Gaussian 2	Gaussian 3
Set 1: FWHM (ps)	214.8 ± 5.3	250.9 ± 8.4	498.3 ± 66.3
Intensity (%)	52	44	4
Shift (ps)	0	-6.9 ±11.4	-15.0 ± 32.2
Set 2: FWHM (ps)	210.6 ± 4.9	202.9 ± 6.6	426.0 ± 47.0
Intensity (%)	52	44	4
Shift (ps)	0	69.3 ± 10.6	211.6 ± 19.4
Set 3: FWHM (ps)	209	252.7 ± 3.5	--
Intensity (%)	53	47	--
Shift (ps)	0	0.3 ± 5.7	--

4.7.1.1 Discussion of the Silicon Results

Tables 4.2 and 4.4 show the lifetimes, intensities, average lifetime, fitting statistics, and total number of counts collected for the analog and digital silicon PALS spectra. The intensities indicate the relative proportion of positrons annihilating in the silicon versus the kapton foils. The analog results suggest that approximately 62% of the positrons annihilate in silicon and 38% in the kapton, while the results from the digital system show a relative intensity closer to 70% for silicon and 30% for kapton. The intensities from the digital system concur with studies done for the fraction of annihilations occurring in source supporting foils for PALS experiments. N. Djourelov et al., for example, performed studies

on positron annihilation in kapton foils for various thicknesses of kapton and obtained a fit with an approximate 70/30% prediction for similar thickness [20].

The good fitting statistics and the correct iteration of the kapton lifetime and intensity show that the extraction of the resolution function from the silicon is valid. Furthermore, the results showed stability across the changing of the 'non-model' parameters – those that do not directly enter into Equation 4.6 as the b_i – such as the fitting range and background subtraction. In other words, when the fitting range was modified, the variation of the results (kapton lifetime, lifetime intensities, fitting statistics, resolution function etc.) was small and within the reported uncertainty values. When this is not the case, more counts are usually required to remedy this or the material possesses lifetimes that are too many or too close to one another to be properly resolved [32].

The resolution functions of the analog and digital systems shown in Tables 4.3 and 4.5 were similar in terms of the lifetimes, intensities, and shifts. Some variation between the two is expected because the timing algorithms and means of processing data are somewhat different. The first and third sets were also tested with two Gaussian components for the resolution function under the hypothesis that the rejection might filter out some events, such as backscatter events, that contribute to the distortion of the resolution function. Further testing with the collection of more counts and/or using materials that have only one or two well-known and documented lifetimes would show more conclusively if a resolution function represented by two Gaussians is feasible for a digital system.

The results from the digital system, Tables 4.4 and 4.5, were characterized by a lower average lifetime than the results from the analog system and a ratio of silicon to kapton

intensities closer to what was expected from the literature [20]. This is due to the nearly identical lifetime values but differing intensities. Data from both systems iterated to the correct range of the kapton lifetime but the relative values of the silicon and kapton intensity from the digital system best matched studies in the literature.

4.7.2 Results of the PALSFit Analysis for the Graphitic Materials

Obtaining results for the silicon samples was more straightforward than for the graphite samples since the lifetimes were known in advance through previous studies. One pertinent PALS study on pyrolytic graphite and reactor grade graphite, however, was done in the past by Iwata. It provided strong results for more highly oriented graphites and explained less about reactor grade and pyrolytic graphite. Iwata's results on high purity, highly ordered and annealed graphites showed a consistent lifetime for positrons in the perfect crystalline graphite structure of about 200 ps and a second lifetime of about 400 ps that is attributed to positron trapping at grain boundaries [7]. The data is shown below in Table 4.6.

Table 4.6. Iwata's lifetime results for various types of graphite [7]

Material	τ_1 (ps)	τ_2 (ps)	I_1 (%)	I_2 (%)	τ_{ave} (ps)	χ^2/ν
Glassy Carbon	261	477	13.3	86.7	448	1.36
Pyrolytic Graphite (as-deposited)	200	444	19.4	80.6	397	1.37
Nuclear Graphite	213	422	42.3	57.7	334	1.23
Pyrolytic Graphite (3000 °C @ 1h)	160	408	40.5	59.5	308	1.24
Pyrolytic Graphite (3000 °C @ 4h)	178	394	60.2	39.8	264	1.09
Natural Powder Graphite (Compacted)	208	400	70.6	29.4	264	1.18
Pyrolytic Graphite (Monochromator Grade)	206	400	90.2	9.8	225	1.12
Natural Flake Graphite	214	394	92.2	7.8	228	1.28

The graphite types are listed in order of increasing structural perfection and purity, as determined independently through the testing of other physical properties [7]. A trend of a first lifetime approaching 200 ps and approaching about 400 ps for the second lifetime is clear with the progression of graphite types down the table. The trend of the intensities also matches the listed order of graphite in increasing perfection as the value of the first intensity tends to increase and the second intensity decrease. More highly ordered graphite materials have larger regions of perfect structure, larger grains of these regions, and as a result fewer grain boundaries and therefore fewer microstructural irregularities. Iwata's two-lifetime analyses on reactor grade and pyrolytic graphite samples yielded second lifetimes (τ_2) greater than the 400 ps result obtained for more perfect graphitic microstructures. Iwata hypothesized that other microstructural features were present but none of his three-lifetime fits converged or produced reasonable results to confirm this [7].

Additionally, the results of the analyses were more sensitive to changes in the fitting range and background range selected than for the silicon. This is expected since the graphites have more microstructural features and hence lifetimes than the high purity silicon, but is also an indication that better statistics (more counts) might be beneficial, as discussed later. The next sections present the results of the PALSFit analyses for the reactor grade, pyrolytic, and foam graphites, including both the analog and digital data sets.

4.7.2.1 Reactor Grade Graphite

The results for the three reactor grade graphite datasets are shown below. The table shows all results where a two-lifetime model was assumed. Each entry is labeled by the

number of lifetimes fit and whether the data is from the analog (A) or digital (D) system. The label *2τA*, for example, means that the data on that row is derived from the analog spectrometer and analyzed using a two-lifetime fit. The column containing the probability of obtaining a reduced chi squared value greater than that fit by the model is represented by $P > \chi^2$. Lifetime and intensity values are reported with their associated one-sigma uncertainty as calculated by PALSfit. Lifetime values presented without an uncertainty were input to PALSFit as a fixed constant and as such cannot have a calculated uncertainty. A lifetime value was occasionally fixed if the results were not consistent with the data sets or bore no resemblance to the typical values found in graphite.

Table 4.7. PALSFit results for reactor grade graphite

Type of Fit	τ_1 (ps)	τ_2 (ps)	I_1 (%)	I_2 (%)	τ_{avg} (ps)	χ^2/λ	$P > \chi^2$ (%)	No. Counts
Set 1								
2τ A	201 ± 6.7	459.8 ±3.4	27.4 ± 1.5	72.6 ± 1.5	390	1.168	99%	$1.72x10^6$
2τ D	209 ± 8.2	412 ± 4.5	30 ± 2.5	70.0 ± 2.5	351	1.021	61%	$1.24x10^6$
Set 2								
2τ A	203 ± 7.2	461 ±1.8	29.2 ± 0.5	70.8 ± 0.5	388	1.260	99.9%	$1.79x10^6$
2τ D	210 (F)	389.6 ± 2.4	31 ± 0.9	69.0 ± 0.9	334	1.111	87%	$1.15x10^6$
Set 3								
2τ A	197.5 ± 5.1	470.4± 3.0	29.3 ± 1.2	70.7 ± 1.2	390	1.189	99%	$2.11x10^6$
2τ D	222.1 ± 8.8	418.4 ± 5.3	32.0 ± 3.0	68.0 ± 3.0	355	1.083	83%	$1.40x10^6$

Analog and digital results for a two-lifetime fitting are in good agreement amongst each other and Iwata for the first lifetime of about 200 ps. The lifetimes iterate to the values shown without dependence on the specific guess used. In other words, the result does not change if the guess is 150 ps or 250 ps instead of a value near 200 ps. Fitting statistics for the digital system are better than the analog. The digital results yield a first lifetime in the range of 209 ps to 222 ps with an uncertainty of about 8 to 9 ps as calculated by PALSfit.

The analog results for the first lifetime range between 197 ps and 203 ps, but differ from the digital results more greatly for the second lifetime. The second lifetime from the analog data lies between 460 ps and 470 ps while for the digital system it lies between about 410 and 420 ps, with the exception of the second set where it is about 390 ps. The average lifetime is otherwise consistent across data sets from the same spectrometer, so this second set seems to be an anomaly since the average lifetime value of 334 ps differs from the approximately 353 ps value from the other data sets.

The results of the digital system agree most closely with the data from Iwata reported in Table 4.6 which show a 213 ps first lifetime, 422 ps second lifetime, and 42% and 58% relative intensity between the lifetimes. This is in reasonable agreement with the approximately 30% and 70% relative intensity of the first and second lifetimes found from the digital system since some differences are to be expected among different samples of reactor grade graphite. As seen in Table 4.5, there is a large difference between the intensities of Iwata's pyrolytic and reactor grade graphites, (20% and 80% compared to 42% and 58%) so it is reasonable that graphites from different sources may show some variation but still fall between the range of intensities between these two types of graphite. Furthermore, the mean lifetime of about 350 ps is closer to the 334 ps value found by Iwata than the analog system's results of 390 ps. The mean lifetime is a characteristic of the data in the spectrum and is independent of the number of lifetimes used in the fit. In the data above, it did not matter whether two or three lifetimes were fit or whether the second and third lifetimes made sense, the mean lifetime was always the same. The mean lifetime is less difficult to obtain than many lifetimes [1]. As such, the differences in mean lifetime are most

likely due to differences between the reactor grade graphite specimens used in this study and in Iwata's. Overall, the better results from the digital system are attributed to its greater flexibility in timing and the ability to optimize the constant fraction timing level.

4.7.2.2 Pyrolytic Graphite

Results from PALSFit for the pyrolytic graphite samples are shown in Table 4.8. The pyrolytic graphite has the highest mean lifetime of the graphites studied in this work and the next to highest mean lifetime of the graphites studied by Iwata, next only to glassy carbon, a non-crystalline, non-graphite substance [41]. The pyrolytic graphite structure contains regions of oriented graphite and showed a first lifetime near 200 ps for the analog system and closer to 220 ps for the digital system. The intensity of this lifetime component was about 20% for the data from the digital system and closer to 15% for the data from the analog system. The second lifetime ranged from 421 ps to 425 ps with an intensity of about 80% for the data from the digital system and ranged from 477 to 488 ps with a lifetime of about 85% for the data from the analog system. The Iwata data yielded a 200 ps first lifetime with an intensity of about 20% and a 444 ps second lifetime with an intensity of about 80%.

Table 4.8. PALSFit results for pyrolytic graphite

Type of Fit	τ_1 (ps)	τ_2 (ps)	I_1 (%)	I_2 (%)	τ_{avg} (ps)	χ^2/ν	$P > \chi^2$ (%)	No. Counts
Set 1								
2τ A	204.6 ± 12.1	476.9 ± 3.4	15.9 ± 1.5	84.1 ±1.5	435	1.063	82%	$1.82x10^6$
2τ D	226.2 ± 13.4	425.5 ± 4.3	20.6 ± 2.9	79.4 ± 2.9	384	1.011	56%	$1.36x10^6$
Set 2								
2τ A	203	481.8 ± 1.6	18.5 ± 0.5	81.5± 0.5	431	1.36	100%	$1.82x10^6$
2τ D	210	422.1± 3.1	21.5 ± 0.9	78.5 ± 0.9	377	0.956	36.3%	$1.22x10^6$
Set 3								
2τ A	183.5 ± 9.2	477.7 ± 2.5	15.3 ± 1	84.7 ± 1	435	1.048	76%	$1.64x10^6$
2τ D	224. ± 15.7	421.6 ± 3.7	18.4 ± 3.0	81.6 ± 3.0	388	1.041	69.5%	$1.06x10^6$

As with the reactor grade graphite, the results from the digital system match the Iwata results more closely, as seen by the comparison of the lifetimes listed above as well as the mean lifetime values, which were about 384 ps for the data from the digital system, 435 ps from the analog system, and 397 ps from Iwata's study. In addition, the fitting statistics were also better for the data from the digital system. Some differences between the results of this work and Iwata's are expected since pyrolytic graphites are produced with a wide range in degree of grain orientation or mosaic spread.

The data from the pyrolytic graphite was more sensitive to changes in fitting range and background than the reactor grade graphite data, but still fit well. Three-lifetime fits were attempted to see if a third lifetime could be inferred from the data but all such fits yielded inconsistent results – sometimes a third lifetime with a very low lifetime (near zero ps), one with a high lifetime and even larger uncertainty, and others where the first two lifetimes had to be fixed in order to get a third lifetime on the order of 500-600 ps. Even in this last case there was significant variation in the results and much larger uncertainties. Overall it was not possible to show that a third lifetime made a better fit and more sensible results. Section 5.2 outlines possible means for improvement of the experimental methods and setup.

4.7.2.3 Foam Graphite

The PALSFit results for the foam graphite are shown below in Table 4.9. The foam graphite exhibits the smallest mean lifetime of the graphite materials studied in this work. This is due to the first lifetime which is on the order of 125 ps with an intensity of over 20%

and a second lifetime that is under 400 ps. These lifetimes are significantly smaller than the approximately 200 ps first lifetime and 415 ps or greater second lifetime in the other graphites studied. The analog data shows a first lifetime ranging from about 119 ps to 140 ps, and the digital data a range of about 122 ps to 131 ps. The second lifetime for the analog data ranges between 371 ps and 381 ps for the two-lifetime analog results, 337-357 ps for the three-lifetime analog results, and 317-338 ps for the digital results.

The value of the first lifetime matches the lifetime of para-positronium, whose theoretical value is 129.3 ps [1]. Positronium forms in regions of low electron density, plentiful in the porous graphite foam. Other studies have found a lifetime of about 125-130 ps in porous materials such as porous silicon and ascribed it to para-Ps [49,53,54].

Table 4.9. PALSFit results for foam graphite

Type of Fit	τ_1 (ps)	τ_2 (ps)	I_1 (%)	I_2 (%)	τ_{avg} (ps)	χ^2/ν	$P > \chi^2$ (%)	No. Counts
Set 1								
2τ A	138.9 ± 4.9	380.9 ± 3,8	31.9 ± 1.3	68.1 ± 1.3	304	1.031	67.0%	$1.65x10^6$
2τ A	129 (f)	374.1 ± 1.8	29.4 ± 0.5	70.6 ± 0.5	302	1.039	70.4%	$1.65x10^6$
2τ D	125.3 ± 5.3	330.3 ± 2.1	22.6 ± 1.1	77.4 ± 1.1	284	1.046	69.8%	$1.27x10^6$
Set 2								
2τ A	128.1 ± 3.6	371.6 ± 1.9	28.9 ± 0.8	71.1 ± 0.8	301	1.184	99.0%	$2.03x10^6$
2τ D	122.0 ± 4.4	317.1 ± 1.9	24.0 ± 1.1	76.0 ± 1.1	270	0.919	18.0%	$1.73x10^6$
Set 3								
2τ A	126.5 ± 3.9	376.9 ± 2.8	29.7 ± 0.9	70.3 ± 0.9	303	1.050	75.8%	$1.60x10^6$
2τ D	130.9 ± 5.4	338.9 ± 2.4	24.4 ± 1.2	75.6 ± 1.2	288	0.983	43.9%	$1.10x10^6$

The first lifetime, with an average value of 126 ps across the digital system data sets is attributed to the annihilation of para-Positronium in pores, while the second lifetime must be associated with the graphite itself. Neither a lifetime of 200 ps corresponding to the perfect graphite crystalline structure nor a lifetime of 400 ps corresponding to graphite grain boundaries was found. The second lifetime value, however, does lie between these two

values and may represent the two lifetimes combined into one. In interpreting the second lifetime, it is reasonable to focus on the results from the digital system since its results for the reactor grade and pyrolytic graphites were in agreement with published data. As such, it is observed that the second lifetime in foam (average of 329 ps) was close to the reactor grade graphite mean lifetime of 334 ps. It is conceivable that the graphite component of the foam graphite would yield lifetime results similar to that of the reactor grade graphite, explaining the value of the second foam lifetime and attributing it to the graphite present in the sample. Three-lifetime fits were attempted for the data from each of the graphite samples but the results did not converge to realistic values and did not have acceptable fitting statistics.

Chapter 5
Conclusions and Future Work

5.1 Conclusions

The purpose of this research was three-fold: to evaluate the use of the new $LaBr_3$(Ce) scintillation material for use in PALS compared to the standard BaF_2 material, to design and build a digital PALS spectrometer and improve its time resolution and performance in comparison to an analog system with the same detectors, and to obtain lifetime data on reactor grade, pyrolytic, and foam graphites. The $LaBr_3$(Ce) material was found to have a slightly better time resolution due to its combination of fast scintillation decay and its superior scintillation light production as compared to BaF_2. Furthermore, its excellent energy resolution simplified the task of setting energy windows for the Start and Stop channels of the spectrometer.

A digital PALS spectrometer was built using both BaF_2 and $LaBr_3$ scintillation detectors and a LeCroy WaveRunner 6100A digital oscilloscope. Pulse timing was accomplished using a computer code that ran on the oscilloscope itself or with off-line processing when a single, smaller data set was analyzed many times for timing optimization. The digital spectrometer was found to have an improvement in time resolution over the analog spectrometer for both detector materials. This was due mainly to the flexibility allowed by the digital system to optimize the constant fraction percentage used for time

pickoff on the detector pulses. The rejection of spurious pulses had little effect on the time resolution.

PALS measurements were carried out on reactor grade graphite, pyrolytic graphite, and foam graphite using the $LaBr_3$ scintillation material in an arrangement that allowed the simultaneous collecting of data via a traditional analog pulse processing and timing system as well as the digital oscilloscope. This allowed comparison between the two systems for the same input, and the results showed that the digital system produced more accurate and consistent results than the analog system. The reactor grade and pyrolytic graphite data from the digital system showed a first lifetime ranging from about 210 ps to 225 ps, a result in good agreement with published data on the materials. These values correspond to the lifetime of positrons in a perfect graphite lattice structure. These two graphites also showed a second lifetime of about 410 to 425 ps, close to published data. Published data on very highly oriented graphites showed that a 400 ps lifetime is found in crystalline graphite due to positron trapping at grain boundaries [7]. The foam graphite was shown to have two lifetimes of about 125 ps and 335 ps. The first lifetime is attributable to the annihilation of para-positronium formed in voids and pores, with a theoretical lifetime of 129.3 ps [1]. The 335 ps lifetime is due to the graphite in the graphite foam and appears to be a combination of the 200 ps and 400 ps lifetimes, as it almost exactly matches the mean lifetime of the reactor grade graphite.

5.2 Future Work

Various aspects of the experiment or experimental methods could potentially be improved upon to yield better or more resolvable data or to explore questions or aspects

related to the physics behind the PALS experiment. Studies using simulated, artificially produced lifetime spectra show that a PALS data set is more resolvable with more counts as opposed to having a better timing resolution to the detriment of count rate [35,36]. Energy windows that are too wide, however, can allow more coincidences from scattering events that can corrupt the data. The geometry of the experimental setup also influences the scattering and the coincidence count rate. A study focusing specifically on optimizing the geometry of the experimental setup and the energy windows for count rate and data resolvability could be performed to determine an ideal or more optimized configuration. This could involve comparisons between the count rate and resolution function of different geometries and repeated measurements on a material utilizing different geometries. The effect of the simultaneous detection of 511 keV annihilation quanta in both detectors on the resolution function and quality of data should also be investigated to see if this warrants the placement of the source outside of the detector, as this placement significantly decreases the coincidence count rate. If many more counts could be collected in a practical time the graphite data could yield even more conclusive results.

The duration of data collection is limited because the equipment is not steady over a long period of time without recalibration. The main parameter that will drift over time is the time-zero, the channel at which coincidences with zero time difference are binned. Since the results are highly sensitive to the time-zero, data collected over a long period where this value drifts will not yield good results [28, 32, 50]. Thus it is desirable to have as high a count rate as possible so more counts can be taken within a few to several days at most for an individual run. Data could be taken over several sessions with recalibration of the resolution

between sessions. Combining this data into one data set could be investigated as a means of increasing the total number of counts for a given material while avoiding drift of measurement parameters. Another way to increase the usable amount of data collected is to use a thinner 7 μm kapton foil to seal the ^{22}Na source. This would increase the number of positrons annihilating in the test material without decreasing the count rate or negatively affecting the timing resolution.

Improvements in timing resolution that do not come at the expense of count rate could also be pursued. For instance, a time resolution of 139 ps for a standard analog system with BaF_2 detectors has been achieved [28]. This was accomplished with a few hardware differences as compared to this work, including the cancellation of magnetic fields in the region of the PMTs to decrease the electron time spread; modifications to the voltage divider of the PMT to increase the photocathode and first few dynode voltages; and modifications to the PMT to take the detector signal from an earlier dynode than the last dynode [28]. There are also a few PMTs available with a smaller rise time than the ones used in this work, such as the Hamamatsu H3378 (R2083Q). An improvement in the timing resolution is expected for this since a smaller rise time leads to more accurate timing as discussed in Section 2.4.1.

The performance of the digital system was better than that of the analog system. The digital system count rate, however, was about 70% of the analog system count rate. Additional work could be performed for the digital system in terms of investigating the sources of, and means of reducing, the dead time associated with the digital processing and timing calculations. Creating a more computationally efficient algorithm for calculating the

constant fraction timing would be one step toward this goal. It is also possible to perform timing calculations offline by saving coincident pulse pairs to the hard drive of the oscilloscope or to another PC. Subsequent pulse processing and timing could then be performed independently from data collection.

This work also raises the question of the effect or potential effect of digital rejection of pulses on the resolution function. The question of how rejection of pulses or digital manipulation can be tailored to affect the resolution function and whether these could remove the need for a third Gaussian in fitting the resolution function or generally increase the resolvability of the data is unresolved. From a computational standpoint, the difference between using a two-Gaussian and a three-Gaussian resolution function is negligible as the nonlinear least squares fitting process in either case is simple and not time consuming.

References

[1] Krause-Rehberg, Reinhard and H.S. Leipner, *Positron Annihilation in Semi-conductors: Defect Studies,* Berlin: Springer-Verlag, 1999.

[2] Y.C. Jean, P.E. Mallon, and D.M. Schrader ed, *Principles and Applications of Positron and Positronium Chemistry,* Singapore: World Scientific, 2003.

[3] Coleman, Paul ed, *Positron Beams and Their Applications,* Singapore: World Scientific, 2000.

[4] Turner, James E, *Atoms, Radiation, and Radiation Protection, 2nd Edition,* New York: John Wiley & Sons, Inc., 1995.

[5] *Positron Annihilation.* Ed. Delft University of Technology. 16 October 2007. 2007 < http://www.tnw.tudelft.nl/live/pagina.jsp?id=d1242d73-091e-49a6-bafe-23aa21626e3d&lang=en >

[6] J. Moxom, A.G. Hathaway, E.W. Bodnaruk, A.I. Hawari, and J. Xu, "Performance analysis of the intense slow-positron beam at the NC State University PULSTAR reactor," *Nuclear Instruments and Methods in Physics Research A*, vol. 579, pp. 534-537, 2007.

[7] Iwata, Tadao, et al., "Characterization of Graphites by Positron Lifetimes," *Japanese Journal of Applied Physics*, vol. 20, no. 10, pp. 1799-1806, 1981.

[8] M. Eldrup and O. Morgensen, "Positron Lifetimes in Pure and Doped Ice and in Water," *The Journal of Chemical Physics*, vol. 57, no. 1, pp. 495, 1972.

[9] F. Becvar, J. Cizek, I. Prochazka, J. Janotova, "The Asset of ultra-fast digitizers for positron lifetime spectroscopy," *Nuclear Instruments and Methods in Physics Research A*, vol. 539, pp. 372-385, 2005.

[10] K. Rytsola, J. Nissila, J. Kokkonen, A. Laakso, R. Aavikko, K. Saarinen, "Digital measurement of positron lifetime," *Applied Surface Science*, vol. 194, pp. 260-263, 2002.

[11] *Energy Information Administration: Official Energy Statistics from the U.S. Government*, International Energy Outlook 2007. 20 October 2007. Report #DOE/EIA-0484(2007), May 2007.

[12] LaMarsh, John R., and Anthony J. Baratta, *Introduction to Nuclear Engineering*, 3rd. ed., Upper Saddle River, New Jersey: Prentice Hall, 2001.

[13] Ayman I. Hawari, I.I. Al-qasir, A.M. Ougouag, "Investigation of the Impact of Simple Carbon Interstitial Formations on Thermal Neutron Scattering in Graphite," *Nuclear Science and Engineering*, vol. 155, no. 499, 2007.

[14] Knoll, Glen F., *Radiation Detection and Measurement*, 3rd ed., New York: John Wiley & Sons, Inc., 1999.

[15] Ortec® Advanced Measurement Technology. *Ortec 583B Data Sheet*. Feb 2007. Updated 2007, < http://www.ortec-online.com/pdf/583b.pdf >.

[16] Photonis. *Photomultiplier XP20D0 Data Sheet*. December 2006. 4 June 2006, http://www.photonis.com/data/cms-resources/File/Photomultiplier_tubes/spec/XP20D0.PDF

[17] Photonis. *Photomultiplier XP2020/Q Data Sheet*. December 2006. 1 November 2005, http://www.photonis.com/data/cms-resources/File/Photomultiplier_tubes/spec/XP2020Q.PDF

[18] Saint-Gobain Crystals. *BriLanCe 380 Data Sheet*. Accessed December 2006. 2004-2006. <http://www.detectors.saint-gobain.com/Media/Documents/S0000000000000001004/SGC_BrilLanCe380_0506.pdf>

[19] Saoucha, A. transmission into Kapton: The effective mass absorption coefficient of relevance to positron lifetime experiments," *Journal of Applied Physics*, vol. 85, no. 3, pp. 1802-1809, 1999.

[20] N Djourelov and M Misheva, "Source correction in positron annihilation lifetime spectroscopy," *Journal of Physics: Condensed Matter*, vol. 8, pp. 2081-2087, 1996.

[21] Monge, M A and J del Rio, "Positron annihilation in Kapton source-supporting foils," *Journal of Physics: Condesned Matter*, vol. 6, 2643-6, 1994.

[22] Saito, H., Y. Nagashima, T. Kurihara, and T. Hyodo, "A new positron lifetime spectrometer using a fast digital oscilloscope and BaF_2 scintillators," *Nuclear Instruments and Methods in Physics Research A*, vo. 487, pp. 612-617, 2002.

[23] *Advanced Math Package: XMATH.* LeCroy Oscilloscopes and Protocol Analyzers, March 2007, 2007. <LeCroyhttp://www.lecroy.com/tm/Options/Software/XMATH/default.asp>

[24] Saint-Gobain Crystals. *Barium Fluoride Scintillation Material Data Sheet.* Accessed December 2006. 2004-2006. < http://www.detectors.saint-gobain.com/Media/Documents/S0000000000000001004/SGC%20Barium%20Fluoride%20Data%20Sheet%200105.pdf>

[25] Ortec® Advanced Measurement Technology. *Ortec 566 Time-to-Amplitude Converter Data Sheet*. Feb 2007. Updated 2007, < http://www.ortec-online.com/electronics/tac/566.htm>.

[26] Ortec® Advanced Measurement Technology. *Principles and Applications of Timing Spectroscopy*. Feb 2007. Updated 2007, < www.ortec-online.com/**application**-notes/an42.pdf >.

[27] Ortec® Advanced Measurement Technology. *Trump^{TM} PCI-8k/2k PCI Format MCA Plug-in Card and Software* . Feb 2007. Updated 2007, < http://www.ortec-online.com/pdf/trumppci.pdf>.

[28] F. Becvar, J. Cizek, L. Lestak, I. Novotny, I. Prochazka, F. Sebesta, "A high-resolution BaF_2 positron-lifetime spectrometer and experience with its long-term exploitation," *Nuclear Instruments and Methods in Physics Research A*, vol. 443, pp. 557-577, 2000.

[29] Ortec® Advanced Measurement Technology. *Ortec 671 Spectroscopy Amplifier Data Sheet*. Feb 2007. Updated 2007, < http://www.ortec-online.com/electronics/amp/671.htm>.

[30] Peter Kirkegaard and Morten Eldrup, "PositronFit: A Versatile Program for Analysing Positron Lifetime Spectra," *Computer Physics Communications,* vol. 3, p. 240, 1972.

[31] Peter Kirkegaard and Morten Eldrup, "PositronFit Extended: A New Version of a Program for Analysing Positron Lifetime Spectra*," Computer Physics Communication* vol. 7, p. 402, 1974.

[32] Jens V. Olsen, Peter Kirkegaard, Niels Jorgan Pedersen, and Morton Eldrup, "PALSfit: A Computer Program for Analysing Positron Lifetime Spectra: Part 1 – Mathematical and Physical Foundation." November 9, 2006.

[33] Dorikens-Vanpraet, L, D. Segers, M. Dorikens, "The Influence of Geometry on the Resolution of a Positron Annihilation Lifetime Spectrometer," *Applied Phyiscs* 23, 149-152, 1980.

[34] Rajainmäki, H., "A High Resolution Positron Lifetime Spectrometer with BaF_2 Scintillators," *Applied Physics A*, vol. 42, pp. 205-208, 1987.

[35] Dannefaer, S., "On the Effect of Backscattering of Gamma Quanta and Statistics in Positron Annihilation Lifetime Measurements," *Applied Physics A* vol. 26, pp. 255-259, 1981.

[36] Dryzek and J. Kansy. "Comparison of Three Programs: Positronfit, Resolution, and LT Used Deconvolution of Positron Lifetime Spectra," *Nuclear Instruments and Methods in Physics Research A*, vol. 380, pp. 576-581, 1996.

[37] K. Wharburton, "DBLCON: A Version of POSITRONFIT with Non-Gaussian Prompt for Analysing Positron Lifetime Spectra," *Computer Physics Communication 13*, 371-379, 1978.

[38] Puff, W. PFPOSFIT: A New Version of a Program for Analyzing Positron Lifetime Spectra with Non-Gaussian Prompt Curve. Computer Physics Communication 30 (1983) 359-368.

[39] B Somieski, TEM Staab, R. Krause-Rehberg, "The data treatment influence on the spectra decomposition in positron lifetime spectroscopy Part 1: On the interpretation of multi- component analysis studied by Monte Carlo simulated model spectra," *Nuclear Instruments and Methods in Physics Research A*, vol. 381, pp. 128-140, 1996.

[40] W.G. Schmidt and W.S. Verwoerd, "Annihilation of delocalized positrons: a comparison of diamond and silicon," *Physics Letters A*, vol. 222, pp. 275-280, 1996.

[41] E. Fitzer, K.-H. Kochling, H.P. Boehm and H. Marsh, "Recommended Terminology for the Description of Carbon as a Solid (IUPAC Recommendations)," *Pure & Applied* Chemistry, vol. 67, no.3, pp. 473-508, 1995.

[42] Y.C. Jean, K. Venkateswaran, E. Parsai, and K.L. Cheng, "Temperature Dependence of Positron Annihilation Characteristics on the Surfaces of Graphite Powders," *Applied Physics A*, vol. 35, pp. 169-176, 1984

[43] Michio Shimotmai, Tadao Iwata, Tohru Takahashi and Masao Doyama, "Vacancy in Graphite: Positron Studies," *Journal of the Physical Society of Japan*, vol. 52, no. 2, pp. 694-702, 1983.

[44] *Highly Oriented Pyrolytic Graphite*. SPI Supplies. "High quality HOPG for scientific research and graphite HOPG monochromators" 5 Dec 2007 < http://www.2spi.com/catalog/new/hopgsub.shtml > Dec 2007

[45] *High Thermal Conductivity Graphite Foam.* James Klett, Oak Ridge National Laboratories. 5 Dec 2007. <http://www.ms.ornl.gov/researchgroups/CMT/FOAM/foams.htm>, 2007.

[46] *POCO Foam Properties and Characteristics*. 5 December 2007. <http://www.poco.com/tabid/130/Default.aspx> 2007.

[47] S. Dannefaer, D. Keer, D. Craigen, T. Bretagnon, T. Taliercio, and A. Foucaran. "A positron annihilation investigation of porous silicon," *Journal of Applied Physics*, vol. 79, No. 12, pp. 9110-9117, 1996.

[48] Bevington, Philip and D. Keith Robinson. *Data Reduction and Error Analysis for the Physical Sciences*, New York: McGraw-Hill, Inc., 1992.

[49] T. Onitsuka, H. Ohkubo, M. Akenaka, N. Tsukuda, and E. Kuramoto, "Positron lifetime calculation for defects and defect clusters in graphite," *Journal of Nuclear Materials*, vols. 283-287, pp. 922-926, 2000

[50] J. Nissila, M. Karppinen, K. Rytsola, J. Oila, K. Saarinen, P. Hantojarvi. "The stabilization of a positron lifetime spectrometer with a high-accuracy time reference," *Nuclear Instruments and Methods in Physics Research A*, vol. 466, pp. 527-537, 2001.

Appendices

Appendix A: Histogramming Program to Determine Pulse Rejection Criteria

The rejection criteria used for pulse rejection were determined by histogramming the baseline parameters and selecting a range from the histograms. The program written to accomplish this is shown below. It consists of a *for* loop that is used to read each text file containing a pulse pair. Within this loop, it calculates the minima, maxima, position of the minima and maxima, the baseline mean value, and baseline rms value for each pulse and allocates each value into a separate dedicated matrix named after the information it contains. The variable/matrix *pulse1maxes*, for instance, will have a length of 10,000 for a set of 10,000 pulses and its entries will contain the maximum voltage value of the first pulse (pulse 1) from each text file. The variable *pulse2maxes* will contain the maximum voltage value of the second pulse from each text file. Once the program was run, the variables were saved so the program would not have to be re-run to recall the information. Each matrix was then histogrammed using the Matlab *hist* command and these histograms were also saved for convenient recall.

```
% This program takes the text file pulses and compiles information
% about the spread of the min/max voltage, the spread of the coordinate of
% the min/max position, and information about the baseline.

nfile = 10000; % number of files/pulses to analyze
result = zeros(nfile,1); % used to initiate the matrices
iones = 0; itens = 0; ihunds = 0; ithous = 0; iten_thous = 0;
% variables to count through the full number of pulses:
% start with file number zero, the first file.

%matrices of zeros to store the mins, maxes, positions of
%extrema, and so forth.

template = zeros(nfile,1);  %preallocation increases speed
pulse1mins = zeros(nfile,1);  % voltage value of min
pulse2mins = zeros(nfile,1);
pulse1maxes = zeros(nfile,1); % voltage value of max
```

```
pulse2maxes = zeros(nfile,1);
minpos1 = zeros(nfile,1);     % position of min
minpos2 = zeros(nfile,1);
maxpos1 = zeros(nfile,1);     % position of max
maxpos2 = zeros(nfile,1);
baseline1 = zeros(nfile,1);   % value of baseline
baseline2 = zeros(nfile,1);
rms1ct = zeros(nfile,1);      % RMS value of baseline
rms2ct = zeros(nfile,1);

for ifile=0:nfile-1  % loop that goes through all 10,000 pulses
  file1 = ['F6PosPulse2_' num2str(iten_thous) num2str(ithous)...
           num2str(ihunds) num2str(itens) num2str(iones) '.txt'];
% creates the filename of the pulse pair for each iteration of the loop

  if ithous == 9 && ihunds == 9 && itens == 9 && iones == 9
      iten_thous = iten_thous + 1;
      ithous = 0; ihunds = 0;  itens = 0; iones = 0;

  elseif ihunds == 9 && itens == 9 && iones == 9 %takes care of thousands
                                                 %place
      ithous = ithous + 1; ihunds = 0;  itens = 0; iones = 0;

  elseif itens == 9 && iones == 9 % takes care of hundreds place
      ihunds = ihunds + 1; itens = 0; iones = 0;

  elseif iones == 9 %takes care of tens and ones place
      iones = 0;  itens = itens + 1;
  else
      iones = iones + 1;  % if it's NOT 9 I can just add one to it
  end

  %the saved concatenated pulses contain pulse 1 in 1:4000 and pulse 2
  %in 4051:8050 (this can change based on the pulse set used)

  p1 = dlmread(file1,' ',5,0);
  X = p1(1:4000,2); %just taking voltage info (second column)
  Y = p1(4051:8050,2); % padded 50 zeros between the pulses.

  % mines baseline information
  BL1 = X(1:1500); BL2 = Y(1:1500); n = length(BL1);
  bmean1 = mean(BL1);  % average of the baseline
  bmean2 = mean(BL2);
  rms1 = norm(BL1)/sqrt(n); % rms value of the baseline
  rms2 = norm(BL2)/sqrt(n);

  baseline1(ifile+1) = bmean1;
  baseline2(ifile+1) = bmean2;
  rms1ct(ifile+1) = rms1;
  rms2ct(ifile+1) = rms2;

  % mines minima and position of minima
  [a b] = min(X);  % [min_value min_index]
```

```
  [c d] = min(Y);

  pulse1mins(ifile+1) = a; % assigns min value of the pulse1
                           %to the matrix of min values for pulse 1
  minpos1(ifile+1) = b;
  pulse2mins(ifile+1) = c;
  minpos2(ifile+1) = d;

  % mines maxima and position of max
  [e f] = max(X);
  [g h] = max(Y);

  pulse1maxes(ifile+1) = e;
  maxpos1(ifile+1) = f;
  pulse2maxes(ifile+1) = g;
  maxpos2(ifile+1) = h;

end

  pulse1maxes  % will display the matrix of pulse 1 maximum values

  %All of the matrices are stored in Matlab and are histogrammed
  %using the 'hist' command
```

Appendix B: Pulse Rejection Time Resolution Results

The following table outlines a series of tests performed on a set of 10,000 pulses from the $LaBr_3$ detectors using the ^{60}Co source. Various criteria were set for the pulses' baseline, max/min voltage, position of the max/min voltage and the FWHM and number of pulses accepted were recorded. Criteria on the pulse minimum and maximum values excluding all values outside the major part of the distribution of these values were the most effective.

Table B.1. Criteria and results of digital filtering of detector pulses on the timing response to Co-60

Rejection Case #	FWHM (ps)	# Pulses Accepted (out of 10,000)	Description
1	188 ± 4	955	Baseline 1 criteria: RMS < 15 mV, |Mean| < 15 mV, RMS-|Mean| < 1mV
2	N/A: too few pulses	320	Same as (1) but on both Baselines 1 & 2 (both pulses)
3	196 ± 2	7490	Baseline 1 criteria: RMS < 14 mV, |Mean| < 14 mV, RMS-|Mean| < 4mV **(3-5 focus on RMS-|Mean| difference)**
4	196 ± 2	6375	Baseline 1 criteria: RMS < 14 mV, |Mean| < 14 mV, RMS-|Mean| < **3mV**
5	195 ± 2	4157	Baseline 1 criteria: RMS < 14 mV, |Mean| < 14 mV, RMS-|Mean| < **2mV**
6	184 ± 2	6023	Same as (3) but with minimum voltage criteria/window: -250 mV to -350 mV accepted. (**6-8 repeat 3-5 but with voltage criteria added**)
7	185 ± 3	5136	Same as (4) but with [-250 to 350 mv] voltage window criteria
8	185 ± 4	3350	Same as (5) but with [-250 to 350 mv] voltage window criteria
9	197 ± 1	8628	**See how stricter RMS requirement affects the resolution:** RMS11 < 10 mV, RMS21 < 10 mV, [-15 < Mean11 < 5 mV] and [-6 < Mean21 < 12 mV].
10	196 ± 1	8051	**Keep same RMS** criteria as in (9), but cut into Mean distribution: [-10 < Mean11 < 0mV] [-2.5 < Mean21 < 8.5 mV]. **(9-10 focus on rejection based on cutting into the RMS or Mean distribution…see figures)**
11	183 ± 1.4	6836	**Testing the effect of *just* the min voltage criteria.** Pulse1: [-280 to -350 mV], Pulse2: [-284 to -350 mV] (based on histograms). Basic baseline 1 values of 14 mV and means in (9).

Table B.1 (Continued)

12	182 ± 1.4	6681	Pulse1: [-280 to -323 mV] Pulse2: [-284 to -336 mV]
13	180.5 ± 1.7	5445	Pulse1: [-295 to -320 mV] Pulse2: [-295 to -331 mV]
14	197 ± 1.3	9537	Pulse1 min must lie in range: sample pt. [3200-3700] where timescale = 5 ps/pt. Pulse2 in range [2900-3400]. (**14 & 15 are testing based on *position* of the minimum value)**
15	195 ± 1.4	8738	Pulse 1 min in range [3250-3570] Pulse 2 min in range [2965-3300]
16	182 ± 2.3	4095	**16-19: Testing of Baseline 2** (a second baseline testing region in addition to Baseline 1) for BL11: mean is -15 to 5 mV, RMS < 14 mV BL21: mean is -6 to 12 mV, RMS < 14 mV Pulse 1 min: -330 to -280 mV Pulse 2 min: -336 to -284 mV **(above criteria are used for tests 16-19**) Baseline 2's are varied. BL12c: RMS < 12 mV, mean is -17 to 5 mV BL22c: RMS < 8 mV, mean is -9 to 15 mV
17	181 ± 3.5	1391	Same as (16) but with BL12c: RMS - |Mean| < 1 mV BL22c: RMS - |Mean| < 1 mV
18	182 ± 1.9	2055	Same as (16) but with BL12d and BL22d instead: BL12d: RMS < 16 mV, Mean is -20 to 2 mV BL22d: RMS < 15 mV, Mean is -8 to 12 mV
19	178 ± 1.8	2596	Cut more into pulse minimum value distribution since min value was most fruitful for the FWHM Pulse 1 Min: -295 to -314 mV Pulse 2 Min: -300 to -323 mV
20	182 ± 1.7	6543	**20-23 incorporate pulse Maximum Values:** (23) is Normal Baseline 1 with Max 1 criteria: 1.30 to 1.375 V Max 2 criteria: 1.27 to 1.325 V
21	181.5 ± 1.7	6481	Adding Min Voltage Criteria in addition to Max Criteria of (20): Min 1 is -330 to -280 mV Min 2 is -336 to -284 mV
22	180.5 ± 1.7	5256	Narrower Vmin and Vmax limits: Max 1: 1.325 to 1.362 V, Min1: -314 to -295 mV Max 2 is 1.28 to 1.313 V, Min2: -323 to -300 mV
23	181 ± 1.8	4909	Same narrower Vmax of (22) with normal Vmin of (19) Max 1: 1.325 to 1.362 V, Min1: -330 to -280 mV Max 2: 1.28 to 1.313 V, Min2: -336 to -284 mV
24	182 ± 1.6	6601	Repeat of (20) with extremely minor difference in criteria. Testing if the Vmax criteria independently has same effect as the Vmin criteria
25	182 ± 1.7	6537	Repeat of (21) but with extremely small difference in criteria: -323 mV to -280 mV and -284 mV to -336 mV
26	181 ± 1.2	6226	Min 1: -280 mV to -323 mV, Min 2: -284 to -336 mV

Appendix C: PALSFit Data Structure and Data Manipulation Programs

The data obtained from the digital and analog PALS systems (the oscilloscope and MCA emulator, respectively) are not produced in the proper form for use in PALSFit and furthermore, the data cannot be entered from within the graphical user interface. This data must be manipulated into the proper form and manually pasted into the .rcf or .pcf PALSFit input file. The required form is a tabular format specified by a set of FORTRAN identifiers, *xfy.0*, where *x* is the number of data entries per for row, and *y* is the number of characters between right justified entries. For instance, 10f6.0 calls for a matrix of data that has 10 columns and where all entered data is right justified and has six spaces until the next entry. The character *f* specifies that the entries are numbers and restricts their form to integers and must be used in PALSFit [10]. An example representing 60 channels or bins of counts is shown below:

```
   4    18    14    16    11    19    13    18    19    32
  33    49    46    54    63    84    76    96   142   155
 169   193   215   283   296   390   450   500   611   689
 789   914  1075  1245  1482  1677  1923  2132  2481  2708
3147  3532  3982  4420  4899  5465  6008  6782  7438  8136
8935  9514 10478 11186 12188 12972 13674 14533 15646 16452
```

Figure C.1. Sample PALSfit data formatting. Data in such a format must be entered into the .pcf or .rcf input file to represent the lifetime spectrum.

The digital system (oscilloscope) output contained several lines of header followed by two columns of data: the first column was time (time difference calculated between the pulses) and the second column was the number of counts. The analog system output from the MCA emulator had six columns of data. The first column represented a channel number

and the second through sixth columns represent counts in successive channels beginning with the channel number in the first row. An example of the format is shown below for both types of output, with the digital on the left.

-1410 303	5500:	10	9	6	5	12
-1400 371	5505:	8	12	10	9	5
-1390 424	5510:	9	19	11	16	25
-1380 556	5515:	24	34	22	36	32
-1370 799	5520:	55	64	71	73	106
-1360 896	5525:	92	113	157	175	210
-1350 1104	5530:	253	283	367	399	439
-1340 1406	5535:	520	558	695	830	998
-1330 1709	5540:	1100	1323	1401	1682	1886
-1320 2045	5545:	2233	2494	2687	3194	3489
-1310 2427	5550:	3889	4258	4698	5165	5797
-1300 2954	5555:	6437	6902	7412	8222	8740
-1290 3438	5560:	9514	10055	10699	11527	12163

Figure C.2. Format of the data produced by the digital system (left) and the analog system (right). The first column on the left is a time difference, and the number of counts in that bin is in the second column. The analog system's format lists the channel number of the first entry of each row.

A FORTRAN program was written that takes a single column of data and arranges it in a desired format specified by a given number of columns and characters between columns. To manipulate the digital system data into this format it was pasted into Excel, the *Text to Columns* option chosen to place the data into distinct rows, and then the second column was pasted into a text file. The analog system data was similarly pasted into Excel and the five columns of data were copied into Matlab. In Matlab the following program was run to place the data into a single column:

```
function [array] = single(inarray)

%takes an array and breaks it down into one long array with one column.

a = size(inarray);
row=a(1); % num rows
col=a(2); % num cols
num = row*col; % total number of entries
Z = zeros(num,1); % creates a blank single column matrix of the proper
                  % length
```

```
for i=1:row
    for j=1:col
        Z(col*(i-1)+j)=inarray(i,j); %enters the values into the new array
    end
end
array = Z;
```

The following FORTRAN program takes a single column of data and puts it into a tabular format required by PALSFit. The program requires the user to input the name of a file and then reads the file, outputs an error message if the file cannot be opened, and otherwise proceeds to read the data and manipulate it into the proper form. The code is shown below.

```
PROGRAM datamanip
!This program opens a file with a list of data and puts it in a
!multi-column format.  This is intended for use with the positron
!lifetime spectrum data.

IMPLICIT NONE

CHARACTER(len=20) :: filename
INTEGER :: status, ioerr, ioerr1, nvals=0, value

!Get the file name
WRITE(*, '(A)', ADVANCE="NO")"Please enter the name of the PALS data file: "
READ(*,*) filename

!Open file and check for error
OPEN(UNIT = 12, FILE = filename, STATUS = "OLD", iostat = ioerr)
IF(ioerr /= 0) STOP "The file didn't open.  Try again"  ! status must be zero

OPEN(16, FILE = 'data.dat', STATUS = 'NEW', iostat = ioerr1)
! opens file for the data in the new format to be written.


!read in values and write them to the file.
DO
 READ(12, *, iostat = status)value
 IF(status /= 0) EXIT   !exits on error or end of file
 nvals = nvals + 1
 WRITE(16,100,ADVANCE = "NO")value
 100 FORMAT(I6.0)  ! FORTRAN spacing specification
 IF(MOD(nvals,10) == 0) THEN   ! If multiple of 10 start new line
  WRITE(16,200,ADVANCE= "NO")
  200 FORMAT(/)
 END IF
```

END DO

CLOSE(12)

END PROGRAM datamanip

Appendix D: Use of PALSFit

The user's manual supplied with PALSFit provides an in-depth explanation of the mathematical foundation and principles behind the program's calculations and algorithms. It also provides a clear explanation of the input structure of the file containing the positron lifetime spectra data and parameters, called the control file [33]. Even so, a brief tutorial here will supply additional help in learning and using the program.

PALSFit uses a different data file for the resolution fitting and for the positron lifetime fitting, called ResolutionFit (ResFit) and PositronFit (PosFit), respectively. The former file has suffix .rcf and the latter has suffix .pcf, which stand for ResFit control file and PosFit control file. The control files are edited with a standard text editor such as Wordpad or Notepad, and are also manipulated within the PALSFit graphical user interface, shown below in Figure D.1.

The model parameters can be entered directly into the file via a text editor or through the PALSFit graphical user interface. The model parameters for ResFit are the number of Gaussian components comprising the resolution function; the FWHM (ns), Intensity (%), and shift (ns) of each Gaussian component; the channel number for the time-zero (T_0) channel; and the number of lifetime components and their relative intensities. The shift of one of the Gaussian components of the resolution function must be fixed to zero to serve as a reference point for the position of the other components. The rest of the

parameters may be fixed or guessed, with guesses serving as initial values in the iteration process. All of these can be entered, specified, and toggled between fixed or guessed in the PALSFit user interface. There are some additional user inputs that are not model parameters and these are the total number of channels in the input spectrum, the background range (in channels) for subtraction of the chance coincidence background, and the upper and lower fitting range that specifies the range of the total number of channels to fit the model to.

The PositronFit file or module takes the same model parameters as ResFit except for a few differences. The resolution function parameters are all fixed, constant inputs and there is a source correction whereby the user specifies the lifetime and intensity of positrons annihilating in the isotopic source and its surrounding foils (multiple lifetimes and intensities can be entered if appropriate). The resolution function is always fixed in PosFit because it is determined from ResFit and is required to deconvolute experimental spectra where the lifetimes and intensities are not known a priori. The ResFit module also provides an option to run a second iteration cycle with different guesses for lifetimes, intensities, and the time-zero channel. This can be useful for comparing the goodness of fit before and after the source correction or to compare two different fits at the same time, such as a two-lifetime fit and a three-lifetime fit.

The control file itself contains eight different control blocks, or sections. The first allows the user to define the output options. The second contains the data representing the positron lifetime spectrum, including the definition of the FORTRAN data formatting delimiter (i.e. 10f6.0). The third block contains the definition of the channel range used in the fit, the time scale (time interval per channel), and the time zero channel, as a fixed value

or as a guess to be iterated. The fourth contains the resolution function and the fifth contains the lifetime and intensity constraints and guesses. The sixth block contains the range of channels used to define the background subtraction, and the seventh block contains the range of channels over which the total number of counts, and hence the area, of the spectrum is summed. The eighth block contains the source correction information, and is absent in a resolution control file since the purpose of this module is in part to determine the source correction [33].

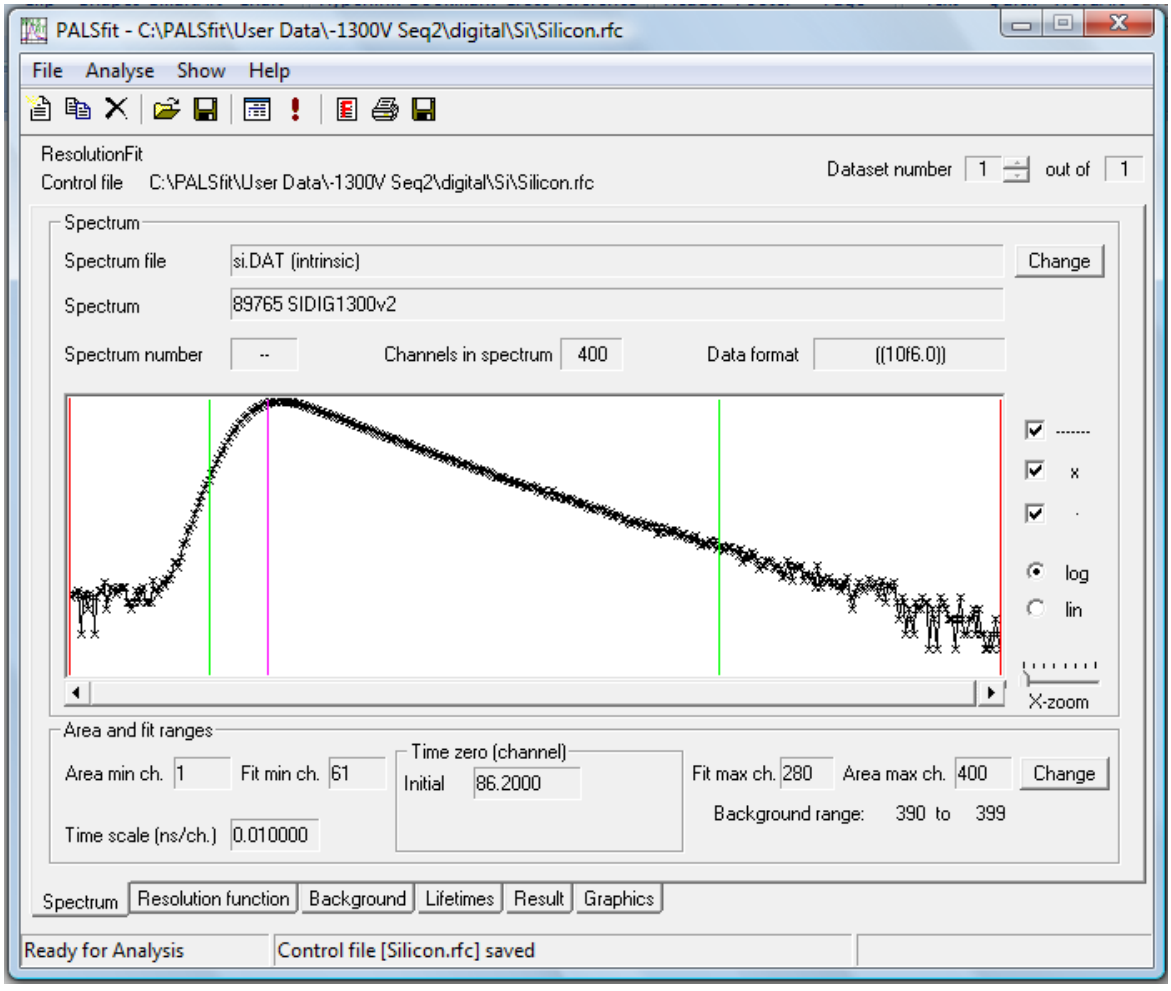

Figure D.1. The primary PALSFit graphical user interface

In general, the easiest way to create a new positron or resolution control file is to copy an existing one provided as an example with the program, or one that already exists based on previous experiments. Then the spectrum data is pasted in and the total number of channels is entered. Each block is clearly marked as to its identity and function, for example block two is labeled *POSITRONFIT DATA BLOCK: SPECTRUM*. The channel ranges in the third, sixth, and seventh blocks should not be outside of the bounds of the new spectra data. This ensures that the program will open successfully. At this point, it is easiest to make all other changes from within the graphical user interface, since it provides a visual link between the ranges entered and their location on the actual positron lifetime spectrum. In the figure above, the red lines correspond to the channel range used in the calculation of the area under the curve (block 7), the green to the region that is fitted by PALSFit (block 3), and the purple line to the time-zero channel (also block 3). Other information is displayed on this screen such as the total number of channels in the spectrum, the time scale (time/channel), and the file name. The channel ranges may be changed by clicking the *Change* button near the bottom right of the interface. The tabs at the bottom of the screen, *Spectrum, Resolution Function, Background, Lifetimes, Result, and Graphics* provide the means of entering the rest of the relevant data and for reviewing the results and graphical representation of the fit to the data. Any changes made in to parameters in the graphical user interface are made in the control file so this is a very convenient and intuitive way to set up the file.

The graphical user interface is also useful because it allows for the fast and efficient user's modification and variation of the fitting parameters between different runs or analyses of the data. The parameters are changed as desired and then the program is run by clicking

the red exclamation mark in the toolbar at the top of the screen or by pressing the word *Analyse* above the toolbar. The analyses take less than a second to perform on modern computers so it is very easy to change the fitting parameters to see how the results change. In general, the results of the fit (lifetimes and their intensities and the resolution function) should remain relatively stable across reasonable portions of the fitting range and time-zero guesses. The results are not expected to be stable, for instance, across a fitting range that incorporates too much of the left-hand side of the spectrum or does not overlap with the bounds of the spectrum at all.

Appendix E: Timing Algorithm Programs

Two nearly identical timing algorithms were used to perform the desired timing on the radiation pulses corresponding to the birth and annihilation of the positrons. Elements of the codes are identical so they are not repeated. The first program shown performs the timing algorithm on the detector pulses in real time on the oscilloscope. The second program performs the timing algorithm with pulse rejection on detector pulses saved to files on a personal computer. They are both written as Matlab .m files and the main difference is in the section of the second program that uses a *for* loop to load pulse data from files saved to hard drive.

```
function [tdiff] = CFtime(WformIn1,WformIn2)

sfactor = 20;  % factor increase in interpolation of points

tstep = 100/sfactor;  % time between points in ps

X = WformIn1; Y = WformIn2;  % redefines pulses as X and Y

% BASELINE SEARCH
  BL1 = X(1:2500); BL2 = Y(1:2500);
  n = length(BL1);
  bmean1 = mean(BL1);  % calculates overall baseline
  bmean2 = mean(BL2);

% Baseline region 5 ns before the actual pulse (1000 pts = 5 ns)
  BL11 = X(2900:3900); BL22 = Y(2900:3900); m = length(BL11);
  bmean11 = mean(BL11); bmean22 = mean(BL22);
  rms1 = norm(BL1)/sqrt(n); % rms value of the baseline
  rms2 = norm(BL2)/sqrt(n);
  rms11 = norm(BL11)/sqrt(m);
  rms22 = norm(BL22)/sqrt(m);

  % Channel range limits for portion of the pulse to be timed
  ch1 = 3000;   ch2 = 4900;    % was 3900 and 3850 ch1 and ch3
  ch3 = 2950;   ch4 = 4850;

  XX=X(ch1:ch2);
  YY=Y(ch3:ch4);
```

```
  [min1 min1p] = min(XX);  %picks off max and min voltage values of the
                           %pulses
  max1 = max(XX);

  [min2 min2p] = min(YY);  %picks off max and min of the pulse
  max2 = max(YY);

  amp1 = max1-min1; % overall pulse amplitude
  amp2 = max2-min2;

  Xlen = length(XX);
  Ylen = length(YY);


% want find min and max level of both, and use this
% to find the constant fraction level desired.

CF = 0.25;  %desired constant fraction level
CF1 = CF*amp1 + min1;  %voltage level at CF
CF2 = CF*amp2 + min2;  %now need find time at these voltages

index1 = 0;  index2 = 0; tol1 = 1e-3; tol2 = 1e-3;

% can speed up process by searching through less of the pulse,
% b/c I know roughly where it will be based on the CF I choose

for i = min1p:Xlen;  % searches starting from the minimum
                     for the CF time index
    if abs(CF1 - XX(i)) < tol1
         index1 = i;
         break    % gets the first such value
    end
end

for i = 1:Ylen; % can increase lower lim if know is ok
    if abs(CF2 - YY(i)) < tol6
         index2 = i;
         break
    end
end

tdiff = (index2-index1)*tstep;  %time difference in picoseconds
```

The following code performs the constant fraction timing on pulses saved to a computer's hard drive.

```
% This does my interpolated CF search on the positive edge of the pulse,
% for the OFFLINE data.

tstep = 5;  % 5 ps/pt

% ------ FOR loop part to handle analyze all 10,000 pulses  ------------
nfile = 10000; % number of pulses to analyze (10,000)
result = zeros(nfile,1); %initializes matrix with length nfile to hold
                         all the delta t values
iones = 1; itens = 0; ihunds = 0; ithous = 0; iten_thous = 0;
% variables to keep track of which pulse is being analyzed.
% counts from one to ten thousand with the code below.

% pulses are named F6PulseGrp2_xxxxx.txt where xxxxx is the file number
% for example 00003 or 09874.

for ifile=0:nfile-1
  file1 = ['F6PulseGrp2_' num2str(iten_thous) num2str(ithous)...
           num2str(ihunds) num2str(itens) num2str(iones) '.txt'];

  if ithous == 9 && ihunds == 9 && itens == 9 && iones == 9
      iten_thous = iten_thous + 1; %increments ten thousand place
      ithous = 0; ihunds = 0;  itens = 0; iones = 0;

  elseif ihunds == 9 && itens == 9 && iones == 9 %increments thousands
place
      ithous = ithous + 1; ihunds = 0;  itens = 0; iones = 0;

  elseif itens == 9 && iones == 9 % increments hundreds place
      ihunds = ihunds + 1; itens = 0; iones = 0;

  elseif iones == 9 %takes care of tens and ones place
      iones = 0;  itens = itens + 1;

  else
      iones = iones + 1;  % if the ones place is NOT 9, then increment
  end

  %concatenated pulse has pulse 1 in 1:5000 and pulse 2 in 5051:10050

  p1 = dlmread(file1,' ',5,0); % reads the data from the file
  X = p1(1:5000,2); % saves pulse 1 as X
  Y = p1(5051:10050,2); % saves pulse 2 as Y

  %line(1:5000,X);   % can plot while all this is going on.
  %line(1:5000,Y);

  % BASELINE INFORMATION
  BL1 = X(1:2500); BL2 = Y(1:2500);
```

```
  n = length(BL1);
  bmean1 = mean(BL1);  % mean of pulse 1 baseline
  bmean2 = mean(BL2);  % mean of pulse 2 baseline

  % the baseline just 5 ns before the pulse
  BL11 = X(2900:3900); BL22 = Y(2900:3900); m = length(BL11);
  bmean11 = mean(BL11); bmean22 = mean(BL22);
  rms1 = norm(BL1)/sqrt(n); % rms value of the baseline
  rms2 = norm(BL2)/sqrt(n);
  rms11 = norm(BL11)/sqrt(m);
  rms22 = norm(BL22)/sqrt(m);

  % Channel range limits for portion of the pulse to be timed
  ch1 = 3000;   ch2 = 4900;
  ch3 = 2950;   ch4 = 4850;

  XX=X(ch1:ch2);
  YY=Y(ch3:ch4);

  [min1 min1p] = min(XX);  % picks off max and min voltage
                             values of the pulses
  max1 = max(XX);

  [min2 min2p] = min(YY);
  max2 = max(YY);  % FOR pos PULSE TESTING

  amp1 = max1-min1; % overall pulse amplitude
  amp2 = max2-min2;

  Xlen = length(XX);
  Ylen = length(YY);

   % ----------------- REJECTION CRITERIA ---------------------

%   rmslim = 0.015;  % rms must be under this
%   blim1 = 0.015;   % abs(baseline) must be under this
%   difflim = 0.005; % difference between baseline and rms
                       must be less than this
%   basecheck = [bmean1 rms1 bmean2 rms2;bmean11 rms11 bmean22 rms22];
%   % voltage range limit for minimum
%   vmin1bot = -0.400; vmin1top = -0.100; vmin2bot = -0.400;
%   vmin2top = -0.100;

%   if (rms1 < rmslim && rms2 < rmslim && rms11 < rmslim && rms22 <
rmslim...
%   && abs(bmean1) < blim1 && abs(bmean2) < blim1 && abs(bmean11) <
blim1...
%   && abs(bmean22) < blim1...
%&& abs((rms1-abs(bmean1))) < difflim && abs((rms2-abs(bmean2))) <
difflim...
%   && abs((rms11-abs(bmean11))) < difflim && abs((rms22-abs(bmean22)))
<...
    && difflim...
```

```
%    && abs(bmean1 - bmean11) < 0.005 && abs(bmean2 - bmean22) < 0.005...
%    && vmin1bot < min1 && min1 < vmin1top && vmin2bot < min2 && min2 < ...
     && vmin2top)…
%    && i1bot < i1 && i1 < i1top && i2bot < i2 && i2 < i2top) % pos. of
%
     CFa = 0.5;  %desired constant fraction level
     CFb = 0.5;

     CFtest = 0.5; %test to compare to normal method
     CF1 = -CFa*amp1 + min1;  %voltage at CF level of pulse 1
     CF2 = -CFb*amp2 + min2;  %voltage at CF level of pulse 2

     %now find time at these voltages
     index5 = 1;  index6 = 1; tol5 = 1e-3; tol6 = 1e-3;

     for i = 1:Xlen;  % searches the pulse for CF time index
        if abs(CF1 - XX(i)) < tol5
          index5 = i;
          break    % gets the first such value
        end
     end

     for i = 1:Ylen; % can increase lower lim if know is ok
         if abs(CF2 - YY(i)) < tol6
          index6 = i;
          break
         end
     end

     %noreject = 1;
     tdiff = (index6-index5)*tstep;  %time difference in picoseconds

   else  % if pulse is rejected then the time difference is set to a single
         % value well outside of the spectra values so the rejects do not
         % interfere and can be counted

     tdiff = -1000;
     %reject = 1;
     % index = [index1 index2] % more error checking

   end  % end of rejection criteria IF

   result(ifile+1) = tdiff;  % places the time difference result
                             % in the results matrix
%
%
end  % end of data searching loop
%
% %result;            %views the matrix/array of delta t's
% % hist(result,100)  %histograms the matrix of time differences
```